Aus der Klinik und Poliklinik für Neurologie
der Technischen Universität München
(Direktor: Univ.-Prof. Dr. med. Bernhard Hemmer)

Voxel-basierte Morphometrie des menschlichen Gehirns:

Transversaluntersuchungen physiologischer Parameter und neuropsychiatrischer Störungen

Zusammenstellung wissenschaftlicher Veröffentlichungen
zur Erlangung der Lehrbefähigung (Habilitation) für das Fach Neurologie
an der Fakultät für Medizin
der Technischen Universität München

Vorgelegt von
Dr. med. Mark Mühlau
München im Mai 2007
(letzte Aktualisierung der Anlage im November 2008)

meinen Eltern

meiner Frau Tina

meinen Söhnen Marvin und Lukas

Inhalt

1 Zusammenfassung

Die vorliegende Habilitationsleistung wurde mit zwischen 2002 und 2006 (in Kooperation mit der Neuroradiologie der Technischen Universität) durchgeführten Untersuchungen kumulativ erbracht. Der Schwerpunkt, auf den sich die folgende Zusammenfassung konzentriert, war dabei die Visualisierung charakteristischer struktureller Veränderungen der grauen Substanz des menschlichen Gehirns, die durch physiologische Zustände bedingt sind oder mit neuropsychiatrischen Störungen einhergehen. Dazu wurden hochaufgelöste T1-gewichtete Kernspinotomografien mit Hilfe der sog. Voxel-basierten Morphometrie analysiert.

1.1 Die Voxel-basierte Morphometrie (VBM)

Mit der Verfügbarkeit der Kernspintomografie seit Mitte/Ende der 80er Jahre wurde es möglich *in vivo* die Struktur des menschlichen Gehirns im Millimeterbereich zu analysieren. Das bedeutete zunächst für den klinischen Alltag einen Durchbruch. Später wurden Sequenzen entwickelt, mit denen die aktivitätsbedingte regionale Durchblutungssteigerung (BOLD Effekt) sichtbar gemacht werden konnte, so dass neben der Struktur auch die Funktion während bestimmter Aufgaben (Paradigmen) untersucht werden konnte (funktionelle Kernspintomografie), was zum heutigen Verständnis von Physiologie und Pathophysiologie der verschieden funktionellen Systeme des zentralen Nervensystems beitrug (z.B. **Ref. 3.1**). Die Untersuchung von neuropsychiatrischen Störungen mit der funktionellen Kernspintomografie hat allerdings methodisch bedingte Grenzen. Es kann häufig keine adäquate Kontrollbedingung gefunden werden. Zum Beispiel ist die Untersuchung von Patienten mit Tinnitus nur bedingt möglich, da das Ohrgeräusch meist permanent wahrgenommen wird und damit keine Kontrollbedingung existiert.

Vor diesem Hintergrund wurde Ende der 90er Jahre das Augenmerk verstärkt auf die vergleichende Analyse der Hirnstruktur gelenkt. Hierbei wurde insbesondere versucht, subtile regionale strukturelle Veränderungen zu detektieren, die sich lediglich in Intensitätsunterschieden anatomisch korrespondierender Bildpunkte niederschlagen und so dem bloßen Auge entgehen. Gruppenanalysen werden dadurch erschwert, dass die Form des Gehirns auch physiologischer Weise erhebliche interindividuelle Unterschiede aufweist. Mit den weithin bekannten, linearen geometrischen Operationen (Verschiebung, Drehung, Streckung) kann ein Teil dieser Variabilität ausgeglichen werden. Der entscheidende methodische Durchbruch waren jedoch Algorithmen, die mit Hilfe nichtlinearer geometrischer Operationen die „Verschiebung“ anatomisch korrespondierender Bildpunkte zueinander in einer Weise ermöglichten, dass diese (anatomisch korrespondierenden Bildpunkte) im dreidimensionalen Raum auch als Bildpunkte bzw. Voxel (Kunstwort aus engl. **vo**lume und **el**ement) übereinander zum Liegen kommen, ohne die Intensitätswerte zu verändern. Zwar ist die Idee, mit nichtlinearen Operatoren biologische Formen ineinander zu überführen, alt (Thompson, 1917.), Algorithmen, die in annehmbaren Zeiträumen die Verarbeitung datenträchtiger dreidimensionaler Datensätze ermöglichen, wurden jedoch erst Ende der 90er Jahre publiziert (Ashburner and Friston, 2000). Damit wurde auch unter praktischen Gesichtspunkten der Gruppenvergleich der Hirnstruktur Bildpunkt für Bildpunkt bzw. Voxel für Voxel – also „Voxel-basiert“ – möglich.

Im Einzelnen wurde Folgendes untersucht:

Der Einfluss der physiologischen Parameter Alter und Geschlecht auf die graue Substanz des menschlichen Gehirns **(Ref. 3.2)**

Veränderungen der Struktur des menschlichen Gehirnes bei neuropsychiatrischen Erkrankungen

- Chorea Huntington

  - vom Erkrankungsprozess ausgesparte Areale **(Ref. 3.3)**

  - Asymmetrie der morphologischen Veränderungen **(Ref. 3.4)**

- Blepharospasmus **(Ref. 3.5)**

- Tinnitus aurium **(Ref. 3.6)**

- Anorexia nervosa **(Ref. 3.7)**

1.2 Der Einfluss der physiologischen Parameter Alter und Geschlecht auf die graue Substanz des menschlichen Gehirns

Seit langem ist bekannt, dass das Gehirn altersbedingten Involutionsprozessen unterliegt. Mit der Kernspintomografie wurde es möglich den zeitlichen Ablauf *in vivo* in den verschiedenen Hirnregionen zu untersuchen. Es zeigte sich, dass praktisch alle kortikalen und subkortikalen Regionen mit dem Alter einen Substanzverlust erleiden (Good et al., 2001b, Smith et al., 2007, Taki et al., 2004). Jedoch ist die Ausprägung in den einzelnen Hirnregionen sehr unterschiedlich. So nimmt die graue Substanz im Frontallappen schneller ab als im Parietal-, Temporal- und Okzipitallappen (Allen et al., 2005, Cowell et al., 1994, Jernigan et al., 2001), während hippocampale und parahippocampale Areale (gemessen an der globalen Atrophie) unterdurchschnittlich an grauer Substanz verlieren (Good et al., 2001b, Grieve et al., 2005, Raz et al., 2004).

Zahlreiche Studien untersuchten ferner die strukturellen Unterschiede zwischen Mann und Frau. Zumeist fand sich nach Korrektur für die Kopfgröße bei Frauen ein Mehr in verschiedensten kortikalen Regionen (frontal, parietal, lateral temporal, okzipital), wobei Männer - wenn überhaupt - lediglich mehr graue Substanz im Kleinhirn und im medialen Temporallappen (Good et al., 2001a) aufwiesen.

Die eigene Studie untersuchte 133 gesunde Erwachsene (73 Frauen und 60 Männer) im Alter zwischen 29 und 80 Jahren und konnte die beschriebenen Haupteffekte von Alter und Geschlecht bestätigen. Zudem wurde einer umstrittenen Frage nachgegangen, nämlich ob es zwischen Männern und Frauen Unterschiede bezüglich des altersbedingten zerebralen Substanzverlustes gibt. Hier gab es nur wenige konventionelle morphometrische Studien, wobei verblindete Untersucher hypothesengetrieben einzelne Hirnstrukturen händisch ausmaßen. Dabei wurde bei Männern ein schnellerer Substanzverlust im Putamen identifiziert (Raz et al., 2003, Raz et al., 1995). Eine Studie, bei der hypothesenfrei das gesamte Gehirn in

einer größeren Population mit nahezu gleich verteilter Altersstruktur beider Geschlechter untersucht wurde, stand noch aus. Bemerkenswerter Weise konnten wir **(Ref. 3.2)** den schnelleren Substanzverlust im Putamen bei Männern im Vergleich zu Frauen bestätigen. Auch Verhaltensdaten sind damit vereinbar. So nimmt bei bestimmten motorischen Funktionen die Leistungsfähigkeit bei Frauen langsamer ab als bei Männern (Kennedy and Raz, 2005). Zudem beginnt die häufigste Erkrankung, die mit einer Fehlfunktion des Putamens einhergeht, der Morbus Parkinson, – auf Gruppenebene betrachtet – bei Frauen später und verläuft weniger schwerwiegend als bei Männern (Baldereschi et al., 2000, Haaxma et al., 2006). Dies könnte durchaus durch den langsameren altersbedingten Substanzverlust im Putamen bei Frauen bedingt sein.

1.3-7 Veränderungen der grauen Substanz des menschlichen Gehirnes bei neuropsychiatrischen Erkrankungen

1.3 Chorea Huntington

– vom Erkrankungsprozess verschonte Areale –

Die Chorea Huntington ist eine neurodegenerative Erkrankung, die klinisch durch die Trias aus Hyperkinesien, Verhaltensauffälligkeiten und Demenz gekennzeichnet ist. Bereits 1993 wurden der Genlocus und das Genprodukt, Huntingtin, entdeckt (Huntington's Disease Collaborative Research Group, 1993). Dennoch ist der genaue Pathomechanismus vom Gendefekt über den Untergang vorwiegend der „medium-sized spiny neurons“ im Corpus striatum zum Phänotyp nicht bekannt, auch wenn bis dato zahlreiche Schädigungsmechanismen des Huntingtins auf zellulärer Ebene beschrieben wurden (Gardian and Vecsei, 2004, Leegwater-Kim and Cha, 2004). Pathophysiologische Modelle der Chorea Huntington müssen in der Lage sein, mit molekularen Mechanismen makrostrukturelle Veränderungen und schließlich die klinische Phänomenologie zu erklären. Insofern ist die genaue Kenntnis der makrostrukturellen Veränderungen für das Verständnis der Chorea Huntington unerlässlich. Mit der VBM wurde bereits gezeigt, dass auch nahezu asymptomatische Patienten ein Weniger an grauer Substanz im Putamen aufweisen (Thieben et al., 2002). Mit zunehmend besseren morphometrischen Techniken wurden auch in frühen Erkrankungsstadien immer ausgedehntere Veränderungen beschrieben (Rosas et al., 2005, Rosas et al., 2003, Rosas et al., 2002), so dass sich die Frage stellte, ob nicht alle Hirnareale von der Erkrankung bereits sehr früh betroffen sind, wenn nur ausreichend genau gemessen wird.

Wir haben daher eine Gruppe von 48 an Chorea Huntington erkrankten Patienten in frühen Krankheitsstadien mit VBM dahingehend untersucht, ob Hirnareale existieren, die – gemessen an der globalen Atrophie – überdurchschnittlich gut erhalten sind **(Ref. 3.3)**. Dies

traf für den präfrontalen limbischen Kortex zu. Hier unterschieden sich auch absolut betrachtet (ohne Korrektur für die globale Atrophie) die an Chorea Huntington erkrankten Patienten nicht signifikant von den Kontrollpersonen. Dazu passend gibt es funktionelle Untersuchungen, die dort eine Überaktivierung bei bestimmten motorischen Paradigmen nachwiesen, was als Kompensation einer frühen Beeinträchtigung innerhalb der motorischen Schleife (s.u.) interpretiert wurde (Rosas et al., 2004). Zudem wurde bereits mehrfach postuliert, dass die Subsysteme der kortiko-striato-thalamo-kortikalen Schleifen in unterschiedlichem Maße vom Krankheitsprozess betroffen sind. Es werden zumindest drei dieser Schleifen unterschieden: die motorische Schleife (Putamen), die kognitive Schleife (Caudatum) und die limbische Schleife (ventrales Striatum). Da der präfrontale limbische Kortex zur sog. limbischen Schleife gehört, unterstützen unsere strukturellen Daten die Annahme, dass die einzelnen kortiko-striato-thalamo-kortikalen Schleifen bei der Chorea Huntington in ganz unterschiedlicher Weise in den Krankheitsprozess einbezogen sind (Joel, 2001).

1.4 Chorea Huntington

– Lateralisation des Erkrankungsprozesses –

Eine weitere Frage, die Untersuchungen der makrostrukturellen Veränderungen bei der Chorea Huntington aufwarfen, ist jene nach einer Linkslateralisierung des zerebralen Substanzverlustes. Fast alle Publikationen über die makrostrukturellen Veränderungen bei der Chorea Huntington beinhalteten Bilder, auf denen die jeweiligen Veränderungen links deutlicher als rechts zu erkennen waren. In einer VBM-Studie wurde explizit auf diesen Unterschied hingewiesen (Thieben et al., 2002), während eine MR-spektroskopische Untersuchung diese Lateralisierung sogar statistisch untermauerte (Jenkins et al., 1998).

In der eigenen Studie wurde mit einer Erweiterung der VBM (Luders et al., 2004) die hemisphärale Asymmetrie von 46 rechtshändigen Huntington-Patienten in frühen Krankheitsstadien mit jener von 46 rechtshändigen Kontrollpersonen verglichen **(Ref. 3.4)**. Auch hier zeigte sich eine Linkslateralisierung des zerebralen Substanzverlustes im Striatum. Diese Asymmetrie nahm mit der Erkrankungsschwere zu.

Auf der Grundlage dieser Lateralisierung haben wir die Hypothese vorgeschlagen **(Ref. 3.4)**, dass bei der Chorea Huntington die linke, dominante Hemisphäre früher in den Krankheitsprozess einbezogen wird, da linkshemisphäral die Lebenszeitaktivität höher ist. Dies wiederum legt die Relevanz von Pathomechanismen nahe, die durch die Aktivierung von Neuronen eine Verstärkung erfahren (z.B. glutaminerge Exzitotoxizität, Fehlfunktion der Mitochondrien).

1.5 Blepharospasmus

Der Blepharospasmus ist eine fokale Dystonie, bei der die Betroffenen immer wieder, krampfhaft beide Augen schließen, ohne dass dies willentlich unterdrückt werden kann. Die Pathogenese dieser Erkrankung ist unklar. In den meisten Fällen ist das diagnostische Kernspintomogramm unauffällig. Symptomatische Fälle wurden nach Läsionen im Bereich des Hirnstamms, des Diencephalons, der Basalganglien und des Kleinhirns beschrieben (Grandas et al., 2004, Jankovic and Patel, 1983, Larumbe et al., 1993, Lee and Marsden, 1994, Verghese et al., 1999). In einem Rattenmodell konnte eine dem Blepharospasmus ähnliche Störung durch zwei „Modifikationen“ ausgelöst werden, nämlich einer dopaminergen Depletion im Striatum und einer Schwächung des Musculus orbicularis oculi, wobei letzteres zu einer Reduktion der tonischen Inhibition des Blinkreflexbogens führt, so das der Blepharospasmus im Sinne eines enthemmten Blinkreflexes interpretiert wurde (Evinger and Perlmutter, 2003, Hallett, 2002). Funktionelle Bildgebungsstudien identifizierten ebenfalls striatale Strukturen, jedoch auch andere zerebrale Areale, so dass diese Ergebnisse zusammenfassend nicht schlüssig interpretiert werden können (Baker et al., 2003, Esmaeli-Gutstein et al., 1999, Hutchinson et al., 2000, Perlmutter et al., 1997, Schmidt et al., 2003).

In der eigenen VBM-Studie wurden 16 Blepharospasmus-Patienten mit 16 Kontrollpersonen verglichen **(Ref. 3.5)**. Es zeigte sich ein Mehr an grauer Substanz beiderseits im hinteren Putamen und ein Weniger an grauer Substanz im linken Parietallappen, wobei nur die letztere, von uns identifizierte strukturelle Veränderung mit der Erkrankungs- und Behandlungsdauer korrelierte. Dies stützt Hypothesen, welche dem Putamen eine originäre Rolle in der Pathogenese des Blepharospasmus zuschreiben.

1.6 Tinnitus aurium

Der Tinnitus aurium (lat. Geklingel der [in den] Ohren) ist eine Störung, bei der die Betroffenen ein zumeist hochfrequentes, monotones Geräusch wahrnehmen, ohne dass eine adäquate Geräuschquelle ausgemacht werden kann. Der Tinnitus ist ein weit verbreitetes Phänomen; viele Betroffene glauben, ernsthaft erkrankt zu sein und nehmen wiederholt ärztliche Hilfe in Anspruch (Lockwood et al., 2002).

Die Pathogenese dieser Störung ist weitgehend unklar. Die meisten wissenschaftlichen Untersuchungen haben sich mit peripheren, dass heißt im Innenohr lokalisierten Mechanismen befasst (Eggermont and Roberts, 2004). Eine umschriebene Schädigung vorwiegend der äußeren Haarzellen der Cochlea kann zum Beispiel zu einem funktionellen Ungleichgewicht zwischen inneren und äußeren Haarzellen und somit zu einem mit der entsprechenden Frequenz korrespondierenden Tinnitus führen. Dafür spricht auch die Tatsache, dass Schwerhörigkeit überzufällig häufig mit einem Tinnitus einhergeht. Zentrale Mechanismen (dass heißt im zentralen Nervensystem lokalisiert) müssen allerdings auch in der Pathogenese des Tinnitus eine entscheidende Rolle spielen. Dafür sprechen zahlreiche Argumente, von denen im Folgenden drei genannt seien:

1. Nach einer operativen Durchtrennung des Hörnerven bleibt der Tinnitus in der Mehrzahl der Fälle bestehen (Andersson et al., 1997, Eggermont and Roberts, 2004, Wiegand et al., 1996).
2. In völliger Stille nimmt die Mehrzahl der Menschen Tinnitus-ähnliche Geräusche wahr (Heller and Bergman, 1953).

3. Die psychometrisch gemessene Intensität des Tinnitus korreliert praktisch nicht mit dem Leidensdruck (Eggermont and Roberts, 2004). So geben unabhängig vom Leidensdruck die meisten Betroffenen bei Darbietung von Vergleichstönen eine Lautstärke von 2-3 dB (Vergleichstöne innerhalb der Tinnitus-Frequenz) bzw. von 10-15 dB (Vergleichstöne außerhalb der Tinnitus-Frequenz) an.

Tinnitus-Modelle, die von einer peripheren Schädigung und einer darauf folgenden zentralen Entstehung des Tinnitus ausgehen, postulieren eine entscheidende Rolle des primären auditorischen Kortex, der als Ort der bewussten Wahrnehmung des Tinnitus gilt (Arnold et al., 1996). So soll es Gemeinsamkeiten von Tinnitus und Schmerz (Rauschecker, 1999) geben, wonach der Tinnitus mit neuroplastischen Veränderungen des auditorischen Kortex einhergeht, wie dies auch beim Phantomschmerz (Flor et al., 1995) nachgewiesen wurde. Hinweise dafür erbrachte eine Magnetenzephalografie-Studie, bei der eine veränderte kortikale Repräsentation der Frequenzen im Bereich des Tinnitusfrequenz nachgewiesen wurde (Mühlnickel et al., 1998). Im letzten Jahrzehnt wurde der Tinnitus auch intensiv mit funktioneller Bildgebung untersucht. Das größte methodische Problem ist dabei das Fehlen einer adäquaten Kontrollbedingung, so dass zumeist Sonderformen des Tinnitus untersucht wurden, die sich durch eine strenge Seitenbetonung (Melcher et al., 2000) auszeichnen oder dadurch, dass sie modulierbar sind, sei es durch Bewegungen der Gesichtsmuskulatur (Lockwood et al., 1998) bzw. der Augen (Lockwood et al., 2001) oder durch Infusion von Lidocain (Mirz et al., 1999). Inwieweit die aus diesen Studien gewonnenen Erkenntnisse auf den „gewöhnlichen“ Tinnitus übertragbar sind, bleibt unklar.

Insbesondere angesichts des sehr unterschiedlichen Leidensdruckes bei – psychometrisch betrachtet – ähnlichen Ausprägungen des Tinnitus wird auch der emotionalen Bewertung und einer darauf aufbauenden Modulation des Tinnitus-Perzeptes eine entscheidende Bedeutung beigemessen, was in einem in sich schlüssigen Modell erstmals von Jastreboff vorgeschlagen wurde (Jastreboff, 1990). Allerdings konnte bezüglich der emotionalen Bewertung und der

darauf aufbauenden Modulation des Tinnitus-Perzeptes keine konkrete Hirnregion benannt werden.

Vor diesem Hintergrund erschien es insbesondere angesichts der mit funktionellen Untersuchungen verbundenen Schwierigkeiten nahe liegend, Tinnitus-Patienten mit VBM zu untersuchen. Unter der Vorstellung, dass bei Normalhörenden die zentralen Mechanismen eine vergleichsweise größere Rollen spielen, wurden mit Hilfe der HNO-Klinik der Technischen Universität München 28 normalhörende Tinnitus-Patienten sowie 28 gesunde Kontrollpersonen untersucht **(Ref. 3.6)**. Innerhalb der Hörbahn fand sich lediglich im Thalamus im Bereich des Corpus geniculatum mediale ein Mehr an grauer Substanz, während im auditorischen Kortex keine strukturellen Veränderungen entdeckt wurden, was mit Befunden vereinbar ist, wonach sich neuroplastische Veränderungen mehr auf thalamischer denn auf kortikaler Ebene abspielen (Chowdhury et al., 2004, Ergenzinger et al., 1998, Rauschecker, 1998). Außerhalb der Hörbahn wies die Area subcallosa bzw. der Nucleus accumbens ein Weniger an grauer Substanz auf. Letztere Region wurde bemerkenswerter Weise mit der emotionalen Bewertung und darauf aufbauenden Modulation von unangenehmen Geräuschwahrnehmungen in Verbindung gebracht. So wies genau diese Region bei Darbietung von Musik, die in unterschiedlichem Maße Dissonanzen enthielt, eine mit der unangenehmen Empfindung korrelierende Minderaktivierung auf (Blood et al., 1999).

Auf der Grundlage dieser Ergebnisse haben wir ein neues Tinnitus-Modell vorgeschlagen **(Ref. 3.6)**:

Eine zumeist im Innenohr lokalisierte Fehlfunktion führt zu einer Tinnitus-spezifischen Aktivität, welche wiederum neuroplastische, den Tinnitus unterhaltende Vorgänge im Corpus geniculatum mediale thalami anstößt, so sie nicht als Konsequenz der emotionalen Bewertung über die vom Nucleus accumbens zum Nucleus reticularis thalami reichende direkte Projektion unterdrückt wird. Nur wenn dieser letztgenannte Mechanismus versagt, entwickelt sich aus einer peripheren Fehlfunktion ein Tinnitus.

1.7 Anorexia nervosa

Essstörungen, insbesondere die Anorexia nervosa, sind ein wesentlicher Grund für seelische und körperliche Morbidität junger Mädchen und Frauen (Fairburn and Harrison, 2003). Nach DSM-IV werden folgende diagnostischen Kriterien gefordert: Verweigerung, das Körpergewicht zumindest an der Untergrenze der Norm (Body-Mass-Index von 17,5 kg/m^2) zu halten, irrationale Angst zuzunehmen oder gar „fett“ zu werden, Körperschemastörung und Amenorrhoe. Die neurobiologischen Grundlagen der Anorexia nervosa sind weitgehend unklar. Ein Suszeptibilitätsgen für die restriktive Form der Anorexia nervosa wird auf Chromosom 1 vermutet (Grice et al., 2002). Ferner sind Risikofaktoren wie weibliches Geschlecht, Aufwachsen in der westlichen Welt, depressive Störungen in der Familienanamnese, sexueller Missbrauch oder eine „gestörte Beziehung zur Mutter“ hinreichend bekannt, jedoch gibt es über die Pathogenese im engeren Sinne oder gar die individuellen Kausalitätsketten, die schließlich zu einer manifesten Erkrankung führen, fast keine gesicherten Erkenntnisse (Fairburn and Harrison, 2003).

Die Unkenntnis der neurobiologischen Grundlagen der Anorexie hat bisher die Weiterentwicklung wirksamer Therapieverfahren vereitelt. Auch bei dieser Störung ist nicht bekannt, welche Hirnareale entscheidend für die Entstehung sind. Eine Metaanalyse von Läsionsstudien folgerte, dass komplexe, der Anorexia nervosa ähnliche Essstörungen nach Schädigungen im Bereich des Frontal-, aber auch des Temporallappens entstehen können (Uher and Treasure, 2005). Andere Untersuchungstechniken sehen sich zumeist mit dem Problem konfrontiert, dass die jeweiligen Ergebnisse nicht sicher den der Anorexia nervosa zugrunde liegenden Pathomechanismen zugeschrieben werden können, da Epiphänomene dieser Essstörung wie die unterschiedlichen Lebenserfahrungen (z.B. häufige Hospitalisierungen) und die Malnutrition ebenso gut dafür verantwortlich gemacht werden können. So ist unmittelbar verständlich, dass auch eine in Remission befindliche Anorexia-

nervosa-Patientin zum Beispiel im Rahmen einer funktionellen Kernspintomographie beim Anblick eines Hamburgers andere Assoziationen hat und damit auch andere Aktivierungsmuster aufweist, als eine gesunde Kontrollperson und dass diese Aktivierungsunterschiede kaum Rückschlüsse auf die Erkrankungsursache zulassen dürften. Wohl auch deshalb wurden Anorexia-nervosa-Patientinnen zunächst in Ruhe mit Single-Photon-Emission-Computer-Tomografie (SPECT) untersucht. Alle Studien zeigten dabei einen *Hypo*metabolismus im anterioren Cingulum – sogar nach Wiedererlangen des Normalgewichtes (Kojima et al., 2005, Naruo et al., 2001, Takano et al., 2001). Demgegenüber wiesen Anorexia-nervosa-Patientinnen nach visueller Darbietung von Nahrung neben anderen Aktivierungsunterschieden im Vergleich zum Kontrollkollektiv eine *Über*aktivierung im anterioren Cingulum auf.

Vor diesem Hintergrund wurden auch Anorexia-nervosa-Patientinnen mit VBM hinsichtlich subtiler struktureller Veränderungen der grauen Substanz untersucht **(Ref. 3.7)**. Allerdings war auch mit dieser Untersuchungstechnik ein methodisches Problem verbunden, nämlich die mit einer Malnutrition verbundene Hirnatrophie, von der nicht genau bekannt ist, ob sie komplett reversibel ist (Katzman et al., 2001, Katzman et al., 1997, Lambe et al., 1997, Swayze et al., 1996, Swayze et al., 2003). Deshalb haben wir nach einem aufwendigen Screeningverfahren, an dem drei Therapiezentren (TCE München, ANAD München und Klinikum Roseneck) beteiligt waren, von über 100 Anorexia-nervosa-Patientinnen lediglich 22 Patientinnen mit VBM untersucht, da nur bei diesen Patientinnen sowohl psychiatrische Begleiterkrankungen mit hinlänglicher Sicherheit ausgeschlossen werden konnten als auch eine körperliche Kompensation konstatiert werden konnte (für mindestens sechs Monate: Body-Mass-Index >17,0 regelmäßige Menstruationen). Dennoch fanden wir bei Betrachtung der Globalwerte ein signifikantes Weniger an grauer Substanz von einem Prozent, was zumindest für ein längerfristiges Bestehen der Hirnatrophie in der Folge der Malnutrition spricht. Dieser einprozentige Unterschied der Globalwerte der grauen Substanz wurde nun

auch in der VBM-Analyse berücksichtigt, in dem er als Kovariate in die Voxel-basierte Kovarianzanalyse einging. Diese Analyse zeigte nur eine Veränderung, nämlich ein Weniger an grauer Substanz im anterioren Cingulum. Um den Einfluss anderer Größen auf diese strukturelle Veränderung zu eruieren, wurden die Grauwerte dieser Region integriert und als abhängige Variable einer Varianzanalyse zugeführt. Zahlreiche klinische Parameter dienten dabei als unabhängige Variablen, wobei nur einer signifikant mit dem Gesamtgrauwert des anterioren Cingulums korrelierte, nämlich die Erkrankungsschwere (niedrigster im Krankheitsverlauf erreichter Body-Mass-Index), was für einen direkten Zusammenhang der entdeckten strukturellen Veränderung mit der Erkrankung spricht. Allerdings kann anhand dieses Ergebnisses aus zwei Gründen kein in sich schlüssiges Krankheitsmodell entwickelt werden. Einerseits ist das anteriore Cingulum eine Hirnregion, die mit zahlreichen Funktionen und deren Konvergenz in Verbindung gebracht wird (Yucel et al., 2003), weshalb es nicht verblüfft, dass andererseits ein Weniger an grauer Substanz im anterioren Cingulum auch bei anderen psychiatrischen Störungen wie der Zwangsstörung (Valente et al., 2005), der Schizophrenie (Honea et al., 2005) und der posttraumatischen Belastungsstörung (Yamasue et al., 2003) beschrieben wurde.

In Zusammenschau mit den in den letzten Jahren veröffentlichten Bildgebungsstudien kann dennoch konstatiert werden, dass bei der Anorexia nervosa sowohl eine funktionelle als auch eine strukturelle Störung im Bereich des anterioren Cingulums vorliegt.

1.8 Fremdreferenzen

Die eigenen, in dieser Zusammenfassung zitierten Arbeiten sind bei den wichtigsten Publikationen unter 3 aufgeführt.

Allen, J.S., Bruss, J., Brown, C.K., Damasio, H., 2005. Normal neuroanatomical variation due to age: the major lobes and a parcellation of the temporal region. Neurobiol Aging. 26, 1245-1260.

Andersson, G., Kinnefors, A., Ekvall, L., Rask-Andersen, H., 1997. Tinnitus and translabyrinthine acoustic neuroma surgery. Audiol Neurootol. 2, 403-409.

Arnold, W., Bartenstein, P., Oestreicher, E., Romer, W., Schwaiger, M., 1996. Focal metabolic activation in the predominant left auditory cortex in patients suffering from tinnitus: a PET study with [18F]deoxyglucose. ORL J Otorhinolaryngol Relat Spec. 58, 195-199.

Ashburner, J., Friston, K.J., 2000. Voxel-based morphometry--the methods. Neuroimage. 11, 805-821.

Baker, R.S., Andersen, A.H., Morecraft, R.J., Smith, C.D., 2003. A functional magnetic resonance imaging study in patients with benign essential blepharospasm. J Neuroophthalmol. 23, 11-15.

Baldereschi, M., Di Carlo, A., Rocca, W.A., Vanni, P., Maggi, S., Perissinotto, E., Grigoletto, F., Amaducci, L., Inzitari, D., 2000. Parkinson's disease and parkinsonism in a longitudinal study: two-fold higher incidence in men. ILSA Working Group. Italian Longitudinal Study on Aging. Neurology. 55, 1358-1363.

Blood, A.J., Zatorre, R.J., Bermudez, P., Evans, A.C., 1999. Emotional responses to pleasant and unpleasant music correlate with activity in paralimbic brain regions. Nat Neurosci. 2, 382-387.

Chowdhury, S.A., Greek, K.A., Rasmusson, D.D., 2004. Changes in corticothalamic modulation of receptive fields during peripheral injury-induced reorganization. Proc Natl Acad Sci U S A. 101, 7135-7140.

Cowell, P.E., Turetsky, B.I., Gur, R.C., Grossman, R.I., Shtasel, D.L., Gur, R.E., 1994. Sex differences in aging of the human frontal and temporal lobes. J Neurosci. 14, 4748-4755.

Eggermont, J.J., Roberts, L.E., 2004. The neuroscience of tinnitus. Trends Neurosci. 27, 676-682.

Ergenzinger, E.R., Glasier, M.M., Hahm, J.O., Pons, T.P., 1998. Cortically induced thalamic plasticity in the primate somatosensory system. Nat Neurosci. 1, 226-229.

Esmaeli-Gutstein, B., Nahmias, C., Thompson, M., Kazdan, M., Harvey, J., 1999. Positron emission tomography in patients with benign essential blepharospasm. Ophthal Plast Reconstr Surg. 15, 23-27.

Evinger, C., Perlmutter, J.S., 2003. Blind men and blinking elephants. Neurology. 60, 1732-1733.

Fairburn, C.G., Harrison, P.J., 2003. Eating disorders. Lancet. 361, 407-416.

Flor, H., Elbert, T., Knecht, S., Wienbruch, C., Pantev, C., Birbaumer, N., Larbig, W., Taub, E., 1995. Phantom-limb pain as a perceptual correlate of cortical reorganization following arm amputation. Nature. 375, 482-484.

Gardian, G., Vecsei, L., 2004. Huntington's disease: pathomechanism and therapeutic perspectives. J Neural Transm. 111, 1485-1494.

Good, C.D., Johnsrude, I., Ashburner, J., Henson, R.N., Friston, K.J., Frackowiak, R.S., 2001a. Cerebral asymmetry and the effects of sex and handedness on brain structure: a voxel-based morphometric analysis of 465 normal adult human brains. Neuroimage. 14, 685-700.

Good, C.D., Johnsrude, I.S., Ashburner, J., Henson, R.N., Friston, K.J., Frackowiak, R.S., 2001b. A voxel-based morphometric study of ageing in 465 normal adult human brains. Neuroimage. 14, 21-36.

Grandas, F., Lopez-Manzanares, L., Traba, A., 2004. Transient blepharospasm secondary to unilateral striatal infarction. Mov Disord. 19, 1100-1102.

Grice, D.E., Halmi, K.A., Fichter, M.M., Strober, M., Woodside, D.B., Treasure, J.T., Kaplan, A.S., Magistretti, P.J., Goldman, D., Bulik, C.M., Kaye, W.H., Berrettini, W.H., 2002. Evidence for a susceptibility gene for anorexia nervosa on chromosome 1. Am J Hum Genet. 70, 787-792.

Grieve, S.M., Clark, C.R., Williams, L.M., Peduto, A.J., Gordon, E., 2005. Preservation of limbic and paralimbic structures in aging. Hum Brain Mapp. 25, 391-401.

Haaxma, C.A., Bloem, B.R., Borm, G.F., Oyen, W.J., Leenders, K.L., Eshuis, S., Booij, J., Dluzen, D.E., Horstink, M.W., 2006. Gender Differences in Parkinson's Disease. J Neurol Neurosurg Psychiatry.

Hallett, M., 2002. Blepharospasm: recent advances. Neurology. 59, 1306-1312.

Heller, M.F., Bergman, M., 1953. Tinnitus aurium in normally hearing persons. Ann Otol Rhinol Laryngol. 62, 73-83.

Honea, R., Crow, T.J., Passingham, D., Mackay, C.E., 2005. Regional deficits in brain volume in schizophrenia: a meta-analysis of voxel-based morphometry studies. Am J Psychiatry. 162, 2233-2245.

Huntington's Disease Collaborative Research Group, 1993. A novel gene containing a trinucleotide repeat that is expanded and unstable on Huntington's disease chromosomes. Cell. 72, 971-983.

Hutchinson, M., Nakamura, T., Moeller, J.R., Antonini, A., Belakhlef, A., Dhawan, V., Eidelberg, D., 2000. The metabolic topography of essential blepharospasm: a focal dystonia with general implications. Neurology. 55, 673-677.

Jankovic, J., Patel, S.C., 1983. Blepharospasm associated with brainstem lesions. Neurology. 33, 1237-1240.

Jastreboff, P.J., 1990. Phantom auditory perception (tinnitus): mechanisms of generation and perception. Neurosci Res. 8, 221-254.

Jenkins, B.G., Rosas, H.D., Chen, Y.C., Makabe, T., Myers, R., MacDonald, M., Rosen, B.R., Beal, M.F., Koroshetz, W.J., 1998. 1H NMR spectroscopy studies of Huntington's disease: correlations with CAG repeat numbers. Neurology. 50, 1357-1365.

Jernigan, T.L., Archibald, S.L., Fennema-Notestine, C., Gamst, A.C., Stout, J.C., Bonner, J., Hesselink, J.R., 2001. Effects of age on tissues and regions of the cerebrum and cerebellum. Neurobiol Aging. 22, 581-594.

Joel, D., 2001. Open interconnected model of basal ganglia-thalamocortical circuitry and its relevance to the clinical syndrome of Huntington's disease. Mov Disord. 16, 407-423.

Katzman, D.K., Christensen, B., Young, A.R., Zipursky, R.B., 2001. Starving the brain: structural abnormalities and cognitive impairment in adolescents with anorexia nervosa. Semin Clin Neuropsychiatry. 6, 146-152.

Katzman, D.K., Zipursky, R.B., Lambe, E.K., Mikulis, D.J., 1997. A longitudinal magnetic resonance imaging study of brain changes in adolescents with anorexia nervosa. Arch Pediatr Adolesc Med. 151, 793-797.

Kennedy, K.M., Raz, N., 2005. Age, sex and regional brain volumes predict perceptual-motor skill acquisition. Cortex. 41, 560-569.

Kojima, S., Nagai, N., Nakabeppu, Y., Muranaga, T., Deguchi, D., Nakajo, M., Masuda, A., Nozoe, S., Naruo, T., 2005. Comparison of regional cerebral blood flow in patients with anorexia nervosa before and after weight gain. Psychiatry Res. 140, 251-258.

Lambe, E.K., Katzman, D.K., Mikulis, D.J., Kennedy, S.H., Zipursky, R.B., 1997. Cerebral gray matter volume deficits after weight recovery from anorexia nervosa. Arch Gen Psychiatry. 54, 537-542.

Larumbe, R., Vaamonde, J., Artieda, J., Zubieta, J.L., Obeso, J.A., 1993. Reflex blepharospasm associated with bilateral basal ganglia lesion. Mov Disord. 8, 198-200.

Lee, M.S., Marsden, C.D., 1994. Movement disorders following lesions of the thalamus or subthalamic region. Mov Disord. 9, 493-507.

Leegwater-Kim, J., Cha, J.H., 2004. The paradigm of Huntington's disease: therapeutic opportunities in neurodegeneration. NeuroRx. 1, 128-138.

Lockwood, A.H., Salvi, R.J., Burkard, R.F., 2002. Tinnitus. N Engl J Med. 347, 904-910.

Lockwood, A.H., Salvi, R.J., Coad, M.L., Towsley, M.L., Wack, D.S., Murphy, B.W., 1998. The functional neuroanatomy of tinnitus: evidence for limbic system links and neural plasticity. Neurology. 50, 114-120.

Lockwood, A.H., Wack, D.S., Burkard, R.F., Coad, M.L., Reyes, S.A., Arnold, S.A., Salvi, R.J., 2001. The functional anatomy of gaze-evoked tinnitus and sustained lateral gaze. Neurology. 56, 472-480.

Luders, E., Gaser, C., Jancke, L., Schlaug, G., 2004. A voxel-based approach to gray matter asymmetries. Neuroimage. 22, 656-664.

Melcher, J.R., Sigalovsky, I.S., Guinan, J.J., Jr., Levine, R.A., 2000. Lateralized tinnitus studied with functional magnetic resonance imaging: abnormal inferior colliculus activation. J Neurophysiol. 83, 1058-1072.

Mirz, F., Pedersen, B., Ishizu, K., Johannsen, P., Ovesen, T., Stodkilde-Jorgensen, H., Gjedde, A., 1999. Positron emission tomography of cortical centers of tinnitus. Hear Res. 134, 133-144.

Mühlnickel, W., Elbert, T., Taub, E., Flor, H., 1998. Reorganization of auditory cortex in tinnitus. Proc Natl Acad Sci U S A. 95, 10340-10343.

Naruo, T., Nakabeppu, Y., Deguchi, D., Nagai, N., Tsutsui, J., Nakajo, M., Nozoe, S., 2001. Decreases in blood perfusion of the anterior cingulate gyri in Anorexia Nervosa Restricters assessed by SPECT image analysis. BMC Psychiatry. 1, 2.

Perlmutter, J.S., Stambuk, M.K., Markham, J., Black, K.J., McGee-Minnich, L., Jankovic, J., Moerlein, S.M., 1997. Decreased [18F]spiperone binding in putamen in idiopathic focal dystonia. J Neurosci. 17, 843-850.

Rauschecker, J.P., 1998. Cortical control of the thalamus: top-down processing and plasticity. Nat Neurosci. 1, 179-180.

Rauschecker, J.P., 1999. Auditory cortical plasticity: a comparison with other sensory systems. Trends Neurosci. 22, 74-80.

Raz, N., Rodrigue, K.M., Head, D., Kennedy, K.M., Acker, J.D., 2004. Differential aging of the medial temporal lobe: a study of a five-year change. Neurology. 62, 433-438.

Raz, N., Rodrigue, K.M., Kennedy, K.M., Head, D., Gunning-Dixon, F., Acker, J.D., 2003. Differential aging of the human striatum: longitudinal evidence. AJNR Am J Neuroradiol. 24, 1849-1856.

Raz, N., Torres, I.J., Acker, J.D., 1995. Age, gender, and hemispheric differences in human striatum: a quantitative review and new data from in vivo MRI morphometry. Neurobiol Learn Mem. 63, 133-142.

Rosas, H.D., Feigin, A.S., Hersch, S.M., 2004. Using advances in neuroimaging to detect, understand, and monitor disease progression in Huntington's disease. NeuroRx. 1, 263-272.

Rosas, H.D., Hevelone, N.D., Zaleta, A.K., Greve, D.N., Salat, D.H., Fischl, B., 2005. Regional cortical thinning in preclinical Huntington disease and its relationship to cognition. Neurology. 65, 745-747.

Rosas, H.D., Koroshetz, W.J., Chen, Y.I., Skeuse, C., Vangel, M., Cudkowicz, M.E., Caplan, K., Marek, K., Seidman, L.J., Makris, N., Jenkins, B.G., Goldstein, J.M., 2003. Evidence for more widespread cerebral pathology in early HD: an MRI-based morphometric analysis. Neurology. 60, 1615-1620.

Rosas, H.D., Liu, A.K., Hersch, S., Glessner, M., Ferrante, R.J., Salat, D.H., van der Kouwe, A., Jenkins, B.G., Dale, A.M., Fischl, B., 2002. Regional and progressive thinning of the cortical ribbon in Huntington's disease. Neurology. 58, 695-701.

Schmidt, K.E., Linden, D.E., Goebel, R., Zanella, F.E., Lanfermann, H., Zubcov, A.A., 2003. Striatal activation during blepharospasm revealed by fMRI. Neurology. 60, 1738-1743.

Smith, C.D., Chebrolu, H., Wekstein, D.R., Schmitt, F.A., Markesbery, W.R., 2007. Age and gender effects on human brain anatomy: a voxel-based morphometric study in healthy elderly. Neurobiol Aging. 28, 1075-1087.

Swayze, V.W., 2nd, Andersen, A., Arndt, S., Rajarethinam, R., Fleming, F., Sato, Y., Andreasen, N.C., 1996. Reversibility of brain tissue loss in anorexia nervosa assessed with a computerized Talairach 3-D proportional grid. Psychol Med. 26, 381-390.

Swayze, V.W., 2nd, Andersen, A.E., Andreasen, N.C., Arndt, S., Sato, Y., Ziebell, S., 2003. Brain tissue volume segmentation in patients with anorexia nervosa before and after weight normalization. Int J Eat Disord. 33, 33-44.

Takano, A., Shiga, T., Kitagawa, N., Koyama, T., Katoh, C., Tsukamoto, E., Tamaki, N., 2001. Abnormal neuronal network in anorexia nervosa studied with I-123-IMP SPECT. Psychiatry Res. 107, 45-50.

Taki, Y., Goto, R., Evans, A., Zijdenbos, A., Neelin, P., Lerch, J., Sato, K., Ono, S., Kinomura, S., Nakagawa, M., Sugiura, M., Watanabe, J., Kawashima, R., Fukuda, H., 2004. Voxel-based morphometry of human brain with age and cerebrovascular risk factors. Neurobiol Aging. 25, 455-463.

Thieben, M.J., Duggins, A.J., Good, C.D., Gomes, L., Mahant, N., Richards, F., McCusker, E., Frackowiak, R.S., 2002. The distribution of structural neuropathology in pre-clinical Huntington's disease. Brain. 125, 1815-1828.

Thompson, D.W.: On Growth and Form. Cambridge, Cambridge University Press, 1917.

Uher, R., Treasure, J., 2005. Brain lesions and eating disorders. J Neurol Neurosurg Psychiatry. 76, 852-857.

Valente, A.A., Jr., Miguel, E.C., Castro, C.C., Amaro, E., Jr., Duran, F.L., Buchpiguel, C.A., Chitnis, X., McGuire, P.K., Busatto, G.F., 2005. Regional gray matter abnormalities in obsessive-compulsive disorder: a voxel-based morphometry study. Biol Psychiatry. 58, 479-487.

Verghese, J., Milling, C., Rosenbaum, D.M., 1999. Ptosis, blepharospasm, and apraxia of eyelid opening secondary to putaminal hemorrhage. Neurology. 53, 652.

Wiegand, D.A., Ojemann, R.G., Fickel, V., 1996. Surgical treatment of acoustic neuroma (vestibular schwannoma) in the United States: report from the Acoustic Neuroma Registry. Laryngoscope. 106, 58-66.

Yamasue, H., Kasai, K., Iwanami, A., Ohtani, T., Yamada, H., Abe, O., Kuroki, N., Fukuda, R., Tochigi, M., Furukawa, S., Sadamatsu, M., Sasaki, T., Aoki, S., Ohtomo, K., Asukai, N., Kato, N., 2003. Voxel-based analysis of MRI reveals anterior cingulate gray-matter volume reduction in posttraumatic stress disorder due to terrorism. Proc Natl Acad Sci U S A. 100, 9039-9043.

Yucel, M., Wood, S.J., Fornito, A., Riffkin, J., Velakoulis, D., Pantelis, C., 2003. Anterior cingulate dysfunction: implications for psychiatric disorders? J Psychiatry Neurosci. 28, 350-354.

2 Schriftenverzeichnis mit Impaktpunkten (IP)

2.1 Erst- und Letztautorenschaften in chronologischer Reihenfolge

1. **Mühlau, M.**, Schlegel, J., Von Einsiedel, H.G., Conrad, B., & Sander, D. (2003). Multiple progressive intracerebral hemorrhages due to an angiosarcoma: a case report. Eur J Neurol, 10(6), 741-742. IF: 2,2
2. **Mühlau, M.**, Bülow, S., Stimmer, H., Schätzl, H., & Berthele, A. (2005a). Seronegative EBV-myeloradiculitis in a 73year-old woman. Neurology, 65(8), 1329-1330. IP: 5,9
3. **Mühlau, M.**, Hermsdörfer, J., Goldenberg, G., Wohlschlager, A.M., Castrop, F., Stahl, R., Röttinger, M., Erhard, P., Haslinger, B., Ceballos-Baumann, A.O., Conrad, B., & Boecker, H. (2005b). Left inferior parietal dominance in gesture imitation: an fMRI study. Neuropsychologia, 43(7), 1086-1098. IP: 4,1
4. **Mühlau, M**., Rauschecker, J.P., Oestreicher, E., Gaser, C., Röttinger, M., Wohlschläger, A.M., Simon, F., Etgen, T., Conrad, B., & Sander, D. (2006). Structural brain changes in tinnitus. Cereb Cortex, 16(9), 1283-1288. IP 6,2
5. **Mühlau, M.**, Weindl, A., Wohlschläger, A.M., Gaser, C., Städtler, M., Valet, M., Zimmer, C., Kassubek, J., & Peinemann, A. (2007a). Voxel-based morphometry indicates relative preservation of the limbic prefrontal cortex in early Huntington disease. J Neural Transm, 114(3), 367-372. IP: 2,6
6. **Mühlau, M.**, Gaser, C., Wohlschläger, A.M., Weindl, A., Städtler, M., Valet, M., Zimmer, C., Kassubek, J., & Peinemann, A. (2007b). Striatal gray matter loss in Huntington's disease is leftward biased. Mov Dis, 22(8), 1169-1173. IP: 2,9
7. **Mühlau, M.**, Gaser, C., Ilg, R., Conrad, B., Leibl, C., Cebulla, M., Backmund, H., Gerlinghoff, M., Lommer, P., Schnebel, A., Wohlschläger, A.M., Zimmer, C., & Nunneman, S. (2007c). Gray-matter decrease of the anterior cingulate cortex in anorexia nervosa. Am J Psychiatry, im Druck. IP: 8,3
8. Nunneman, S., Wohlschläger, A.M., Gaser, C., Ilg, R., Conrad, B., Zimmer, C., & **Mühlau, M.** (2007d). Accelerated aging of the putamen in men but not in women. Neurobiol Aging, im Druck. IP: 5,3

9. Ilg, R., Burazanis, S., Wohlschläger, A.M., Wöller, A., & **Mühlau, M.** (2007a). Evidence for bottom-up processing of perceptual reversals derived from an ambiguous apparent motion task. Perception and Psychophysics, eingereicht.

10. Ilg, R., Burazanis, S., Wohlschläger, A.M., Wöller, A., & **Mühlau, M.** (2007b). Spontaneous reversals in ambiguous apparent motion are generated at early visual areas: an fMRI study. Neuropsychologia, eingereicht.

Summe der Impaktpunkte als Erst/Letztautor: 37,5

2.2 Koautorenschaften in chronologischer Reihenfolge

11. Boecker, H., Lee, A., **Mühlau, M.**, Ceballos-Baumann, A., Ritzl, A., Spilker, M.E., Marquart, C., & Hermsdörfer, J. (2005). Force level independent representations of predictive grip force-load force coupling: a PET activation study. Neuroimage, 25(1), 243-252. IP: 5,3
12. Hermsdörfer, J., Nowak, D.A., Lee, A., Rost, K., Timmann, D., **Mühlau, M.**, & Boecker, H. (2005). The representation of predictive force control and internal forward models: evidence from lesion studies and brain imaging. Cogn Process, 6(1), 48–58. IP: unbekannt (Publication start year: 2004)
13. Etgen, T., **Mühlau, M.**, Gaser, C., & Sander, D. (2006). Bilateral grey-matter increase in the putamen in primary blepharospasm. J Neurol Neurosurg Psychiatry, 77(9), 1017-1020. IP: 3,1
14. Hillerer, C., Wöller, A., **Mühlau, M.**, Stimmer, H., & Zimmer, C. (2007). Neuroradiologische Befunde beim Mobius-Syndrom. Röfo, 179(5), 532-534. IP: 1,9
15. Hermsdörfer, J., Terlinden, G., **Mühlau, M.**, Goldenberg, G., & Wohlschläger, A.M. (2007). Neural representations of pantomimed and actual tool use: Evidence from an event-related fMRI study. Neuroimage, im Druck. IP: 5,3

Summe der Impaktpunkte als Koautor: 15,6

Summe aller Impaktpunkte: 53,1

3 Die wichtigsten Publikationen

Verzeichnis

ELSEVIER

Neuropsychologia 43 (2005) 1086–1098

NEUROPSYCHOLOGIA

www.elsevier.com/locate/neuropsychologia

Left inferior parietal dominance in gesture imitation: an fMRI study

Mark Mühlau [a, *], Joachim Hermsdörfer [c], Georg Goldenberg [c], Afra M. Wohlschläger [a, b, c], Florian Castrop [a], Robert Stahl [a], Michael Röttinger [d], Peter Erhard [a], Bernhard Haslinger [a], Andres O. Ceballos-Baumann [a], Bastian Conrad [a], Henning Boecker [b]

[a] *Neurologische Klinik Rechts der Isar, Technische Universität München, Munich, Germany*
[b] *Nuklearmedizinische Klinik Rechts der Isar, Technische Universität München, Munich, Germany*
[c] *Entwicklungsgruppe Klinische Neuropsychologie (EKN), Städtisches Krankenhaus München-Bogenhausen, Munich, Germany*
[d] *Institut für Röntgendiagnostik, Technische Universität München, Munich, Germany*

Received 18 January 2004; received in revised form 17 September 2004; accepted 1 October 2004

Abstract

The inability to imitate gestures is an essential feature of apraxia. However, discrepancies exist between clinical studies in apraxic patients and neuroimaging findings on imitation. We therefore aimed to investigate: (1) which areas are recruited during imitation under conditions similar to clinical tests for apraxic deficits; (2) whether there are common lateralized areas subserving imitation irrespective of the acting limb side; and also (3) whether there are differences between hand and finger gestures. We used fMRI in 12 healthy, right handed subjects to investigate the imitation of four types of variable gestures that were presented by video clips (16 different finger and 16 different hand gestures with either the right or the left arm). The respective control conditions consisted of stereotyped gestures (only two gestures presented in pseudorandom order). Subtraction analysis of each type of gesture imitation (variable > stereotyped) revealed a bilateral activation pattern including the inferior parietal cortex Brodmann Area (BA 40), the superior parietal cortex, the inferior frontal cortex (opercular region), the prefrontal motor cortex, the lateral occipito-temporal junction, and the cerebellum. These results were supported by statistical conjunction of all four subtraction analyses and by the common analysis of all four types of gesture imitation. The direct comparison of the right and left hemispheric activation revealed a lateralization to the left only of the inferior parietal cortex. Comparisons between different types of gesture imitation yielded no significant results. In conclusion, gesture imitation recruits bilateral fronto-parietal regions, with significant lateralization of only one area, namely the left inferior parietal cortex. These in vivo data indicate left inferior parietal dominance for gesture imitation in right handers, confirming lesion-based theories of apraxia.

Keywords: Apraxia; fMRI; Gestures; Imitation; Parietal cortex

1. Introduction

Imitation is a fundamental principle of behavioral learning (Byrne & Russon, 1998; Kymissis & Poulson, 1990) and an important component of non-verbal communication. The inability to imitate is an essential feature of apraxia, a disorder of skilled movements. Apraxia manifests in tasks like performing verbally instructed gestures, pantomiming the use of an object, and imitating actions demonstrated by the examiner (De Renzi, 1990; Heilman & Rothi, 1993; Rothi, Raymer, & Heilman, 1997; Roy & Hall, 1992). Respective errors occur either during known manual actions, such as conventional gestures, or meaningless and "novel" gestures (De Renzi, Motti, & Nichelli, 1980; Goldenberg, 1996; Kimura & Archibald, 1974; Roy, Square-Storer, Hogg, & Adams, 1991). It is generally acknowledged that apraxic deficits occur after left hemispheric damage, whereas apraxia resulting from lesions of the right hemisphere remains a controversial issue (Alexander, Baker, Naeser, Kaplan, & Palumbo,

* Corresponding author. Present address: Department of Neurology, Technical University of Munich, Möhlstrasse 28, D-81675 Munich, Germany. Tel.: +49 89 4140 4601; fax: +49 89 4140 4919.
E-mail address: m.muehlau@neuro.med.tu-muenchen.de (M. Mühlau).

0028-3932/$ – see front matter © 2004 Elsevier Ltd. All rights reserved.
doi:10.1016/j.neuropsychologia.2004.10.004

1992; De Renzi et al., 1980; Goldenberg, 1996,1999; Haaland & Flaherty, 1984; Heath, Roy, Westwood, & Black, 2001; Kertesz & Ferro, 1984; Kimura et al., 1974; Lehmkuhl, Poeck, & Willmes, 1983; Roy et al., 1991). A possible reason for this debate is that the specific involvement of cerebral areas critically depends on the detailed characteristics of the gesture under examination.

Indeed, different results have been found for hand gestures consisting of different hand positions in relation to the head, and finger gestures defined only by different configurations of the fingers. While left parietal lesions impaired both, hand and finger gestures, right parietal damage impaired primarily finger gesture tasks (Goldenberg, 1995; Hermsdörfer et al., 1996). Furthermore, it has been suggested that apraxia on imitation is primarily a deficit of perceptional analysis, since errors also occur when subjects are to match photographs of gestures (Goldenberg, 1999). This is also supported by PET imaging in healthy subjects, where matching photographs of hand gestures activated the left parietal cortex, whereas matching photographs of finger gestures activated both parietal cortices (Hermsdörfer et al., 2001).

In recent years, in particular, after the discovery of "mirror neurons" in the monkey brain (Gallese, Fadiga, Fogassi, & Rizzolatti, 1996; Rizzolatti, Fadiga, Gallese, & Fogassi, 1996a), imitation has been investigated intensively in neuroimaging studies. "Mirror neurons" were localized at the rostral part of the inferior frontal cortex (area F5) and become active both when the monkey performs a given action and when it observes a similar action performed by the experimenter. The human homologue of monkey area F5 is probably Brodmann Area (BA) 44 within the pars opercularis of the inferior frontal gyrus (Rizzolatti, Fogassi, & Gallese, 2002). Accordingly, Iacoboni et al. (1999) found this area activated during finger movements, regardless of how they were evoked, and, most importantly, their activation increased further when the same movement was elicited by the observation of an identical movement. These results gave further support to the "direct matching hypothesis" which postulates the direct matching of the observed action onto an internal motor representation of that action. However, lesion studies on apraxic patients have failed so far to demonstrate an involvement of the frontal operculum.

With few exceptions (Tanaka & Inui, 2002; Tanaka, Inui, Iwaki, Konishi, & Nakai, 2001), neuroimaging studies on imitation investigated simple movements such as lifting the index finger (Brass, Zysset, & von Cramon, 2001; Iacoboni et al., 1999; Koski et al., 2002; Krams, Rushworth, Deiber, Frackowiak, & Passingham, 1998). In contrast to studies on apraxic patients that mostly demonstrated left parietal dominance, these neuroimaging studies found activation of both parietal cortices at different locations. It seems possible that very simple movements do not lead to activation of the whole network subserving imitation but also that different areas are recruited for copying simple movements. Therefore, investigations of more complex imitative behavior has been proposed (Koski, Iacoboni, Dubeau, Woods, & Mazziotta, 2003).

Finally, the effect of the acting limb side on imitation is not completely resolved. This can be attributed to two facts. Firstly, apraxics are mostly paralyzed on the limb side contralateral to the damaged hemisphere so that only the ipsilesional hand can be investigated. Secondly, while several neuroimaging studies were concerned with active imitation, subjects had to imitate with their right hand exclusively (Brass et al., 2001; Decety, Chaminade, Grezes, & Meltzoff, 2002; Iacoboni et al., 1999; Koski et al., 2002; Krams et al., 1998; Tanaka et al., 2001, 2002).

Hence, the purpose of this study was to investigate the cerebral activation that results from more complex imitation such that under conditions similar to the clinical testing for apraxic deficits, to analyze the influence of the acting limb side, and to search for differences between the imitation of hand and finger gestures.

2. Materials and methods

2.1. Subjects

Twelve volunteer subjects (mean age 50, range 41–60 years, six females) participated in the study. All subjects were right-handed, drug-free, and had no history of neurological or psychiatric disorders. They had been informed about the purpose of the study before giving their written consent, in accordance with the Declaration of Helsinki 2000. The study had been approved by the Ethics Committee of the Faculty of Medicine at the Technical University of Munich.

2.2. General remarks, stimulus material and task

Four types of gesture imitation were investigated; namely, the imitation of finger and hand gestures with either the right or the left arm. Exclusively specular imitation was used, that is when the actor moves the left hand, the imitator moves the right hand.

Video clips of a person performing meaningless gestures were presented one after the other (see Fig. 1). Each clip showed a meaningless gesture and the return to the neutral position (see Fig. 1, upper panels) within two seconds. Then the freeze image was displayed for another two seconds. Subjects were instructed to observe the gesture and to imitate it thoroughly as soon as the image froze.

The clips were taken from colored video recordings of actual movements with the right arm. Stimulus material involved 16 different finger gestures and 16 different hand gestures. All clips were mirrored to obtain gestures performed with the left arm. During one experiment, none of the gestures was displayed more than three times for each side.

To enable imitation of hand gestures in the MRI scanner, the hand was moved into different positions and orientations relative to the opposite forearm, which rested comfortably above the abdomen (see Fig. 1, left panels). During finger

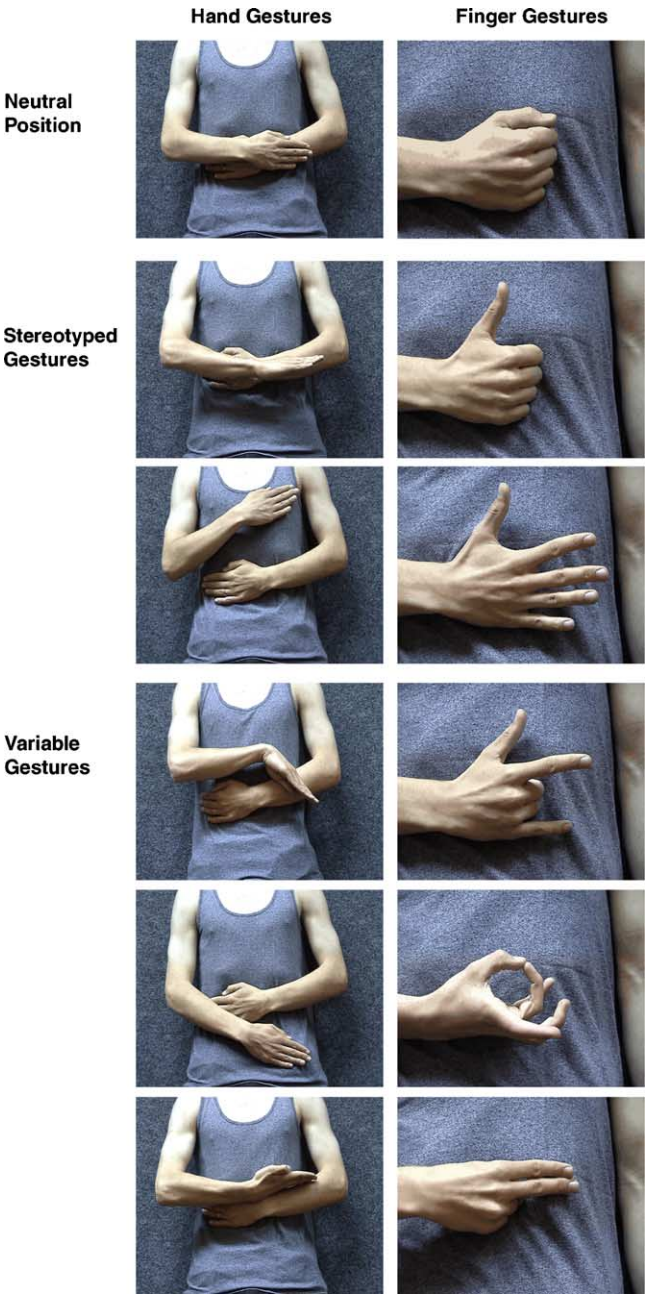

Fig. 1. Hand and finger gestures. Frames were taken from the video clips that were presented during the experiment. For hand (left panels) and finger (right panels) gestures respectively, the neutral position (upper panels), both stereotyped gestures (middle panels), and three examples of variable gestures (lower panels) are shown.

gestures the hand was held in the centre of the abdomen (see Fig. 1, right panels).

In the experimental condition (variable gesture imitation), subjects imitated gestures that were taken from a set of 16 gestures one after the other.

Two control conditions were used. In the first control condition (stereotyped gesture imitation), subjects imitated gestures one after the other like in the experimental condition; but now, the set of the presented gestures consisted of only two gestures (see Fig. 1, middle panels). These gestures were repetitively presented in pseudorandom order, not allowing for the same gesture more than twice in sequence. The second control condition (motor rest), consisted of a clip that showed the trunk with breathing motions and with the arm held in the resting position (see Fig. 1, upper panels). Under this condition, subjects were instructed to attend to motions and not to move.

2.3. Procedure

Each subject underwent four sessions (i.e. imitation of finger and hand gestures with either the right or the left arm). The order of sessions was pseudorandomised over subjects. Each condition (variable and stereotyped gesture imitation as well as motor rest) was presented in form of four blocks (10 different gestures per block, 40 s block duration). A short instruction (10 s) preluded every block. Blocks were ordered pseudorandomly not allowing for the same condition in subsequent blocks (see Fig. 2).

Before the measurement started, each subject was trained with a shorter set of clips outside the scanner. Except for clips that were presented in the control condition of stereotyped gestures, these clips never reappeared during the MRI scans. During gesture imitation inside the scanner, subjects viewed the clips by projection onto a mirror. Performance was observed by an investigator and monitored with a video camera.

2.4. Performance control

As image definition of the monitoring inside the scanner was not good enough to allow an exact error analysis, the same experiment was repeated outside the scanner 6 weeks later and recorded by a digital video camera. Three raters estimated all responses as correct or incorrect. Whenever an imitation was scored as incorrect by at least two raters, it was interpreted as an error. Raters had been instructed to score finger gestures as correct whenever fingers to be extended or to be flexed were correct or whenever the correct finger tips touched each other, respectively. Imitation of hand gestures were only estimated as correct when the end position of the hand moved was correct in relation to the opposite forearm. The scores of the three raters coincided in 96.4% of the ratings (94.4% no error, 2.0% error), in the remaining cases of disagreement either two scorers (2.0%) or one scorer (1.6%) denoted an error. The non-parametric Wilcoxon test was applied to search for differences of error frequencies between imitations of hand and finger gestures as well as between imitations performed with the right and the left arm.

2.5. Magnetic resonance imaging

Imaging was performed using a 1.5-T Siemens scanner (Magnetom Symphony) with a standard birdcage head coil. First, a 3-D structural high-resolution T1-weighted

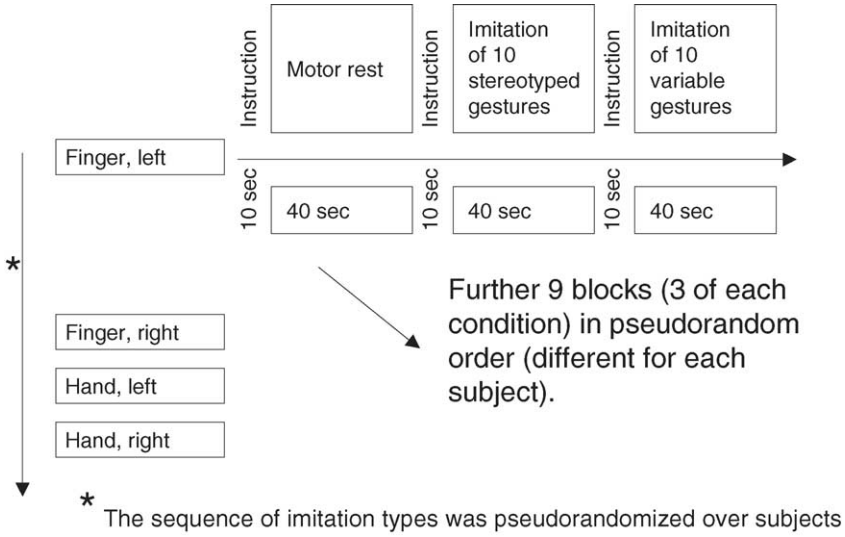

Fig. 2. Schematic representation of all conditions' organization.

MRI using an magnetization prepared rapid gradient echo (MPRAGE) sequence was acquired on each subject (sagittal plane; TR, 11.1 ms; TE, 4.3 ms; field of view, 224 mm × 256 mm; flip angle, 15°; number of slice, 160; slice thickness, 1 mm).

Functional imaging was performed using an ultra fast echo planar gradient echo imaging sequence sensitive to blood oxygenation level-dependent (BOLD) contrast (TR, 3.100 s; TE, 50 ms; FOV, 192; flip angle, 90°) with 34 slices oriented along the anterior and posterior commissure (oblique axial; thickness, 4 mm; gap, 0.4 mm; in-plane resolution, 3 mm × 3 mm).

Prior to each run, four images were acquired and discarded to allow for longitudinal magnetization to reach equilibrium.

2.6. Data analysis

SPM 99 software (Wellcome Department of Cognitive Neurology, London, UK), based on the general linear model (Friston, 1996) was applied for data analysis. Calculations were performed on dual-Pentium 400 PCs running LINUX.

For each subject, images were realigned to the first image of the first session to account for head-motion in time. The mean image of all realigned images was used for the determination of the individual parameters for the normalization into a standard space, the MNI brain-based system. After normalization, images were smoothed with a Gaussian filter of 10 mm × 10 mm × 10 mm to increase signal to noise ratio and to account for intersubject anatomical variability.

For each subject, movement parameters were calculated over time with an IDL routine by subtracting all six realignment parameters of subsequent images. These movement parameters were added to the general linear model to remove any component that was correlated with this function of movement estimates.

Significance was assessed using the delayed box-car reference that was convolved with the haemodynamic response function. In a first level (fixed effects) analysis, we obtained statistical parametric maps (SPM) and corresponding contrast images for each subject from the following categorical comparisons:

- Variable > stereotyped gesture imitation (separately for each type of imitation).
- Stereotyped gesture imitation > motor rest (separately for each type of imitation).
- Variable hand > finger gestures (separately for each side).
- Variable finger > hand gestures (separately for each side).
- Variable gestures, right > left arm (separately for finger and hand gestures).
- Variable gestures, left > right arm (separately for finger and hand gestures).

To allow more generalized inferences, those contrast images were entered into second level (random effects) analyses using one sample *t*-tests.

In order to identify regions that are specific to the imitation of hand gestures (compared to the imitation of finger gestures), categorical analyses (variable hand > finger gestures) of the right and the left side were statistically conjoined (see Table 1). The conjunction of the converse categorical analyses

Table 1
Conjunction analyses at the second level

Name of conjunction	Conjoined first level contrasts
Hand > finger gestures	LH > LF ∩ RH > RF
Finger > hand gestures	LF > LH ∩ RF > RH
Left > right	LF > RF ∩ LH > RH
Right > left	RF > LF ∩ RH > LH
Variable > stereotyped	LF: V > S ∩ RF: V > S ∩ LH: V > S ∩ RH: V > S

Note: F, finger; H, hand; L, left; R, right; S, stereotyped; V, variable.

was applied to reveal areas that are specific to the imitation of finger gestures (compared to the imitation of hand gestures). Likewise, for the identification of regions that are specific to the imitation performed with the right arm (compared to the imitation performed with the left arm), categorical analyses (right > left) of variable finger and hand gestures were statistically conjoined (see Table 1). The conjunction of the converse categorical analyses was applied to detect areas that are specific to the imitation performed with the left arm (compared to the imitation performed with the right arm). Finally, subtraction analyses of all types of gesture imitation (variable > stereotyped) were statistically conjoined in order to reveal areas that are related to all types of gesture imitation (see Table 1). All conjunctions were performed at the second level by entering different types of imitation (variable > stereotyped) as covariates in a multiple regression model (without a constant) (Friston, Holmes, Price, Buchel, & Worsley, 1999).

To detect left-right differences in hemispheric activation, we modeled all types of gesture imitation as a single main effect at the first level. Then, contrast images were left-right flipped. To compare the original and flipped contrast images the paired *t*-test was applied. This procedure resulted in maps that, on the left side, indicate areas which are more active on the left side compared to the corresponding areas of the right side. Vice versa on the right side, areas appear that are more active on the right side compared to the corresponding areas of the left side. A region of interest (ROI) was defined by the conjunction of all four types of gesture imitation.

A statistical threshold of $P < 0.05$ (family wise error correction, FWE) was considered to show significant activation. Only clusters of activation with an extent exceeding 10 contiguous voxels were considered relevant.

If there were no clusters surviving this level, the threshold was changed to $q < 0.05$, corrected with the false discovery rate (FDR) (Genovese, Lazar, & Nichols, 2002).

Calculated coordinates of activation peaks were converted from the MNI brain-based system into the Talairach brain system (Talairach & Tournoux, 1988) using a non-linear transformation method (http://www.mrc-cbu.cam.ac.uk/Imaging/mnispace.html).

3. Results

3.1. Task performance

Observation of task performance during the MRI-experiment showed that subjects performed the task according to the given instructions. Subsequent error analysis revealed not a single error during the imitation of stereotyped gestures. During the imitation of variable gestures, finger gestures were significantly more difficult than hand gestures (left side, $P = 0.014$; right side, $P = 0.005$; see Fig. 3) whereas the comparison of the acting limb sides did not yield significantly different error rates ($P > 0.1$; see Fig. 3).

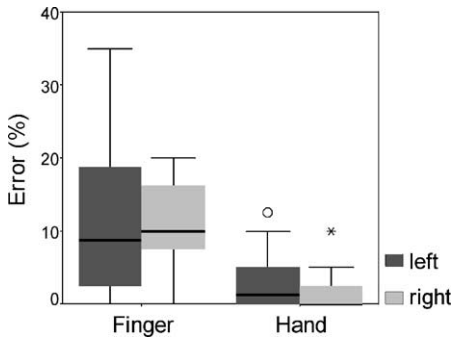

Fig. 3. Performance during imitation of variable gestures. Box plots of the subjects' performance during imitation of variable gestures (bold horizontal line, median; rectangles, quartile range; horizontal lines, 1.5× quartile range; °, *, extreme values). The frequencies of errors are displayed. Individual values represent means from four blocks performed under each condition. Note that the frequencies of errors are similar for the right and left arm while the imitation of finger gestures resulted in significantly more errors than the imitation of hand gestures.

3.2. MRI results

3.2.1. Stereotyped gesture imitation

Compared to motor rest, stereotyped imitation of hand and finger gestures performed with either the right or left arm induced activation (second level, $P < 0.05$, FWE) in the contralateral primary motor and sensory cortex as well as in the ipsilateral cerebellum.

3.2.2. Variable gesture imitation

Within each type of gesture imitation (finger and hand gestures with either the right or the left arm), variable gesture imitation induced nearly no significant activation when compared to stereotyped gesture imitation at a significance threshold of $P < 0.05$ corrected (FWE). After changing the threshold to $q < 0.05$ corrected (FDR), all types of imitation showed bilateral activation of the inferior parietal cortex (BA 40), the superior parietal lobe (precuneus, BA 7), the inferior frontal cortex (opercular region including BA 44 on the right and BA 9/44 on the left hemisphere), the prefrontal motor cortex (BA 6), the lateral occipito-temporal junction (BA 37/19 including MT/V5), and the cerebellum (lobule VI of the vermis and both hemispheres without activation within the nuclei) (Dimitrova et al., 2002; Schmahmann et al., 1999). This activation pattern was also revealed by the conjunction analysis ($P < 0.05$ corrected, FWE) of all types of gesture imitation (variable > stereotyped, see Fig. 4, Table 2) and by the common analysis of all four types of gesture imitation (variable > stereotyped, $P < 0.05$ corrected at the cluster level with an underlying threshold of $P < 0.001$ uncorrected).

The direct comparison of the right and left hemispheric activation revealed a lateralization only of the left inferior parietal cortex (see Fig. 5).

Second level analyses of categorical comparisons between imitation of variable finger and hand gestures for

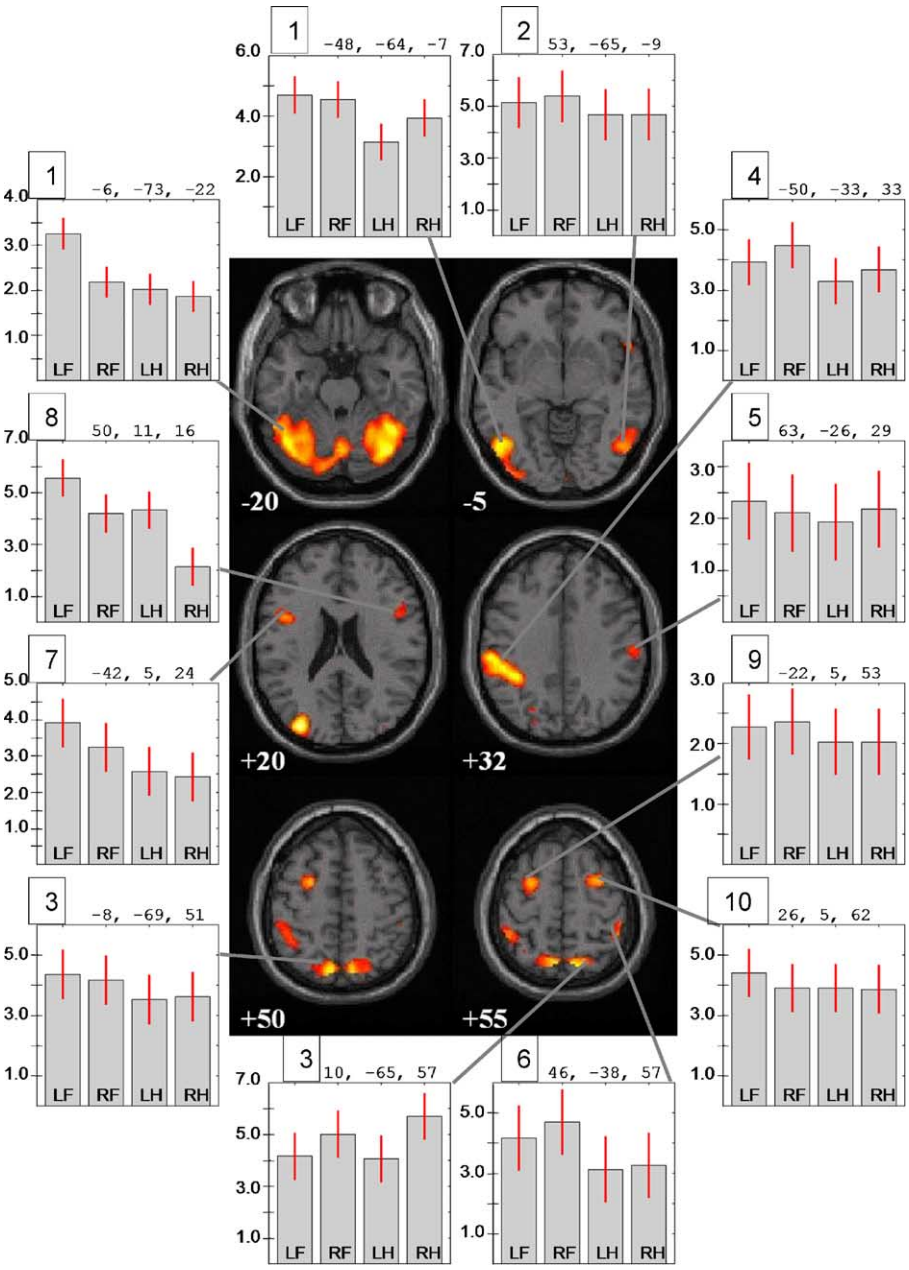

Fig. 4. Conjunction of all types of gesture imitation ($P < 0.05$, corrected with FWE). Clusters of activation are overlaid onto consecutive axial slices of a T1 weighted anatomical magnetic resonance image (right side of image is the right hemisphere). Positions of the slices are indicated in mm relative to the anterior commissure. Histograms show parameter estimates for each type of imitation (bars, standard deviation; F, finger; H, hand; L, left; R, right) at the Talairach coordinates indicated above. The numbers on the upper left corners of the histograms correspond to the first column in Table 2.

both the right and the left side revealed no significantly different activation, even when changing the statistical threshold to $q < 0.05$ (FDR) or $P < 0.001$ (uncorrected). Significant activation was neither shown on conjunction analyses of these comparisons. Likewise, analyses to detect areas that are specific to the imitating limb side yielded no activation difference apart from the contralateral primary motor or sensory cortex and the ipsilateral cerebellum.

4. Discussion

4.1. The paradigm

In this study, we have investigated active imitation of variable meaningless gestures, thereby adopting tests used for clinical evaluation of apraxic deficits (see Fig. 1) to neuroimaging. To control visual input, elementary motor output, and basic aspects of imitation, we compared our experimen-

Table 2
Areas of significant activation for the conjunction analysis of all types of gesture imitation

Number of cluster	Area	Voxels per cluster	Corrected *P*-value (voxel-level)	*Z* score (voxel-level)	Tailarach coordinates of peak (mm)		
					x	*y*	*z*
1	L cerebellum, hemisphere, lobule VI	4006	<0.001	>7	−30	−52	−21
	Cerebellum, vermis, lobule VI		<0.001	>7	2	−65	−15
	R cerebellum, hemisphere, lobule VI		<0.001	>7	24	−53	−18
	L occ. lobe, sup. occ. g., BA 19		<0.001	>7	−32	−80	24
	L occ. lobe, middle occ. g., BA 37		<0.001	>7	−48	−64	−7
2	R temp. lobe, fusiform g., BA37	2373	<0.001	>7	40	−50	−19
	R occ. lobe, fusiform g., BA 19		<0.001	>7	38	−69	−15
	R occ. lobe, middle occ. g., BA 37		<0.001	>7	53	−65	−9
3	R par. lobe, sup. par. lobule, BA7	912	<0.001	>7	10	−65	57
	L par. lobe, precuneus, BA7		<0.001	>7	−8	−69	51
	L par. lobe, precuneus, BA7		<0.001	>7	−4	−63	57
4	L par. lobe, inf. par. lobule, BA 40	1477	<0.001	>7	−55	−25	34
	L par. lobe, inf. par. lobule, BA 40		<0.001	>7	−50	−33	33
	L par. lobe, supramarginal g., BA 40		<0.001	>7	−36	−41	37
5	R par. lobe postcentral g., BA 3	251	<0.001	6.69	57	−21	40
	R par. lobe, inf. par. lobule, BA 40		<0.001	5.94	63	−26	29
6	R par. lobe, inf. par. lobule, BA 40	80	<0.001	6.42	46	−38	57
7	L frontal lobe, inf. frontal g., BA 9/44	244	<0.001	>7	−42	5	24
8	R frontal lobe, inf. frontal g., BA 44	179	<0.001	6.55	50	11	16
9	L frontal lobe, sup. frontal g., BA 6	315	<0.001	>7	−22	5	53
	L frontal lobe, sup. frontal g., BA 6		<0.001	6.56	−16	−6	68
10	R frontal lobe, sup. frontal g., BA 6	242	<0.001	>7	26	5	62
11	R temp. lobe, sup. temp. g., BA 38	52	<0.001	6.53	53	17	−8
12	R occ. lobe, cuneus, BA 18	78	<0.001	6.47	8	−96	18

Note: To attain statistical significance ($P < 0.05$, corrected with family wise error), clusters must include at least 10 voxels and peaks must be separated by 8 mm. BA, Brodmann area; corr., corrected; g., gyrus; inf., inferior; L, left; occ., occipital; par., parietal; R, right; sup., superior; temp., temporal. The numbers of clusters correspond to the numbers on the upper left corner of the histograms in Fig. 4.

tal condition of variable gesture imitation with the imitation of only two gestures repetitively presented in pseudorandom order (stereotyped gesture imitation).

We chose specular imitation (i.e. when the actor moves the left hand, the imitator moves the right hand, as if looking in a mirror) because developmental studies indicate that specular imitation is the more natural behavior, compared to anatomic imitation (i.e. both actor and imitator moving the right arm) (Schofield, 1976).

In theoretical terms, imitation is regarded as a replica of the observed action. According to most ethologists, "true imitation" concerns only motor acts never before performed by

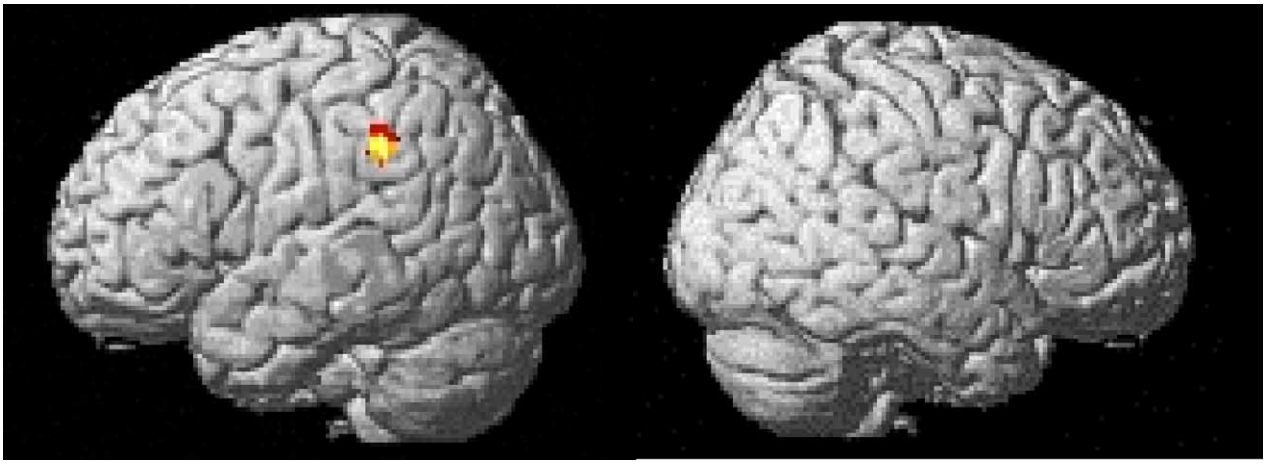

Fig. 5. Differences in hemispheric activation in gesture imitation. The difference in activation is rendered onto the cortex surface. Talairach coordinates of peak activity: $x = 50$, $y = -37$, $z = 37$; $Z = 3.68$ (voxel level); $P = 0.004$ (corrected at the cluster level with an underlying voxel level of 0.001 uncorrected); cluster size: 100 voxels; area, left inferior parietal lobule/Brodmann area 40.

the observer (Rizzolatti, Fogassi, & Gallese, 2001). Support for the validity of this notion is also provided by patients that fail at imitation of meaningless gestures while being able to understand and reproduce meaningful gestures (Goldenberg & Hagmann, 1997).

In contrast to the above summarized ethological view, some behavioral psychologists emphasize that imitation involves a decomposition of the motor patterns into their constituent components and later a reconstruction of the action pattern from these components (Bekkering, Wohlschlager, & Gattis, 2000). According to both theoretical concepts, the actions performed in our experimental condition (variable gesture imitation) can be considered "more imitative" than in our control condition (stereotyped gesture imitation). Thus, we expected our paradigm to provide valuable and novel insights about the neural mechanisms underlying more complex imitative behavior. In particular, we thereby intended to clarify different findings from studies on apraxic patients and from neuroimaging studies concerning the importance of the parietal and frontal cortex, the effect of the acting limb side, and differences between finger and hand gestures.

However, apart from imitation, our experimental condition differed from our control condition in further aspects such as complexity of the executed movements, motor attention, and demands on visual analysis. Thus, our results must be interpreted with caution in regard to the question whether activation can be attributed to the process of imitation or not.

4.2. The activation pattern of gesture imitation

Conjunction analysis as well as the common analysis of all four imitation types revealed a bilaterally distributed fronto-parietal activation pattern, with only the inferior parietal cortex being significantly lateralized, namely to the left hemisphere. Neither of the direct statistical comparisons between the four imitation conditions revealed any significant difference, apart from the respective primary sensori-motor cortex on comparisons between imitations performed with the left versus right arm. Although, performance analysis showed more errors during the imitation of finger gestures than during hand gestures (see Fig. 3), we found no indication for different underlying neuronal processes. The fact that our paradigm did not reveal differences between finger and hand gestures might be due to a lack of statistical power or to the necessary adoption of clinical tests in order to enable their performance within the MRI-scanner and will not be discussed further.

We will now discuss each component of the activation pattern revealed by the conjunction analysis of all types of imitation (see Fig. 4, Table 2).

4.2.1. The parietal cortex

In the inferior parietal cortex, activity was significantly lateralized to the left hemisphere, with peaks in the inferior parietal lobule (BA 40) and in the supramarginal gyrus (BA 40). Two areas within the right anterior inferior parietal lobule (BA 40) were also activated, but to a smaller extent. Furthermore, we found activation in the superior parietal lobe (precuneus, BA 7) bilaterally.

The bilateral activation of the dorsal superior parietal cortex (BA 7) can be attributed to higher demands regarding visual motion analysis in our experimental condition. This region is part of the dorsal, or "where" stream (Ungerleider, 1985). Primate studies have shown that the dorsal stream can be further subdivided into two streams that both terminate in the parietal lobe (Felleman & Van Essen, 1991; Zeki & Shipp, 1988). The first originates from primary visual cortex and projects to V5/V5a (MT/MST). From there, it is relayed to the ventral intraparietal area and the superior parietal lobule. This pathway is involved in processing visual motion. The second projects from V3/V3a to the lateral intraparietal area and specifically to the caudal intraparietal sulcus. Signals conveyed in this stream are related to the perception of spatial properties and three-dimensional structures. Our paradigm requires the analysis of hands regarding to both motion and spatial properties. Thus, our findings corroborate the importance of the dorsal stream for mediating imitation. Comparable activations of the superior parietal cortex was a common finding in imaging studies on imitation (Chaminade, Meltzoff, & Decety, 2002; Koski et al., 2003; Peigneux et al., 2000; Tanaka et al., 2002).

Furthermore, we found activation of the inferior parietal cortex significantly lateralized to the left hemisphere. Comparison of hemispheric activations requires caution as there is neither functional nor complete anatomical brain symmetry. However, in our study, the left inferior parietal activation consists of a cluster of more than 1000 voxels with three maxima. Therefore, it seems very unlikely that the significant differences between both parietal cortices result from imperfect co-registration of the two hemispheres to one another. The lateralization to the left complies with most studies on apraxic patients (Barbieri & De Renzi, 1988; Haaland, Harrington, & Knight, 2000; Kimura et al., 1974; Kolb & Milner, 1981; Lehmkuhl et al., 1983). Haaland et al. (2000) studied left brain damaged stroke patients with the classical syndrome of "ideomotor limb apraxia", analyzed MRI or CT for lesion location and compared areas of overlap. Thereby, the intraparietal sulcus region and the middle frontal gyrus were identified. On the other hand, reports on apraxic disorders resulting from lesions of the right parietal cortex are rare (De Renzi et al., 1980; Goldenberg, 1996, 1999; Haaland et al., 1984; Heath et al., 2001; Kimura et al., 1974; Lehmkuhl et al., 1983; Roy et al., 1991). Based on these findings in apraxic patients, it has been proposed that the inferior portion of the parietal cortex (including the intraparietal sulcus), especially on the left, is the brain area in which gestures are represented irrespective of their content.

In several human neuroimaging studies, parietal cortex activation was found during imitation tasks (Chaminade et al., 2002; Choi et al., 2001; Decety et al., 2002; Iacoboni et al., 1999; Koski et al., 2003; Moll et al., 2000; Tanaka et al., 2001, 2002). The lateralization of the parietal activation differed throughout these studies (see Fig. 6). Notably, the two

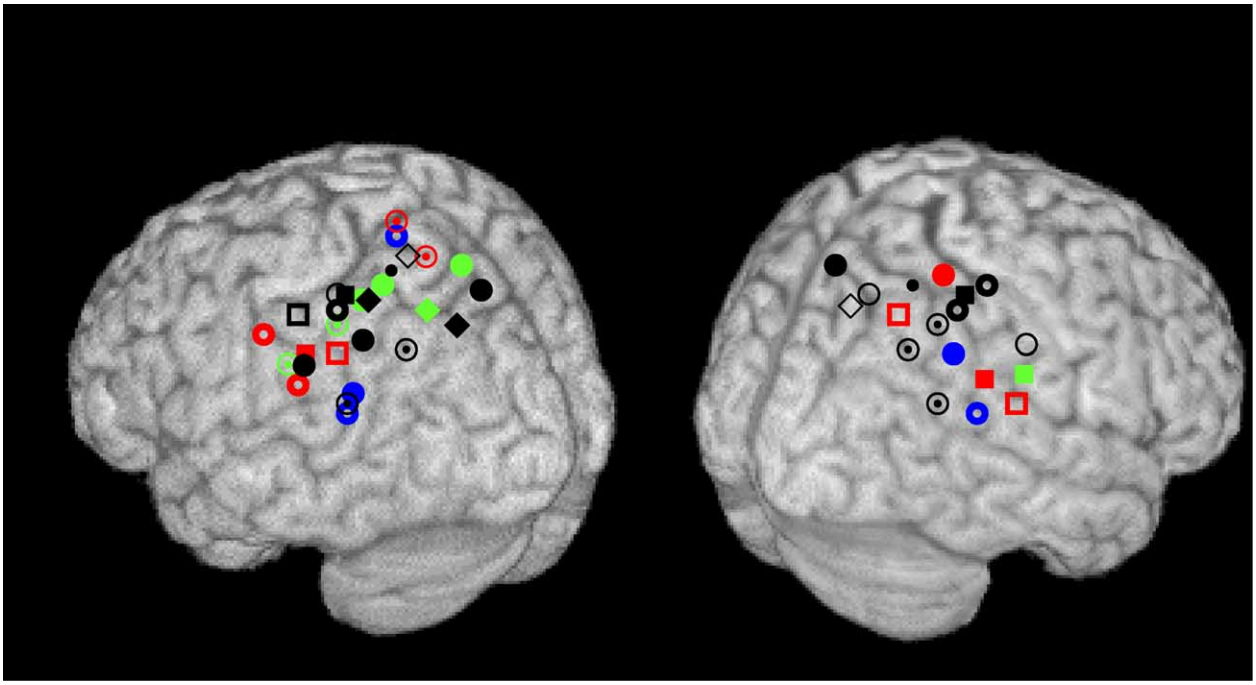

Fig. 6. Summary of parietal activation found in imaging studies on active imitation and pantomiming. Peak activations that were found in the studies named underneath are indicated. Angular symbols refer to experiments with control conditions consisting of motor rest, round symbols refer to experiments with control conditions consisting of movements. Color coding: black, complex imitation; red, imitation of simple finger movements; green, pantomiming; blue, imitation of and with active object manipulation. ◆ (Moll et al., 2000), ● (Choi et al., 2001), ■ ⊙ (Rumiati et al., 2004), ● (Decety et al., 2002), ○ (Chaminade et al., 2002), ● ○ (Grèzes, Armony, Rowe, & Passingham, 2003), ■ ○ □ (Krams et al., 1998), ● (Iacoboni et al., 1999), ⊙ (Koski et al., 2003), ■ □ ○ (Tanaka et al., 2001), ◆ ◇ (Tanaka et al., 2002), ⊙ ○ (Peigneux et al., 2000), ● present study.

studies (Tanaka et al., 2001, 2002) with paradigms probing gestures more similar to those used in the clinical testing of apraxic patients found a lateralization to the left inferior parietal cortex in most conditions (see black angular symbols in Fig. 6). The gestures were presented on photographs and had to be performed with the right arm exclusively. The experimental conditions were compared to motor rest. Therefore, it remained to be resolved whether the activation in the left parietal cortex originates from complex imitation or whether copying simple movements alone would also result in such an activation pattern. Moreover, the lateralization to the left hemisphere could result from the acting limb side. Now, our study indicates that the activation of the left inferior parietal cortex cannot be attributed to the acting limb side but to the higher variability and complexity of the gestures presented.

It has to be recognized that the exact location within the parietal cortex differed remarkably throughout the available imaging studies on active imitation (see Fig. 6). It is impossible to explain this variability stringently. This might be due to the fact that methods, thresholds, as well as experimental and control conditions differed throughout these studies.

Another two studies investigated cerebral activation during pantomiming tool-use. Here, tools were presented verbally (Moll et al., 2000) or visually (Choi et al., 2001). Thus, both paradigms resembled clinical tests for apraxic deficits. Interestingly, in both studies a lateralization to the left was found (see green symbols ● and ◆ in Fig. 6). The involvement of the left inferior parietal cortex in both pantomiming tool-use and imitation is comprehensible as both tasks share common components. Both tasks include the need to access a visual description of the movement, then to assemble this complex movement, and finally to execute it. Correspondingly, both tasks are typically disturbed in apraxia.

Moreover, the left parietal cortex is activated by observation of movements (Bonda, Petrides, Ostry, & Evans, 1996; Grafton, Mazziotta, Woods, & Phelps, 1992), motor imagery (Grafton, Arbib, Fadiga, & Rizzolatti, 1996; Ruby & Decety, 2001), movement preparation (Deiber, Ibanez, Sadato, & Hallett, 1996; Krams et al., 1998; Stephan et al., 1995), and analysis of photographs showing the end positions of meaningless gestures (Hermsdörfer et al., 2001). These functions are primarily devoted to perceptual analysis of body movements and postures and thus closely related to imitation.

Furthermore, this region has also been related to motor attention and selection (for review see Rushworth, Johansen-Berg, Gobel, & Devlin, 2003). Accordingly, it has also been proposed that the difficulties, apraxic patients frequently experience when sequencing movements (see also Haaland, Elsinger, Mayer, Durgerian, & Rao, 2004; Harrington & Haaland, 1992), may partly be due to an inability to redirect movement attention (Rushworth, Nixon, Renowden, Wade, & Passingham, 1997). Moreover, imaging studies on motor attention and selection found the left parietal cortex ac-

tivated. While motor attention and movement selection are inherent aspects of complex imitation, the critical question appears whether these factors alone might explain the activation found in our study. However, imaging studies on motor attention and movement selection found the left parietal cortex activated when subjects covertly prepared movements (e.g. Rushworth, Krams, & Passingham, 2001) or switched intended movements (e.g. Rushworth, Paus, & Sipila, 2001; Schluter, Krams, Rushworth, & Passingham, 2001). These paradigms cannot easily be compared with our task that required the spontaneous imitation of observed movements with a very predictable procedure. Considering further the ample evidence for leftward lateralized parietal activation in gesture imitation from clinical studies and from neuroimaging studies, we rate the possibility that motor attention and movement selection alone caused the left inferior parietal activation in our study unlikely. However, we do not want to rule out that motor attention and movement selection contributed to the activation. In summary, we attribute the left inferior parietal dominance demonstrated in our study primarily to the process of imitation.

4.2.2. The frontal cortex

In the frontal cortex, we found bilateral activation, namely occurring in the dorsal premotor cortex (BA 6) and the opercular region including BA 44 on the right and BA 9/44 on the left hemisphere.

Imaging experiments have identified activation of the dorsal premotor cortex during free selection of movements (compared with repetitive movements), during sensory-guided movement, new learning (compared with prelearned sequences), when subjects await a trigger signal to move or when subjects attend to their performance (Colebatch, Deiber, Passingham, Friston, & Frackowiak, 1991; Deiber et al., 1991; Jenkins, Brooks, Nixon, Frackowiak, & Passingham, 1994; Jueptner et al., 1997; Toni, Schluter, Josephs, Friston, & Passingham, 1999). Specular imitation is a sensory-guided task. Compared with our control condition, the experimental condition consisted of novel postures requiring continuously higher attentional demands. Nonetheless, the absence of activation differences in primary sensorimotor cortex between the imitation condition and the control state (stereotyped gesture imitation) indicate that our experimental design was balanced with respect to motor output. We conclude, therefore, that differences in motor control required for task performance were responsible for the higher activation in the dorsal premotor cortex. Interestingly, we did not disclose any differences in dorsal premotor cortex activation when comparing the more difficult finger with the hand imitation task.

Further more, we detected activation of the opercular region including BA 44 on the right and BA 9/44 on the left hemisphere. If activation of the frontal opercular region during imitation were functionally relevant; one would expect lesions within this region to result in deficits, similar to those found in apraxia. To the best of our knowledge, we are not aware of such cases, even in patients with apraxia following frontal lesions (Haaland et al., 2000). However, a recent study on imitation conducted with repetitive transcranial magnetic stimulation showed a temporarily degraded imitation capacity after the stimulation of either the right or the left Broca's area (Heiser, Iacoboni, Maeda, Marcus, & Mazziotta, 2003).

In contrast to lesion studies on apraxia, several imaging studies focusing on active imitation have shown recruitment of the frontal opercular region (Grèzes, Armony, Rowe, & Passingham, 2003; Iacoboni et al., 1999; Koski et al., 2002; Krams et al., 1998; Tanaka et al., 2002). Further imaging studies indicate, that the opercular region of the inferior frontal gyrus, beyond speech control, is recruited during the execution of hand movements (Ehrsson, Fagergren, & Forssberg, 2001; Schlaug, Knorr, & Seitz, 1994), during mental imagery of hand movements (Binkofski et al., 2000; Decety et al., 1994; Grafton et al., 1996), during observation of body movements (Buccino et al., 2001), and during object manipulation (Binkofski et al., 1999a,b). Notably, object manipulation alone yielded activation in the opercular part of BA 44 whereas object manipulation and naming of the object revealed additional activation in the pars triangularis of the inferior frontal gyrus (BA 45) (Binkofski et al., 1999a). Likewise activation of only BA 44 during imagery of right finger movements could be demonstrated by the co-registration of fMRI data with cytoarchitectonic maps of BA 44 and 45 in a common reference space (Binkofski et al., 2000). Therefore, it has been suggested that BA 44 mediates higher-order forelimb movement control resembling the neuronal mechanisms subserving speech as also necessary in our experimental condition. In conclusion, our finding of an activated frontal operculum is in line with imaging findings. The fact that apraxic deficits do not occur after lesions of the frontal operculum might be due to a bilateral distribution and the ability to functionally compensate unilateral damage on the long term.

4.2.3. The occipito-temporal junction

Bilaterally, we found the occipito-temporal junction including MT/V5 (BA 19/37) activated. This area is responsible for visual motion processing (Watson et al., 1993; Zeki et al., 1991) and was frequently found to be activated when subjects observed hand movements, irrespectively of the exact experimental conditions. In previous studies, activation was either bilateral (Decety & Grezes, 1999; Grezes & Costes, 1998) or shifted to the left hemisphere (Decety et al., 1994; Hermsdörfer et al., 2001; Rizzolatti et al., 1996b). This region is not only activated during the observation of real movements. Its functional implications are more complex. For example, viewing pictures that suggest movements compared to viewing mere static pictures also results in a recruitment of V5/MT (Kourtzi & Kanwisher, 2000). Recently, Peigneux et al. (2000) demonstrated a particular role of V5/MT for the analysis of static upper limb postures compared to the analysis of intransitive three-dimensional objects.

In our study, the observation of movements with varying content compared to repetitively presented movements also resulted in activation of the occipito-temporal junction including V5/MT (BA 19/37). This finding suggests that the involvement of the temporo-occipital junction also correlates with the degree of complexity of the observed biological motion.

4.2.4. The cerebellum

The cerebellar activation in our study included lobule VI of the vermis and both hemispheres but not the nuclei. This finding is in line with the traditional view that the cerebellum controls complex (as opposed to simple) movements preferentially. Correspondingly, involvement of both neocerebellar hemispheres and the vermis was reported during learning of new motor sequences as compared to the automatic performance of a well trained task (Jueptner & Weiller, 1998). Therefore, the cerebellar activation found in this study may be sufficiently explained by differences in the motor tasks between the experimental and the control condition. In recent years, however, evidence has been accumulating that the cerebellum also plays a role in non-motor tasks, such as mental imagery (Lotze et al., 1999; Parsons et al., 1995), sensory processing (Gao et al., 1996; Parsons et al., 2000), planning (Dagher, Owen, Boecker, & Brooks, 1999; Kim, Ugurbil, & Strick, 1994), attention (Allen, Buxton, Wong, & Courchesne, 1997), and language (Leiner, Leiner, & Dow, 1993). Therefore, it cannot be excluded that some of the cerebellar activation is related to the imitation process.

4.3. Conclusions

The current imaging study suggests that gesture imitation in right-handers results in a bilateral fronto-parietal activation pattern, while the inferior parietal cortex is lateralized to the left hemisphere. This activation pattern occurs regardless of the acting limb side. Thus, the paradigm employed here supports the functional relevance of the left inferior parietal cortex in complex aspects of imitation as also revealed by clinical studies in apraxic patients.

Acknowledgments

The work was supported by grant 8764153 of the Kommission für Klinische Forschung (KKF). We are grateful to Helga Gräfin von Einsiedel and her colleagues of the Institut für Röntgendiagnostik, Technische Universität München for making this study possible.

References

Alexander, M. P., Baker, E., Naeser, M. A., Kaplan, E., & Palumbo, C. (1992). Neuropsychological and neuroanatomical dimensions of ideomotor apraxia. *Brain*, *115*(1), 87–107.

Allen, G., Buxton, R. B., Wong, E. C., & Courchesne, E. (1997). Attentional activation of the cerebellum independent of motor involvement. *Science*, *275*(5308), 1940–1943.

Barbieri, C., & De Renzi, E. (1988). The executive and ideational components of apraxia. *Cortex*, *24*(4), 535–543.

Bekkering, H., Wohlschlager, A., & Gattis, M. (2000). Imitation of gestures in children is goal-directed. *Q. J. Exp. Psychol. A*, *53*(1), 153–164.

Binkofski, F., Amunts, K., Stephan, K. M., Posse, S., Schormann, T., Freund, H. J., et al. (2000). Broca's region subserves imagery of motion: A combined cytoarchitectonic and fMRI study. *Hum. Brain Mapp.*, *11*(4), 273–285.

Binkofski, F., Buccino, G., Posse, S., Seitz, R. J., Rizzolatti, G., & Freund, H. (1999). A fronto-parietal circuit for object manipulation in man: Evidence from an fMRI-study. *Eur. J. Neurosci.*, *11*(9), 3276–3286.

Binkofski, F., Buccino, G., Stephan, K. M., Rizzolatti, G., Seitz, R. J., & Freund, H. J. (1999). A parieto-premotor network for object manipulation: Evidence from neuroimaging. *Exp. Brain. Res.*, *128*(1–2), 210–213.

Bonda, E., Petrides, M., Ostry, D., & Evans, A. (1996). Specific involvement of human parietal systems and the amygdala in the perception of biological motion. *J. Neurosci.*, *16*(11), 3737–3744.

Brass, M., Zysset, S., & von Cramon, D. Y. (2001). The inhibition of imitative response tendencies. *Neuroimage*, *14*(6), 1416–1423.

Buccino, G., Binkofski, F., Fink, G. R., Fadiga, L., Fogassi, L., Gallese, V., et al. (2001). Action observation activates premotor and parietal areas in a somatotopic manner: An fMRI study. *Eur. J. Neurosci.*, *13*(2), 400–404.

Byrne, R. W., & Russon, A. E. (1998). Learning by imitation: A hierarchical approach. *Behav. Brain Sci.*, *21*(5), 667–684, Discussion 684–721.

Chaminade, T., Meltzoff, A. N., & Decety, J. (2002). Does the end justify the means? A PET exploration of the mechanisms involved in human imitation. *Neuroimage*, *15*(2), 318–328.

Choi, S. H., Na, D. L., Kang, E., Lee, K. M., Lee, S. W., & Na, D. G. (2001). Functional magnetic resonance imaging during pantomiming tool-use gestures. *Exp. Brain Res.*, *139*(3), 311–317.

Colebatch, J. G., Deiber, M. P., Passingham, R. E., Friston, K. J., & Frackowiak, R. S. (1991). Regional cerebral blood flow during voluntary arm and hand movements in human subjects. *J. Neurophysiol.*, *65*(6), 1392–1401.

Dagher, A., Owen, A. M., Boecker, H., & Brooks, D. J. (1999). Mapping the network for planning: A correlational PET activation study with the Tower of London task. *Brain*, *122*(10), 1973–1987.

De Renzi, E. (1990). Apraxia. In F. Boller & J. Grafman (Eds.), *Handbook of clinical neuropsychology* (pp. 245–263). Amsterdam: Elsevier.

De Renzi, E., Motti, F., & Nichelli, P. (1980). Imitating gestures A quantitative approach to ideomotor apraxia. *Arch. Neurol.*, *37*(1), 6–10.

Decety, J., Chaminade, T., Grezes, J., & Meltzoff, A. N. (2002). A PET exploration of the neural mechanisms involved in reciprocal imitation. *Neuroimage*, *15*(1), 265–272.

Decety, J., & Grezes, J. (1999). Neural mechanisms subserving the perception of human actions. *Trends Cogn. Sci.*, *3*(5), 172–178.

Decety, J., Perani, D., Jeannerod, M., Bettinardi, V., Tadary, B., Woods, R., et al. (1994). Mapping motor representations with positron emission tomography. *Nature*, *371*(6498), 600–602.

Deiber, M. P., Ibanez, V., Sadato, N., & Hallett, M. (1996). Cerebral structures participating in motor preparation in humans: A positron emission tomography study. *J. Neurophysiol.*, *75*(1), 233–247.

Deiber, M. P., Passingham, R. E., Colebatch, J. G., Friston, K. J., Nixon, P. D., & Frackowiak, R. S. (1991). Cortical areas and the selection of movement: A study with positron emission tomography. *Exp. Brain Res.*, *84*(2), 393–402.

Dimitrova, A., Weber, J., Redies, C., Kindsvater, K., Maschke, M., Kolb, F. P., et al. (2002). MRI atlas of the human cerebellar nuclei. *Neuroimage*, *17*(1), 240–255.

Ehrsson, H. H., Fagergren, E., & Forssberg, H. (2001). Differential fronto-parietal activation depending on force used in a precision grip task: An fMRI study. *J. Neurophysiol.*, *85*(6), 2613–2623.

Ehrsson, H. H., Fagergren, A., Jonsson, T., Westling, G., Johansson, R. S., & Forssberg, H. (2000). Cortical activity in precision versus power-grip tasks: An fMRI study. *J. Neurophysiol.*, *83*(1), 528–536.

Felleman, D. J., & Van Essen, D. C. (1991). Distributed hierarchical processing in the primate cerebral cortex. *Cereb. Cortex*, *1*(1), 1–47.

Friston, K. J. (1996). Statistical parametric mapping and other analyses of functional imaging data. In A. W. Toga & J. C. Mazziotta (Eds.), *Brain mapping: The methods* (pp. 363–386). New York: Academic Press.

Friston, K. J., Holmes, A. P., Price, C. J., Buchel, C., & Worsley, K. J. (1999). Multisubject fMRI studies and conjunction analyses. *Neuroimage*, *10*(4), 385–396.

Gallese, V., Fadiga, L., Fogassi, L., & Rizzolatti, G. (1996). Action recognition in the premotor cortex. *Brain*, *119*(2), 593–609.

Gao, J. H., Parsons, L. M., Bower, J. M., Xiong, J., Li, J., & Fox, P. T. (1996). Cerebellum implicated in sensory acquisition and discrimination rather than motor control. *Science*, *272*(5261), 545–547.

Genovese, C. R., Lazar, N. A., & Nichols, T. (2002). Thresholding of statistical maps in functional neuroimaging using the false discovery rate. *Neuroimage*, *15*(4), 870–878.

Goldenberg, G. (1995). Imitating gestures and manipulating a manikin: The representation of the human body in ideomotor apraxia. *Neuropsychologia*, *33*(1), 63–72.

Goldenberg, G. (1996). Defective imitation of gestures in patients with damage in the left or right hemispheres. *J. Neurol. Neurosurg. Psychiatr.*, *61*(2), 176–180.

Goldenberg, G. (1999). Matching and imitation of hand and finger postures in patients with damage in the left or right hemispheres. *Neuropsychologia*, *37*(5), 559–566.

Goldenberg, G., & Hagmann, S. (1997). The meaning of meaningless gestures: A study of visuo-imitative apraxia. *Neuropsychologia*, *35*(3), 333–341.

Grafton, S. T., Arbib, M. A., Fadiga, L., & Rizzolatti, G. (1996). Localization of grasp representations in humans by positron emission tomography. 2. Observation compared with imagination. *Exp. Brain Res.*, *112*(1), 103–111.

Grafton, S. T., Mazziotta, J. C., Woods, R. P., & Phelps, M. E. (1992). Human functional anatomy of visually guided finger movements. *Brain*, *115*(2), 565–587.

Grèzes, J., Armony, J. L., Rowe, J., & Passingham, R. E. (2003). Activations related to "mirror" and "canonical" neurones in the human brain: An fMRI study. *Neuroimage*, *18*(4), 928–937.

Grezes, J., & Costes, N. (1998). Top-down effect of strategy on the perception of human biological motion: A pet investigation. *Cogn. Neuropsychol.*, *15*, 553–582.

Haaland, K. Y., Elsinger, C. L., Mayer, A. R., Durgerian, S., & Rao, S. M. (2004). Motor sequence complexity and performing hand produce differential patterns of hemispheric lateralization. *J. Cogn. Neurosci.*, *16*(4), 621–636.

Haaland, K. Y., & Flaherty, D. (1984). The different types of limb apraxia errors made by patients with left vs. right hemisphere damage. *Brain Cogn.*, *3*(4), 370–384.

Haaland, K. Y., Harrington, D. L., & Knight, R. T. (2000). Neural representations of skilled movement. *Brain*, *123*(11), 2306–2313.

Harrington, D. L., & Haaland, K. Y. (1992). Motor sequencing with left hemisphere damage. Are some cognitive deficits specific to limb apraxia? *Brain*, *115*(3), 857–874.

Heath, M., Roy, E. A., Westwood, D., & Black, S. E. (2001). Patterns of apraxia associated with the production of intransitive limb gestures following left and right hemisphere stroke. *Brain Cogn.*, *46*(1/2), 165–169.

Heilman, K. M., & Rothi, L. J. G. (1993). Apraxia. In K. M. Heilman & E. Valenstein (Eds.), *Clinical neuropsychology* (pp. 141–163). New York: Oxford University Press.

Heiser, M., Iacoboni, M., Maeda, F., Marcus, J., & Mazziotta, J. C. (2003). The essential role of Broca's area in imitation. *Eur. J. Neurosci.*, *17*(5), 1123–1128.

Hermsdörfer, J., Goldenberg, G., Wachsmuth, C., Conrad, B., Ceballos-Baumann, A. O., Bartenstein, P., et al. (2001). Cortical correlates of gesture processing: Clues to the cerebral mechanisms underlying apraxia during the imitation of meaningless gestures. *Neuroimage*, *14*(1 Pt 1), 149–161.

Hermsdörfer, J., Mai, N., Spatt, J., Marquardt, C., Veltkamp, R., & Goldenberg, G. (1996). Kinematic analysis of movement imitation in apraxia. *Brain*, *119*(Pt 5), 1575–1586.

Iacoboni, M., Woods, R. P., Brass, M., Bekkering, H., Mazziotta, J. C., & Rizzolatti, G. (1999). Cortical mechanisms of human imitation. *Science*, *286*(5449), 2526–2528.

Jenkins, I. H., Brooks, D. J., Nixon, P. D., Frackowiak, R. S., & Passingham, R. E. (1994). Motor sequence learning: A study with positron emission tomography. *J. Neurosci.*, *14*(6), 3775–3790.

Jueptner, M., Stephan, K. M., Frith, C. D., Brooks, D. J., Frackowiak, R. S., & Passingham, R. E. (1997). Anatomy of motor learning. I. Frontal cortex and attention to action. *J. Neurophysiol.*, *77*(3), 1313–1324.

Jueptner, M., & Weiller, C. (1998). A review of differences between basal ganglia and cerebellar control of movements as revealed by functional imaging studies. *Brain*, *121*(Pt 8), 1437–1449.

Kertesz, A., & Ferro, J. M. (1984). Lesion size and location in ideomotor apraxia. *Brain*, *107*(3), 921–933.

Kim, S. G., Ugurbil, K., & Strick, P. L. (1994). Activation of a cerebellar output nucleus during cognitive processing. *Science*, *265*(5174), 949–951.

Kimura, D., & Archibald, Y. (1974). Motor functions of the left hemisphere. *Brain*, *97*(2), 337–350.

Kolb, B., & Milner, B. (1981). Performance of complex arm and facial movements after focal brain lesions. *Neuropsychologia*, *19*(4), 491–503.

Koski, L., Iacoboni, M., Dubeau, M. C., Woods, R. P., & Mazziotta, J. C. (2003). Modulation of cortical activity during different imitative behaviors. *J. Neurophysiol.*, *89*(1), 460–471.

Koski, L., Wohlschlager, A., Bekkering, H., Woods, R. P., Dubeau, M. C., Mazziotta, J. C., et al. (2002). Modulation of motor and premotor activity during imitation of target-directed actions. *Cereb. Cortex*, *12*(8), 847–855.

Kourtzi, Z., & Kanwisher, N. (2000). Activation in human MT/MST by static images with implied motion. *J. Cogn. Neurosci.*, *12*(1), 48–55.

Krams, M., Rushworth, M. F., Deiber, M. P., Frackowiak, R. S., & Passingham, R. E. (1998). The preparation, execution and suppression of copied movements in the human brain. *Exp. Brain Res.*, *120*(3), 386–398.

Kymissis, E., & Poulson, C. L. (1990). The history of imitation in learning theory: The language acquisition process. *J. Exp. Anal. Behav.*, *54*(2), 113–127.

Lehmkuhl, G., Poeck, K., & Willmes, K. (1983). Ideomotor apraxia and aphasia: An examination of types and manifestations of apraxic symptoms. *Neuropsychologia*, *21*(3), 199–212.

Leiner, H. C., Leiner, A. L., & Dow, R. S. (1993). Cognitive and language functions of the human cerebellum. *Trends Neurosci.*, *16*(11), 444–447.

Lotze, M., Montoya, P., Erb, M., Hulsmann, E., Flor, H., Klose, U., et al. (1999). Activation of cortical and cerebellar motor areas during executed and imagined hand movements: An fMRI study. *J. Cogn. Neurosci.*, *11*(5), 491–501.

Moll, J., de Oliveira-Souza, R., Passman, L. J., Cunha, F. C., Souza-Lima, F., & Andreiuolo, P. A. (2000). Functional MRI correlates of real and imagined tool-use pantomimes. *Neurology*, *54*(6), 1331–1336.

Parsons, L. M., Denton, D., Egan, G., McKinley, M., Shade, R., Lancaster, J., & Fox, P. T. (2000). Neuroimaging evidence implicating cerebellum in support of sensory/cognitive processes associated with thirst. *Proc. Natl. Acad. Sci. U.S.A.*, *97*(5), 2332–2336.

Parsons, L. M., Fox, P. T., Downs, J. H., Glass, T., Hirsch, T. B., Martin, C. C., et al. (1995). Use of implicit motor imagery for visual shape discrimination as revealed by PET. *Nature*, *375*(6526), 54–58.

Peigneux, P., Salmon, E., van der Linden, M., Garraux, G., Aerts, J., Delfiore, G., et al. (2000). The role of lateral occipitotemporal junction and area MT/V5 in the visual analysis of upper-limb postures. *Neuroimage*, *11*(6 Pt 1), 644–655.

Rizzolatti, G., Fadiga, L., Gallese, V., & Fogassi, L. (1996). Premotor cortex and the recognition of motor actions. *Brain Res. Cogn. Brain Res.*, *3*(2), 131–141.

Rizzolatti, G., Fadiga, L., Matelli, M., Bettinardi, V., Paulesu, E., Perani, D., et al. (1996). Localization of grasp representations in humans by PET. 1. Observation versus execution. *Exp. Brain Res.*, *111*(2), 246–252.

Rizzolatti, G., Fogassi, L., & Gallese, V. (2001). Neurophysiological mechanisms underlying the understanding and imitation of action. *Nat. Rev. Neurosci.*, *2*(9), 661–670.

Rizzolatti, G., Fogassi, L., & Gallese, V. (2002). Motor and cognitive functions of the ventral premotor cortex. *Curr. Opin. Neurobiol.*, *12*(2), 149–154.

Rothi, L. J. G., Raymer, A. M., & Heilman, K. M. (1997). Limb praxis assessment. In L. J. G. Rothi & K. M. Heilman (Eds.), *Apraxia: The neuropsychology of action east Sussex* (pp. 61–73). UK: Psychology Press.

Roy, E. A., & Hall, C. (1992). Limb apraxia: A process approach. In D. Elliott & L. Proteau (Eds.), *Vision and motor control* (pp. 261–282). Amsterdam: Elsevier.

Roy, E. A., Square-Storer, P., Hogg, S., & Adams, S. (1991). Analysis of task demands in apraxia. *Int. J. Neurosci.*, *56*(1–4), 177–186.

Ruby, P., & Decety, J. (2001). Effect of subjective perspective taking during simulation of action: A PET investigation of agency. *Nat. Neurosci.*, *4*(5), 546–550.

Rumiati, R. I., Weiss, P. H., Shallice, T., Ottoboni, G., Noth, J., Zilles, K., et al. (2004). Neural basis of pantomiming the use of visually presented objects. *Neuroimage*, *21*(4), 1224–1231.

Rushworth, M. F., Johansen-Berg, H., Gobel, S. M., & Devlin, J. T. (2003). The left parietal and premotor cortices: Motor attention and selection. *Neuroimage*, *20*(Suppl 1), 89–100.

Rushworth, M. F., Krams, M., & Passingham, R. E. (2001). The attentional role of the left parietal cortex: The distinct lateralization and localization of motor attention in the human brain. *J. Cogn. Neurosci.*, *13*(5), 698–710.

Rushworth, M. F., Nixon, P. D., Renowden, S., Wade, D. T., & Passingham, R. E. (1997). The left parietal cortex and motor attention. *Neuropsychologia*, *35*(9), 1261–1273.

Rushworth, M. F., Paus, T., & Sipila, P. K. (2001). Attention systems and the organization of the human parietal cortex. *J. Neurosci.*, *21*(14), 5262–5271.

Schlaug, G., Knorr, U., & Seitz, R. (1994). Inter-subject variability of cerebral activations in acquiring a motor skill: A study with positron emission tomography. *Exp. Brain Res.*, *98*(3), 523–534.

Schluter, N. D., Krams, M., Rushworth, M. F., & Passingham, R. E. (2001). Cerebral dominance for action in the human brain: The selection of actions. *Neuropsychologia*, *39*(2), 105–113.

Schmahmann, J. D., Doyon, J., McDonald, D., Holmes, C., Lavoie, K., Hurwitz, A. S., et al. (1999). Three-dimensional MRI atlas of the human cerebellum in proportional stereotaxic space. *Neuroimage*, *10*(3 Pt 1), 233–260.

Schofield, W. N. (1976). Hand movements which cross the body midline: Findings relating age differences to handedness. *Percept. Mot. Skills*, *42*(2), 643–646.

Stephan, K. M., Fink, G. R., Passingham, R. E., Silbersweig, D., Ceballos-Baumann, A. O., Frith, C. D., et al. (1995). Functional anatomy of the mental representation of upper extremity movements in healthy subjects. *J. Neurophysiol.*, *73*(1), 373–386.

Talairach, J., & Tournoux, P. (1988). *A co-planar stereotaxic atlas of a human brain*. Stuttgart, Germany: Thieme.

Tanaka, S., & Inui, T. (2002). Cortical involvement for action imitation of hand/arm postures versus finger configurations: An fMRI study. *Neuroreport*, *13*(13), 1599–1602.

Tanaka, S., Inui, T., Iwaki, S., Konishi, J., & Nakai, T. (2001). Neural substrates involved in imitating finger configurations: An fMRI study. *Neuroreport*, *12*(6), 1171–1174.

Toni, I., Schluter, N. D., Josephs, O., Friston, K., & Passingham, R. E. (1999). Signal-, set- and movement-related activity in the human brain: An event-related fMRI study. *Cereb. Cortex*, *9*(1), 35–49.

Ungerleider, L. G. (1985). The corticocortical pathways for object recognition and spatial perception. In C. Chagas, R. Gattas, & C. Gross (Eds.), *Pattern recognition mechanisms* (pp. 21–37). New York: Springer.

Watson, J. D., Myers, R., Frackowiak, R. S., Hajnal, J. V., Woods, R. P., Mazziotta, J. C., et al. (1993). Area V5 of the human brain: Evidence from a combined study using positron emission tomography and magnetic resonance imaging. *Cereb. Cortex*, *3*(2), 79–94.

Zeki, S., & Shipp, S. (1988). The functional logic of cortical connections. *Nature*, *335*(6188), 311–317.

Zeki, S., Watson, J. D., Lueck, C. J., Friston, K. J., Kennard, C., & Frackowiak, R. S. (1991). A direct demonstration of functional specialization in human visual cortex. *J. Neurosci.*, *11*(3), 641–649.

ELSEVIER

Neurobiology of Aging 30 (2009) 147–151

NEUROBIOLOGY OF AGING

www.elsevier.com/locate/neuaging

Brief communication

Accelerated aging of the putamen in men but not in women

Sabine Nunnemann [a], Afra M. Wohlschläger [a,b,c], Rüdiger Ilg [a], Christian Gaser [d], Thorleif Etgen [a], Bastian Conrad [a], Claus Zimmer [b], Mark Mühlau [a,*]

[a] *Department of Neurology, Technische Universität München, Ismaninger Str. 22, D-81675 München, Germany*
[b] *Department of Neuroradiology, Technische Universität München, Ismaninger Str. 22, 81675 München, Germany*
[c] *Department of Nuclear Medicine Technische, Technische Universität München, Ismaninger Str. 22, 81675 München, Germany*
[d] *Department of Psychiatry, University of Jena, Philosophenweg 3, 07743 Jena, Germany*

Received 3 January 2007; received in revised form 7 May 2007; accepted 21 May 2007
Available online 3 July 2007

Abstract

Age-related structural brain changes have been demonstrated repeatedly but data on the effect of gender on age-related structural brain changes are conflicting. Using high-resolution T1-weighted magnetic resonance imaging and voxel-based morphometry, we examined a population of 133 healthy adults (women, 73; men, 60; age range, 29–80 years) focusing on differential aging between men and women (i.e., interaction of age and gender). Compared to women, men showed accelerated age-related gray matter (GM) loss in the posterior putamen. Our data may constitute the structural substrate for age-related differences in motor function between men and women such as the higher incidence and earlier onset of Parkinson's disease in men.

Keywords: Putamen; Gender; Aging; Voxel-based morphometry

1. Introduction

Age- and gender-related effects on the human brain have been extensively studied *post mortem* and *in vivo*. Beyond doubt, brain mass declines with age. Magnetic resonance imaging (MRI) studies showed that gray matter (GM) of almost all cortical and subcortical areas negatively correlates with age (Good et al., 2001b; Smith et al., 2006; Taki et al., 2004). Yet MRI studies also indicate a remarkable heterogeneity in the regional pattern of age-related GM decline. For example, several studies suggest that the frontal lobe declines more rapidly with age compared to other major lobes (Allen et al., 2005; Cowell et al., 1994; Jernigan et al., 2001).

A number of further MRI studies have demonstrated age- and/or gender-related effects on brain morphology (Coffey et al., 1998; Cowell et al., 1994; Good et al., 2001a,b; Grieve et al., 2005; Gur et al., 1991; Tisserand et al., 2002, 2004; Van Laere and Dierckx, 2001; Xu et al., 2000). However, although significant main effects of gender and/or age were detected in most of these studies, differences in aging between men and women (i.e., an interaction of age and gender) have been reported only in some studies (Coffey et al., 1998; Cowell et al., 1994; Gunning-Dixon et al., 1998; Gur et al., 1991; Raz et al., 1995; Xu et al., 2000). For example, Xu et al. reported significantly more brain atrophy with aging in men than in women in the posterior parts of the right frontal lobe, the middle part of the right temporal lobe, the parietal lobe, the cerebellum and the left basal ganglia (Xu et al., 2000). Another two studies reported that age-related shrinkage of (parts of) the basal ganglia is restricted to men (Gunning-Dixon et al., 1998; Raz et al., 1995). Despite conflicting results on gender differences in age-related brain changes, differences were, if detected, to the disadvantage of men. Yet these studies differ greatly with regard to the techniques applied, the populations examined, and the statistical models used. Addressing this issue, we decided to use voxel-based

* Corresponding author.
E-mail address: m.muehlau@neuro.med.tum.de (M. Mühlau).

0197-4580/$ – see front matter © 2007 Elsevier Inc. All rights reserved.
doi:10.1016/j.neurobiolaging.2007.05.016

morphometry since this technique is rater-independent and allows the hypothesis-free analysis of GM across the whole brain.

2. Subjects and methods

Images were derived from volunteers who had participated in imaging studies as healthy controls at our department. Before scanning, subjects were interviewed by an experienced neurologist and only included if there was no indication for any neurological or psychiatric disorder. All images were screened by an experienced neuroradiologist and excluded if there were unusual or abnormal findings. We could include the images of 133 subjects (60 men: range, 29–76 years, median, 54 years; 73 women: range, 32–80 years; median, 57 years).

Three-dimensional structural images were acquired on one and the same scanner (Siemens MAGNETOM Symphony; field intensity, 1.5 T; headcoil, standard 2-channel birdcage; sequence, T1 magnetization prepared rapid gradient echo (MP-RAGE); TR, 11.1 ms; TE, 4.3 ms; TI, 800 ms; flip angle, 15°; matrix size, 224 mm × 256 mm; orientation, sagittal; slices, 160; voxel size, 1 mm × 1 mm × 1 mm).

We used SPM2 software (Wellcome Department of Imaging Neuroscience Group, London, UK; http://www.fil.ion.ucl.ac.uk/spm). Image preprocessing was performed according to the optimized protocol (Ashburner and Friston, 2000; Good et al., 2001b) using study-specific prior probability maps. The resulting GM images were smoothed with a Gaussian kernel of 8 mm full width at half maximum.

As a result of nonlinear spatial normalization, the volumes of certain brain regions may grow, whereas others may shrink. These volume changes can be corrected by an additional step prior to smoothing. This additional step, the modulation, comprises multiplication of voxel values of the segmented images by the Jacobian determinants derived from the normalization matrix. In effect, an analysis of modulated data tests for regional differences in the absolute amount of GM. Since modulation has been recommended especially for the investigation of age-related effects and neurodegeneration (Ashburner and Friston, 2000; Busatto et al., 2003; Good et al., 2001b, 2002; Karas et al., 2003; Senjem et al., 2005), we applied the modulation step.

We analyzed only voxels that were likely to represent GM according to the study-specific probability maps ("priors") for GM, WM and CSF. Therefore, a voxel was only included if it displayed a GM value greater than both the corresponding WM and CSF value. Accounting for the existence of another class apart from the three tissue classes, the background class, we also applied an absolute voxel threshold of a GM value greater than 0.2 (maximum value: 1).

For the analysis of regional effects, we performed a voxel-by-voxel interaction analysis of age with group (i.e., gender) as implemented in SPM2. According to the default setting,

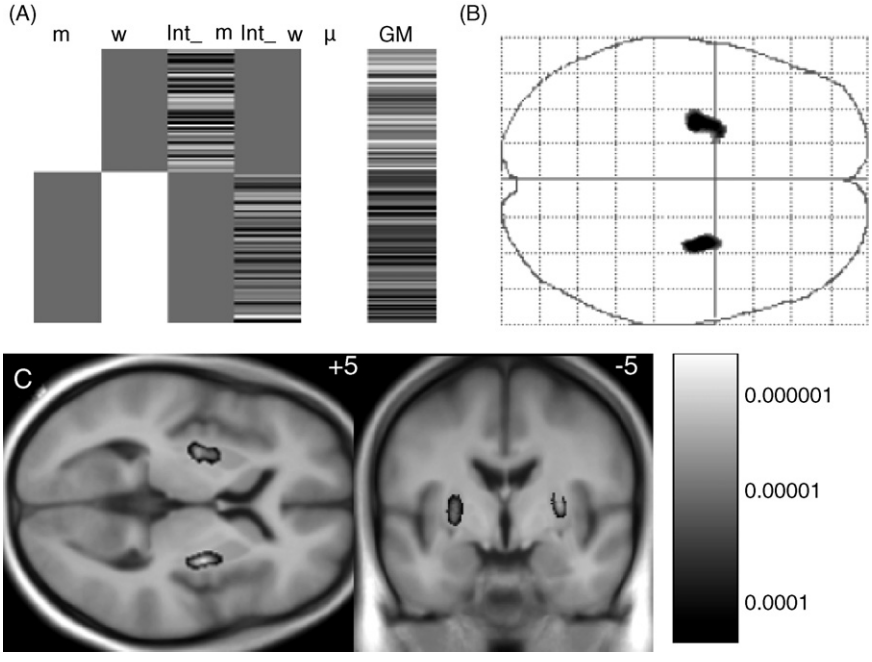

Fig. 1. Interaction of age and gender. The interaction analysis of age and group (i.e., gender) revealed accelerated age-related GM loss bilaterally in the putamen in men compared to women (Montreal Neurological Institute (MNI) coordinates of peak voxels, 30 −5 6 and −26 −10 −5; *Z* values of peak voxels, 4.5 and 4.3; height threshold, $P < 0.05$ corrected with false discovery rate (FDR); extent threshold, >330 voxels corresponding to $P < 0.05$ corrected at the cluster level). (A) Design matrix (Int_m and Int_w, regressors for the interaction of age and gender; GM, global GM volume; m, men; w, women; μ, mean; contrast, 0 0 −1 1). (B) Maximum intensity projection. (C) Projection onto the study-specific averaged T1-image is shown on the left. MNI coordinates are indicated in the right upper corner of each panel. The bar on the right encodes increasing significance.

age was centered around group means. Since our data were modulated, we had to correct for global volumes (Ashburner and Friston, 2000; Busatto et al., 2003; Good et al., 2001b, 2002; Karas et al., 2003; Senjem et al., 2005) and included the global GM volume as nuisance variable in our model (Fig. 1A).

To correct for multiple comparisons, we set a height threshold (voxel-level) of $P<0.0002$ corresponding to a false discovery rate (FDR) of $P<0.05$ (Genovese et al., 2002). In addition, we applied a spatial extent threshold of 330 voxels corresponding to $P<0.05$ corrected for multiple comparisons at the cluster level (Friston et al., 1996). For clusters showing significant interaction, the absolute GM content (i.e., the sum of all voxel values of the cluster) and the "relative GM content" (i.e., the sum of all voxel values divided by the global GM) were analyzed separately for men and women with standard software (SPSS, version 14.0.1).

3. Results

Analyses of regional GM changes with regard to the main effects of age and gender as well as analyses of global GM volumes revealed results that were largely in the range of previous reports (supplementary material).

The interaction of age and gender revealed accelerated age-related GM loss bilaterally in the posterior putamen in men (Fig. 1) whilst women showed no area of accelerated GM loss. Correlation analysis of the GM content (sum of all voxel values of both clusters within the putamen) with age was significant in men (Pearson correlation coefficient, −0.6; 2-sided P value, <0.001) but not in women (Pearson correlation coefficient, 0.1; 2-sided P value, 0.3). Plotting the "relative GM content" (sum of all voxel values of both clusters within the putamen divided by global GM) against age separately for men and women (Fig. 2) revealed accelerated loss of GM in men as indicated by the negative slope (Pearson correlation coefficient, −0.3; 2-sided P value, 0.02) and relative preservation in women as indicated by the positive slope (Pearson correlation coefficient, 0.3; 2-sided P value, 0.01).

4. Discussion

Our study aimed to identify brain regions that display gender differences in age-related GM loss. We analyzed cross-sectional data although this implies inherent limitations due to the potential for confounding age and cohort effects which can only be resolved by a longitudinal design. Nonetheless, we found an interaction of age and gender in the sense of accelerated GM loss within the posterior putamen in men compared to women (Fig. 1). Further analyses showed that the posterior putamen undergoes accelerated GM loss (i.e., faster regional GM loss than estimated from global GM loss) in men in contrast to relative preservation in women (Fig. 2).

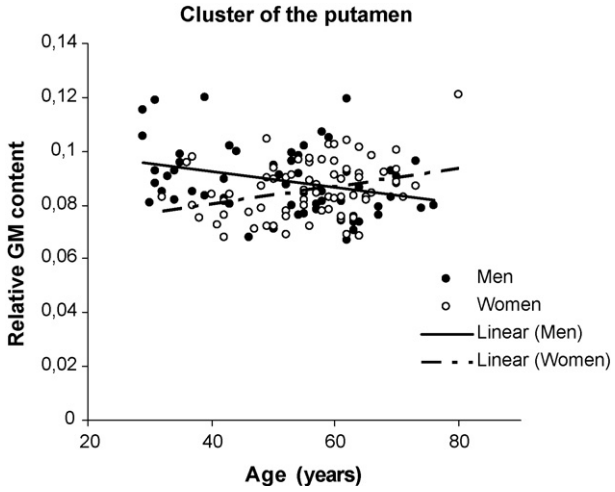

Fig. 2. Relative GM content of the clusters showing an interaction of age and gender. The relative GM content of the significant clusters is plotted against age separately for men and women. In men, the GM content decreases more rapidly than the global GM volume resulting in a negative slope of the regression line (Pearson correlation coefficient, −0.3; 2-sided P value, 0.02). In women, the GM content decreases more slowly than the global GM volume resulting in a positive slope of the regression line (Pearson correlation coefficient, 0.3; 2-sided P value, 0.01).

Addressing the issue of gender differences in age-related brain changes, various morphometry studies have yielded heterogeneous results. A quantitative review of studies on age-related changes in the striatum revealed moderate age-related shrinkage of the striatum (Raz et al., 1995). Based on this finding, a cross-sectional conventional morphometry analysis was performed in 55 healthy adults that, in accordance with our finding, demonstrated age-related shrinkage of the putamen in men but not in women (Raz et al., 1995) although a later longitudinal morphometry study in 53 healthy adults on basal ganglia structures over 5 years yielded only a trend towards an interaction of age and gender (Raz et al., 2003). Another study on differences between men and women with regard to age-related changes in the striatum did not demonstrate an interaction of age and gender either but, in this study, the volume of the whole striatum (caudate, putamen and nucleus accumbens) was measured and only 10 women were included so that the study design may have been inappropriate to demonstrate an interaction of age and gender within the putamen (Koikkalainen et al., 2007). Yet further cross-sectional conventional morphometry studies on populations comparable to ours could not demonstrate an interaction of age and gender within the putamen (Brabec et al., 2003; Brickman et al., 2003; Gunning-Dixon et al., 1998; Xu et al., 2000). Likewise VBM studies have not demonstrated an interaction of age and gender within the putamen so far but the populations of these studies differed remarkably from ours since mainly young adults with a mean age below 30 years (Good et al., 2001b) or older adults exclusively with ages

above 58 (Lemaitre et al., 2005; Smith et al., 2006) had been studied.

However, our finding of differential aging of the putamen in men and women is compatible with evidence derived from animal studies, behavioral studies in humans and epidemiological studies on Parkinson's disease (PD). In animals, neuroprotective properties of estrogens for the nigrostriatal dopaminergic system have been demonstrated repeatedly (Dluzen, 2000). A study on rhesus monkeys demonstrated age-related slowing of motor function in males but not in females although sexual differences in age-related decrease of the striatum could not be shown in the subgroup of 15 monkeys that underwent neuroimaging (Lacreuse et al., 2005). In humans, behavioral studies found age-related decrease of motor skill acquisition to be less pronounced in women than in men. In a mirror drawing task, women performed better than men and age-related decline in speed was greater in men than in women (Kennedy and Raz, 2005). Moreover, the most common disorder associated with a dysfunction of the putamen, PD, shows differences between men and women according to most but not all studies. In men, PD is more frequent (Baldereschi et al., 2000) and starts earlier (Haaxma et al., 2006). In women, the estrogen status (i.e., parity, age at menopause and fertile life span) correlates with a later onset of PD. Accordingly, striatal degeneration measured with [123I]FP-CIT SPECT was less pronounced in women (Haaxma et al., 2006). Notably, evidence exists that the posterior putamen, the site identified by our interaction analysis, is primarily affected in PD (Jellinger, 2002; Ma et al., 2002).

Conflict of interest

There are neither actual nor potential conflicts of interests for any of the authors of the manuscript. Written informed consent was obtained from all subjects in accordance with the Declaration of Helsinki 2000.

Acknowledgements

S. Nunnemann and her colleagues from the Department of Neurology (Technische Universität München) were supported by Fond 766160 of the "Kommission für Klinische Forschung (KKF), Klinikum rechts der Isar, Technische Universität München".

Appendix A. Supplementary data

Supplementary data associated with this article can be found, in the online version, at doi:10.1016/j.neurobiolaging.2007.05.016.

References

Allen, J.S., Bruss, J., Brown, C.K., Damasio, H., 2005. Normal neuroanatomical variation due to age: the major lobes and a parcellation of the temporal region. Neurobiol. Aging 26, 1245–1260 (discussion 1279–1282).

Ashburner, J., Friston, K.J., 2000. Voxel-based morphometry: the methods. Neuroimage 11, 805–821.

Baldereschi, M., Di Carlo, A., Rocca, W.A., Vanni, P., Maggi, S., Perissinotto, E., Grigoletto, F., Amaducci, L., Inzitari, D., 2000. Parkinson's disease and parkinsonism in a longitudinal study: two-fold higher incidence in men. ILSA Working Group. Italian Longitudinal Study on Aging. Neurology. 55, 1358–1363.

Brabec, J., Kraseny, J., Petrovicky, P., 2003. Volumetry of striatum and pallidum in man–anatomy, cytoarchitecture, connections, MRI and aging. Sb. Lek. 104, 13–65.

Brickman, A.M., Buchsbaum, M.S., Shihabuddin, L., Hazlett, E.A., Borod, J.C., Mohs, R.C., 2003. Striatal size, glucose metabolic rate, and verbal learning in normal aging. Brain Res. Cogn. Brain Res. 17, 106–116.

Busatto, G.F., Garrido, G.E., Almeida, O.P., Castro, C.C., Camargo, C.H., Cid, C.G., Buchpiguel, C.A., Furuie, S., Bottino, C.M., 2003. A voxel-based morphometry study of temporal lobe gray matter reductions in Alzheimer's disease. Neurobiol. Aging 24, 221–231.

Coffey, C.E., Lucke, J.F., Saxton, J.A., Ratcliff, G., Unitas, L.J., Billig, B., Bryan, R.N., 1998. Sex differences in brain aging: a quantitative magnetic resonance imaging study. Arch. Neurol. 55, 169–179.

Cowell, P.E., Turetsky, B.I., Gur, R.C., Grossman, R.I., Shtasel, D.L., Gur, R.E., 1994. Sex differences in aging of the human frontal and temporal lobes. J. Neurosci. 14, 4748–4755.

Dluzen, D.E., 2000. Neuroprotective effects of estrogen upon the nigrostriatal dopaminergic system. J. Neurocytol. 29, 387–399.

Friston, K.J., Holmes, A., Poline, J.B., Price, C.J., Frith, C.D., 1996. Detecting activations in PET and fMRI: levels of inference and power. Neuroimage 4, 223–235.

Genovese, C.R., Lazar, N.A., Nichols, T., 2002. Thresholding of statistical maps in functional neuroimaging using the false discovery rate. Neuroimage 15, 870–878.

Good, C.D., Johnsrude, I., Ashburner, J., Henson, R.N., Friston, K.J., Frackowiak, R.S., 2001a. Cerebral asymmetry and the effects of sex and handedness on brain structure: a voxel-based morphometric analysis of 465 normal adult human brains. Neuroimage 14, 685–700.

Good, C.D., Johnsrude, I.S., Ashburner, J., Henson, R.N., Friston, K.J., Frackowiak, R.S., 2001b. A voxel-based morphometric study of ageing in 465 normal adult human brains. Neuroimage 14, 21–36.

Good, C.D., Scahill, R.I., Fox, N.C., Ashburner, J., Friston, K.J., Chan, D., Crum, W.R., Rossor, M.N., Frackowiak, R.S., 2002. Automatic differentiation of anatomical patterns in the human brain: validation with studies of degenerative dementias. Neuroimage 17, 29–46.

Grieve, S.M., Clark, C.R., Williams, L.M., Peduto, A.J., Gordon, E., 2005. Preservation of limbic and paralimbic structures in aging. Hum. Brain Mapp. 25, 391–401.

Gunning-Dixon, F.M., Head, D., McQuain, J., Acker, J.D., Raz, N., 1998. Differential aging of the human striatum: a prospective MR imaging study. AJNR Am. J. Neuroradiol. 19, 1501–1507.

Gur, R.C., Mozley, P.D., Resnick, S.M., Gottlieb, G.L., Kohn, M., Zimmerman, R., Herman, G., Atlas, S., Grossman, R., Berretta, D., et al., 1991. Gender differences in age effect on brain atrophy measured by magnetic resonance imaging. Proc. Natl. Acad. Sci. USA 88, 2845–2849.

Haaxma, C.A., Bloem, B.R., Borm, G.F., Oyen, W.J., Leenders, K.L., Eshuis, S., Booij, J., Dluzen, D.E., Horstink, M.W., 2006. Gender differences in Parkinson's disease. J. Neurol. Neurosurg. Psychiatry.

Jellinger, K.A., 2002. Recent developments in the pathology of Parkinson's disease. J. Neural. Transm. Suppl., 347–376.

Jernigan, T.L., Archibald, S.L., Fennema-Notestine, C., Gamst, A.C., Stout, J.C., Bonner, J., Hesselink, J.R., 2001. Effects of age on tissues and regions of the cerebrum and cerebellum. Neurobiol. Aging 22, 581–594.

Karas, G.B., Burton, E.J., Rombouts, S.A., van Schijndel, R.A., O'Brien, J.T., Scheltens, P., McKeith, I.G., Williams, D., Ballard, C., Barkhof, F., 2003. A comprehensive study of gray matter loss in patients with Alzheimer's disease using optimized voxel-based morphometry. Neuroimage 18, 895–907.

Kennedy, K.M., Raz, N., 2005. Age, sex and regional brain volumes predict perceptual-motor skill acquisition. Cortex 41, 560–569.

Koikkalainen, J., Hirvonen, J., Nyman, M., Lotjonen, J., Hietala, J., Ruotsalainen, U., 2007. Shape variability of the human striatum-Effects of age and gender. Neuroimage 34, 85–93.

Lacreuse, A., Diehl, M.M., Goh, M.Y., Hall, M.J., Volk, A.M., Chhabra, R.K., Herndon, J.G., 2005. Sex differences in age-related motor slowing in the rhesus monkey: behavioral and neuroimaging data. Neurobiol. Aging 26, 543–551.

Lemaitre, H., Crivello, F., Grassiot, B., Alperovitch, A., Tzourio, C., Mazoyer, B., 2005. Age- and sex-related effects on the neuroanatomy of healthy elderly. Neuroimage 26, 900–911.

Ma, Y., Dhawan, V., Mentis, M., Chaly, T., Spetsieris, P.G., Eidelberg, D., 2002. Parametric mapping of [^{18}F]FPCIT binding in early stage Parkinson's disease: a PET study. Synapse 45, 125–133.

Raz, N., Rodrigue, K.M., Kennedy, K.M., Head, D., Gunning-Dixon, F., Acker, J.D., 2003. Differential aging of the human striatum: longitudinal evidence. AJNR Am. J. Neuroradiol. 24, 1849–1856.

Raz, N., Torres, I.J., Acker, J.D., 1995. Age, gender, and hemispheric differences in human striatum: a quantitative review and new data from in vivo MRI morphometry. Neurobiol. Learn. Mem. 63, 133–142.

Senjem, M.L., Gunter, J.L., Shiung, M.M., Petersen, R.C., Jack Jr., C.R., 2005. Comparison of different methodological implementations of voxel-based morphometry in neurodegenerative disease. Neuroimage 26, 600–608.

Smith, C.D., Chebrolu, H., Wekstein, D.R., Schmitt, F.A., Markesbery, W.R., 2006. Age and gender effects on human brain anatomy: a voxel-based morphometric study in healthy elderly. Neurobiol. Aging.

Taki, Y., Goto, R., Evans, A., Zijdenbos, A., Neelin, P., Lerch, J., Sato, K., Ono, S., Kinomura, S., Nakagawa, M., Sugiura, M., Watanabe, J., Kawashima, R., Fukuda, H., 2004. Voxel-based morphometry of human brain with age and cerebrovascular risk factors. Neurobiol. Aging 25, 455–463.

Tisserand, D.J., Pruessner, J.C., Sanz Arigita, E.J., van Boxtel, M.P., Evans, A.C., Jolles, J., Uylings, H.B., 2002. Regional frontal cortical volumes decrease differentially in aging: an MRI study to compare volumetric approaches and voxel-based morphometry. Neuroimage 17, 657–669.

Tisserand, D.J., van Boxtel, M.P., Pruessner, J.C., Hofman, P., Evans, A.C., Jolles, J., 2004. A voxel-based morphometric study to determine individual differences in gray matter density associated with age and cognitive change over time. Cereb. Cortex 14, 966–973.

Van Laere, K.J., Dierckx, R.A., 2001. Brain perfusion SPECT: age- and sex-related effects correlated with voxel-based morphometric findings in healthy adults. Radiology 221, 810–817.

Xu, J., Kobayashi, S., Yamaguchi, S., Iijima, K., Okada, K., Yamashita, K., 2000. Gender effects on age-related changes in brain structure. AJNR Am. J. Neuroradiol. 21, 112–118.

Accelerated aging of the putamen in men but not in women

– Supplementary material –

Sabine Nunnemann, Afra M. Wohlschläger, Rüdiger Ilg, Christian Gaser, Thorleif Etgen, Bastian Conrad, Claus Zimmer, Mark Mühlau

Supplementary introduction

In order to evaluate the plausibility of our data, we also analyzed the main effects of age and gender.

Supplementary methods

Global volumes of gray matter (GM), white matter (WM) and cerebrospinal fluid (CSF) were derived from the first segmentation process. Statistical tests were performed using SPSS software (Statistical Package for the Social Sciences, version 14.0.1, Chicago, Illinois, USA). Total intracranial volume was approximated by the sum of global GM, WM, and CSF. To correct for intracranial volume, fractions of GM (FGM), WM (FWM), and CSF (FCSF) were calculated by dividing the global values by the TIV. For the analysis of gender differences, 2-sided independent t-tests were applied. For the analysis of age-related effects, parametric correlations were used. Moreover, age and gender were fed in an analysis of variances (ANOVA) with global GM volume as dependent variable in order to identify differences in aging between men and women (i.e., the interaction of age and gender) with regard to global GM volumes.

For the voxel-wise analysis of the main effects of age and gender, we applied an analysis of covariance (ANCOVA) model (as implemented in SPM2) for the comparison of 2 groups (i.e., men and women) with age and global GM as covariates in order to identify only regional GM differences that cannot be explained by global effects (supplementary Figure 2E). Therefore, we will refer to these changes as relative gender-related GM differences and decelerated or accelerated age-related GM decrease, respectively.

Supplementary results

The distribution of age is shown in supplementary Figure 1 indicating that younger, middle-aged, and older adults were all represented well in both genders.

Global GM volume decreased significantly with age (P value < 0.001) but we did not find an interaction of age and gender. Compared to women, men displayed higher TIV (1859±132 vs. 1689±166 ml; P value, < 0.001) and higher global GM volumes (676.4±61.7 vs. 618.1±60.5 ml, P value < 0.001). After correcting for the TIV by analyzing FGM, no significant differences were found between men and women (36.4±2.5 vs. 36.7±2.8%; P value, 0.5).

The voxel-wise analysis of age-related effects revealed accelerated GM decrease in frontal, parietal, and occipital cortical areas as well as in the subcortical areas of the medial thalamus, caudate nucleus, and superior insula (supplementary Figure 2A, supplementary Table 1). By contrast, decelerated GM decrease was mainly found in parahippocampal areas, the inferior insula, tectum, and posterior thalamus (supplementary Figure 2B, supplementary Table 1).

Compared to men, women displayed relative GM increase diffusely in frontal, parietal, occipital and lateral temporal cortical areas as well as in the medial thalamus (supplementary Figure 2C, supplementary Table 2). By contrast, men displayed relative GM increase in cerebellar and inferomedial temporal regions as well as in the posterior cingulate (supplementary Figure 2D, supplementary Table 2).

Supplementary discussion

Relating our results on the main effects of age and gender to the results of other morphometry studies is difficult given the marked differences among the studies with regard to the methods applied and the populations examined. Yet our results are largely in the range of previous reports.

Like our study, numerous studies have demonstrated a significant decrease of global GM volume with age (Ge et al., 2002, Good et al., 2001b, Lemaitre et al., 2005, Raz et al., 2005, Resnick et al., 2003, Smith et al., 2006, Taki et al., 2004). In most of these studies, higher TIV and global GM volume in men than in women have been reported. After correcting the global GM volumes for the TIV, some studies reported higher values in men (Good et al., 2001b) whilst others found higher values in women (Lemaitre et al., 2005) or no difference (Riello et al., 2005). Some studies revealed an interaction of age and gender with regard to global GM volumes (Ge et al., 2002, Taki et al., 2004) whilst, in accordance with our results, other studies revealed no such interaction (Lemaitre et al., 2005, Resnick et al., 2003, Riello et al., 2005) or only a trend towards such an interaction (Good et al., 2001b).

With regard to regional changes, relative preservation (i.e., decelerated GM decrease) within hippocampal and parahippocampal structures have not only been demonstrated in our study but also in studies that examined samples of younger subjects with mean ages below 40 years (Good et al., 2001b, Grieve et al., 2005) whilst studies on older populations with mean ages above 60 have not demonstrated a preservation of these regions (Lemaitre et al., 2005, Smith et al., 2006). Both results are compatible with the finding that hippocampal decline accelerates with age (Raz et al., 2004). Furthermore, age-related GM decrease has been shown to be most pronounced around the Sylvian fissure as well as in further frontal and parietal regions (Good et al., 2001b, Lemaitre et al., 2005, Smith et al., 2006, Taki et al., 2004) which, again, largely complies with our data.

Gender differences in human brain anatomy are beyond dispute although the differences shown in numerous studies differ in detail. In accordance with our findings, studies that corrected for differences in global GM volume, demonstrated a diffuse surplus within frontal, parietal, occipital and lateral temporal areas in women (Good et al., 2001a, Luders et al., 2005) whilst men, if at all, displayed a surplus of GM only in medial temporal and cerebellar regions (Good et al., 2001a).

Supplementary figure 1: Distribution of age separately for men and women

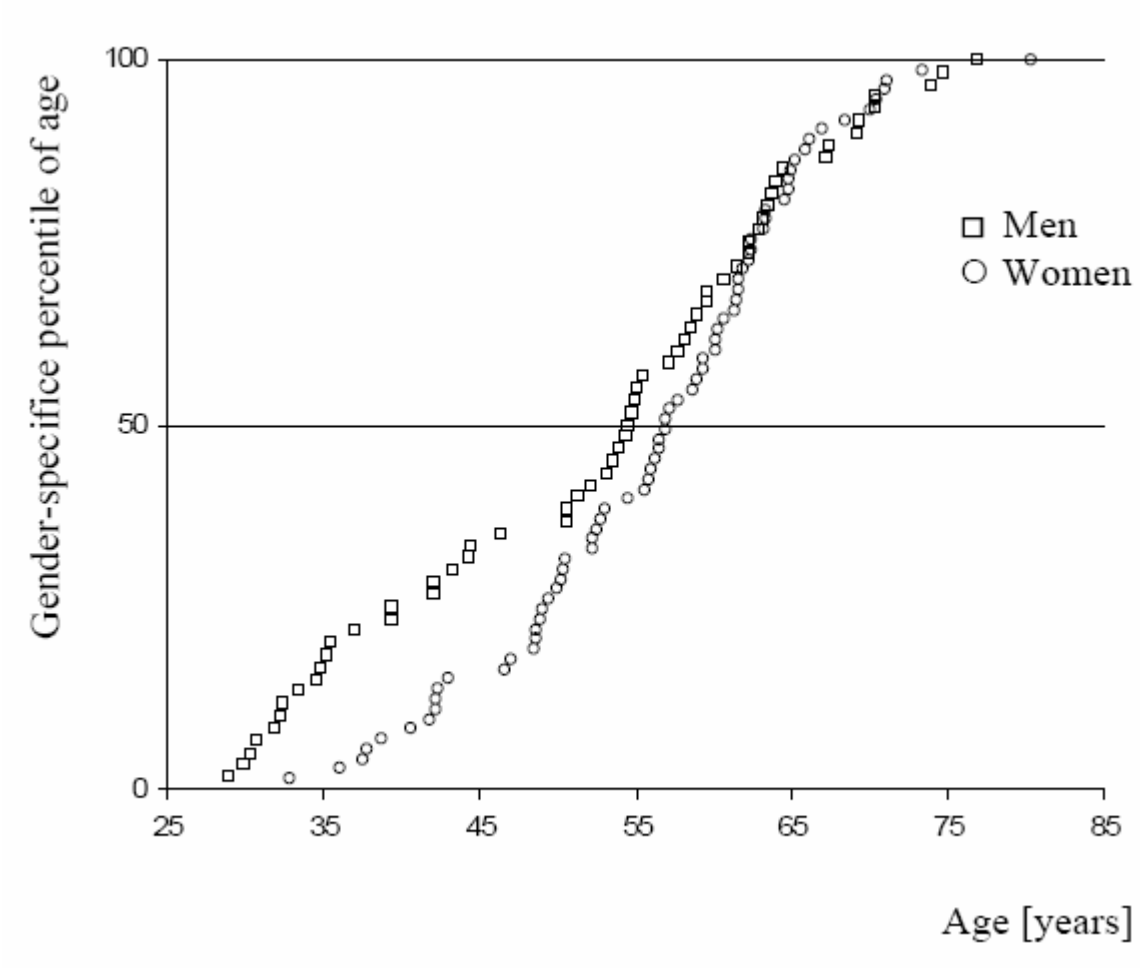

Legend of supplementary figure 1

Separately for men and women, age [years] is plotted against the (gender-specific) percentile of age indicating that younger, middle-aged, and older adults were all represented well in both genders.

Supplementary figure 2: **Main effect of age and gender**

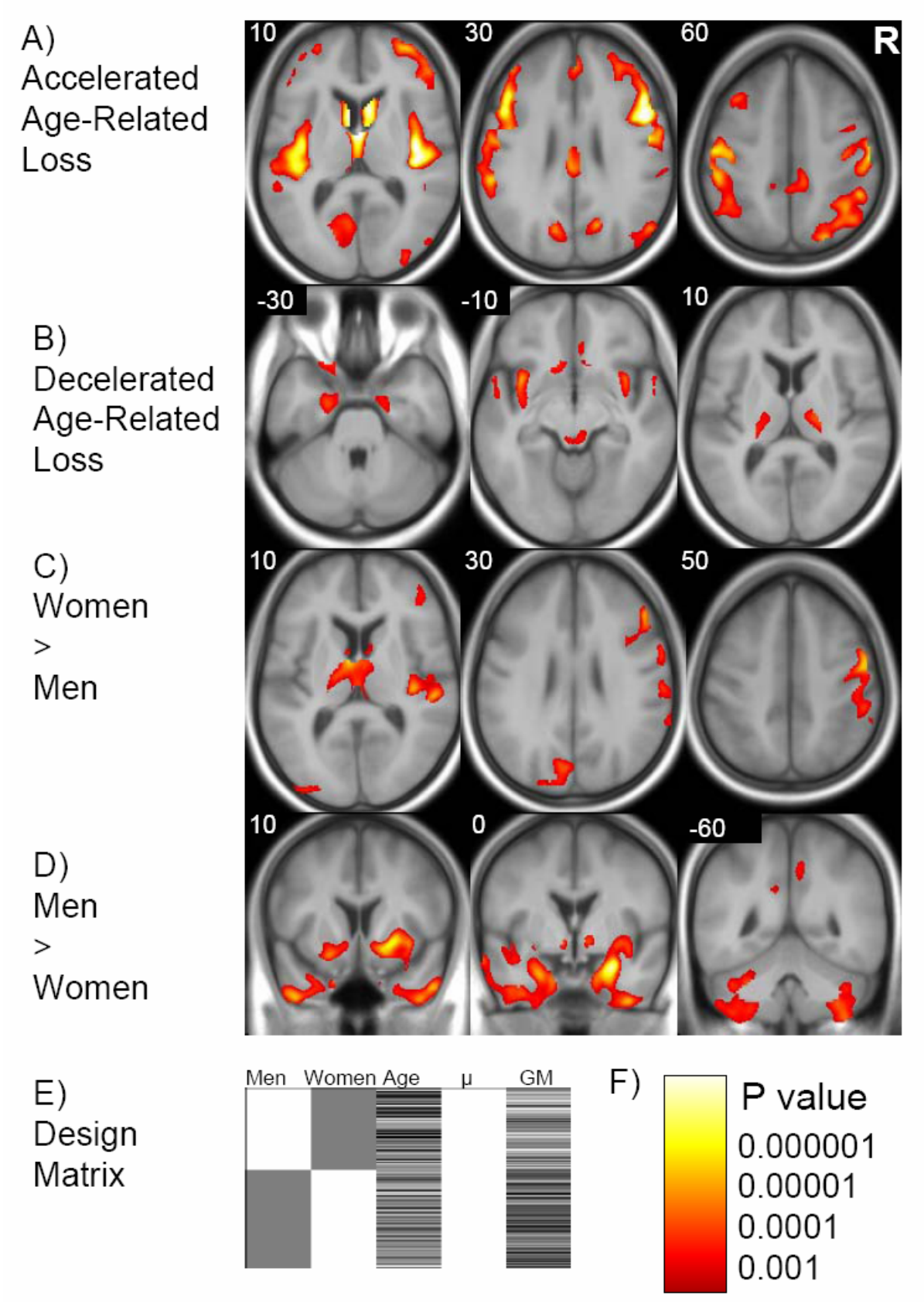

Legend of supplementary figure 2

A-D) Main effects of age and gender are projected onto slices of the study-specific averaged T1 image. Montreal Neurological Institute (MNI) coordinates (panels A-C, Z axis; panel D, Y axis) are indicated in the upper left corner of each slice. The right side of the images corresponds to the right hemisphere as indicated with the letter "R" in the upper right corner. Height threshold, $P < 0.05$ corrected (false discovery rate).

A) Accelerated age-related gray-matter loss [contrast: 0 0 -1].

B) Decelerated age-related gray-matter loss [contrast: 0 0 1].

C) Gray-matter increase in women compared to men [contrast: -1 1 0].

D) Gray-matter increase in men compared to women [contrast: 1 -1 0].

E) Design matrix for the analysis of main effects of age and gender.

F) The bar encodes increasing significance form dark red to light yellow as indicated by the uncorrected P values (voxel level).

Supplementary table 1 Age-related relative gray-matter changes

Cluster extent	MNI coordinates x	y	z	Z value	Region
Decelerated age-related gray matter loss					
740	19	-8	-30	3.84	R parahippocampal g., BA35
	24	-13	-23	3.69	R parahippocampal g., BA28
	24	-4	-23	3.54	R uncus, amygdala
1257	37	10	-9	4.84	R inferior insula
	27	21	-4	4.28	R inferior insula
5123	-23	-5	-26	4.98	L uncus, amygdala
	-36	10	-11	5.69	L inferior insula
	-36	2	-7	4.72	L inferior insula
2296	19	-18	7	4.87	R thalamus
	8	-28	-5	4.26	R thalamus/tectum
1110	-19	-14	17	4.96	L thalamus
	-25	-29	8	4.48	L thalamus, pulvinar
	-20	-22	6	4.16	L thalamus
1121	62	0	-3	4.47	R middle temporal g., BA21
	69	-22	4	4.13	R superior temporal g., BA22
	62	-8	-2	4	R superior temporal g., BA21
818	-54	14	-14	5.19	L superior temporal g., BA38
	-54	0	-9	3.91	L middle temporal g., BA21
1567	2	25	-4	4.28	R anterior cingulate, BA24
	-15	17	-13	4.84	L subcallosal g., BA47
1002	11	19	60	3.89	R superior frontal g., BA6
	13	11	63	3.88	R superior frontal g., BA6
	15	-3	71	3.5	R superior frontal g., BA6
Accelerated age-related gray matter loss					
11344	-6	5	14	6.75	L caudate body
	-12	0	21	6.47	L caudate body
	8	13	11	6.35	R caudate head
	0	-18	3	5.43	L/R medial thalamus
28068	50	10	34	7.27	R middle frontal g., BA9
	52	8	43	6.63	R middle frontal g., BA8
	50	25	26	6.59	R middle frontal g., BA46
	58	-16	48	6.01	R Postcentral g., BA3
6626	-46	22	27	6.58	L middle frontal g., BA46
	-48	14	34	6.08	L middle frontal g., BA9
	-45	1	33	5.25	L Inferior frontal g., BA6
21025	-48	-17	37	6.47	L precentral g., BA4
	-57	-39	20	6.36	L superior insula
	-55	-24	42	6.14	L postcentral g., BA3
	-41	-25	9	5.87	L transverse temporal g., BA41
9031	40	-14	13	6.9	R superior insula
	45	-11	-3	6.66	R superior temporal g., BA22
	50	-15	7	6.02	R superior temporal g., BA22
3228	-14	-68	25	4.76	L precuneus, BA31
	-20	-69	8	4.56	L posterior cingulate, BA30
	-5	-71	17	4.46	L precuneus, BA31

BA, Brodmann area; g., gyrus; L, left; MNI, Montreal Neurological Institute; R, right; voxel size, 1x1x1 mm^3. Voxel threshold, $P < 0.05$ corrected with false discovery rate.

Supplementary table 2 Gender-related relative gray-matter differences

Cluster extent	MNI coordinates x	y	z	Z value	Region
Gray-matter increase in women compared to men					
8385	9	-4	16	4.34	R caudate body
	4	-3	7	4.25	R thalamus
	-12	-7	17	5.82	L caudate body
	-15	-36	-5	5.2	L parahippocampal g., BA30
	-6	-3	10	5.14	L thalamus
4384	54	36	18	5.49	R middle frontal g.
	50	29	31	4.92	R middle frontal g., BA9
	54	20	24	4.52	R Inferior frontal g., BA9
3240	-21	62	-5	5.3	L superior frontal g., BA10
	-33	60	-7	4.51	L middle frontal g., BA10
18263	52	-28	12	5.47	R transverse temporal g., BA41
	53	-7	48	5.21	R precentral g., BA4
	54	-29	22	4.94	R inferior parietal lobule, BA40
	39	-21	9	4.88	R insula
4674	-11	-76	36	4.56	L precuneus, BA7
	-8	-84	36	4.48	L precuneus, BA19
	-33	-91	13	3.91	L middle occipital g., BA19
Gray-matter increase in men compared to women					
20603	27	0	-23	6.14	R parahippocampal g., amygdala
	25	11	-5	5.5	R putamen
	42	7	-46	5.19	R middle temporal g., BA38
17627	-38	5	-17	5.82	L superior temporal g., BA38
	-45	12	-43	5.4	L middle temporal g., BA21
	-20	14	-16	5.08	L Inferior frontal g., BA47
7743	37	-47	-58	4.7	R cerebellum, lobules VIIB/VIIIA, crus II
	34	-50	-49	4.27	R cerebellum, lobules VIIB/VIIIA, crus II
	43	-55	-55	4.21	R cerebellum, lobules VIIB/VIIIA, crus II
7788	-32	-44	-55	4.8	L cerebellum, lobules VIIB/VIIIA/VIIIB
	-27	-56	-33	4.53	L cerebellum, lobules VIIB/VIIIA/VIIIB
	-30	-44	-34	4.37	L cerebellum, lobules VIIB/VIIIA/VIIIB
2326	5	-44	29	4.25	R cingulate g., BA31
	9	-51	48	3.6	R precuneus, BA7
	-6	-44	31	4.71	L posterior cingulate g., BA31

BA, Brodmann area; g., gyrus; L, left; MNI, Montreal Neurological Institute; R, right; voxel size, 1x1x1 mm^3.

Voxel threshold, $P < 0.05$ corrected with false discovery rate.

Cerebellar regions are described according to Schmahmann et al. (Schmahmann et al., 1999).

Supplementary references

Ge, Y., Grossman, R.I., Babb, J.S., Rabin, M.L., Mannon, L.J., Kolson, D.L., 2002. Age-related total gray matter and white matter changes in normal adult brain. Part I: volumetric MR imaging analysis. AJNR Am J Neuroradiol. 23, 1327-1333.

Good, C.D., Johnsrude, I., Ashburner, J., Henson, R.N., Friston, K.J., Frackowiak, R.S., 2001a. Cerebral asymmetry and the effects of sex and handedness on brain structure: a voxel-based morphometric analysis of 465 normal adult human brains. Neuroimage. 14, 685-700.

Good, C.D., Johnsrude, I.S., Ashburner, J., Henson, R.N., Friston, K.J., Frackowiak, R.S., 2001b. A voxel-based morphometric study of ageing in 465 normal adult human brains. Neuroimage. 14, 21-36.

Grieve, S.M., Clark, C.R., Williams, L.M., Peduto, A.J., Gordon, E., 2005. Preservation of limbic and paralimbic structures in aging. Hum Brain Mapp. 25, 391-401.

Lemaitre, H., Crivello, F., Grassiot, B., Alperovitch, A., Tzourio, C., Mazoyer, B., 2005. Age- and sex-related effects on the neuroanatomy of healthy elderly. Neuroimage. 26, 900-911.

Luders, E., Narr, K.L., Thompson, P.M., Woods, R.P., Rex, D.E., Jancke, L., Steinmetz, H., Toga, A.W., 2005. Mapping cortical gray matter in the young adult brain: effects of gender. Neuroimage. 26, 493-501.

Raz, N., Lindenberger, U., Rodrigue, K.M., Kennedy, K.M., Head, D., Williamson, A., Dahle, C., Gerstorf, D., Acker, J.D., 2005. Regional brain changes in aging healthy adults: general trends, individual differences and modifiers. Cereb Cortex. 15, 1676-1689.

Raz, N., Rodrigue, K.M., Head, D., Kennedy, K.M., Acker, J.D., 2004. Differential aging of the medial temporal lobe: a study of a five-year change. Neurology. 62, 433-438.

Resnick, S.M., Pham, D.L., Kraut, M.A., Zonderman, A.B., Davatzikos, C., 2003. Longitudinal magnetic resonance imaging studies of older adults: a shrinking brain. J Neurosci. 23, 3295-3301.

Riello, R., Sabattoli, F., Beltramello, A., Bonetti, M., Bono, G., Falini, A., Magnani, G., Minonzio, G., Piovan, E., Alaimo, G., Ettori, M., Galluzzi, S., Locatelli, E., Noiszewska, M., Testa, C., Frisoni, G.B., 2005. Brain volumes in healthy adults aged 40 years and over: a voxel-based morphometry study. Aging Clin Exp Res. 17, 329-336.

Schmahmann, J.D., Doyon, J., McDonald, D., Holmes, C., Lavoie, K., Hurwitz, A.S., Kabani, N., Toga, A., Evans, A., Petrides, M., 1999. Three-dimensional MRI atlas of the human cerebellum in proportional stereotaxic space. Neuroimage. 10, 233-260.

Smith, C.D., Chebrolu, H., Wekstein, D.R., Schmitt, F.A., Markesbery, W.R., 2006. Age and gender effects on human brain anatomy: A voxel-based morphometric study in healthy elderly. Neurobiol Aging.

Taki, Y., Goto, R., Evans, A., Zijdenbos, A., Neelin, P., Lerch, J., Sato, K., Ono, S., Kinomura, S., Nakagawa, M., Sugiura, M., Watanabe, J., Kawashima, R., Fukuda, H., 2004. Voxel-based morphometry of human brain with age and cerebrovascular risk factors. Neurobiol Aging. 25, 455-463.

J Neural Transm (2007) 114: 367–372
DOI 10.1007/s00702-006-0571-x
Printed in The Netherlands

Journal of Neural Transmission

Voxel-based morphometry indicates relative preservation of the limbic prefrontal cortex in early Huntington disease

M. Mühlau[1], A. Weindl[1], A. M. Wohlschläger[1,2,3], C. Gaser[4], M. Städtler[1], M. Valet[1], C. Zimmer[2], J. Kassubek[5], A. Peinemann[1]

[1] Department of Neurology, Technische Universität München, Munich, Germany
[2] Department of Neuroradiology, Technische Universität München, Munich, Germany
[3] Department of Nuclear Medicine, Technische Universität München, Munich, Germany
[4] Department of Psychiatry, University of Jena, Jena, Germany
[5] Department of Neurology, University of Ulm, Ulm, Germany

Received: June 7, 2006 / Accepted: August 8, 2006 / Published online: October 6, 2006

Summary In Huntington disease (HD), both the genetic defect and mutant gene product huntington are known but the exact mechanisms that lead to neuronal loss are poorly understood. Until now, the distribution of tissue *loss* throughout the brain has been investigated intensively. Here we searched for areas that, antipodal to the striatum, display grey-matter (GM) preservation. We performed high resolution T1-weighted magnetic resonance imaging and voxel-based morphometry in 46 patients in early HD and 46 healthy controls. We applied an analysis of covariance (ANCOVA) model with the total GM volume of each participant as covariate. In accordance with earlier reports, group comparisons revealed GM decrease in the striatum, insula, and thalamus as well as in dorsolateral frontal and occipital areas. In contrast, the limbic prefrontal cortex displayed GM preservation. Our findings support hypotheses that postulate differential involvement of frontosubcortical circuits in the pathophysiology of HD.

Keywords: Grey-matter preservation, Huntington disease, voxel-based morphometry

Introduction

Huntington disease (HD) is an autosomal dominant neurodegenerative disease. Since the discovery that HD results from an expanded CAG trinucleotide repeat within the IT15 gene located on chromosome 4 (1993), HD has become an attractive model for neurodegeneration. However, the pathomechanisms that lead to the typical distribution of pathological changes throughout the brain (i.e., primarily loss of medium-sized spiny neurons in the striatum) (Graveland et al., 1985; Vonsattel et al., 1985) and, finally, to the clinical picture of involuntary movements, dementia, and behavioral disturbances are poorly understood. At the molecular level, numerous pathomechanisms triggered by the mutant gene product huntingtin have been discovered and, far from arriving at a unifying mechanism, robust evidence suggests that multiple – probably interacting – pathomechanisms (e.g., glutamatergic excitotoxicity and mitochondrial dysfunction) occur in HD (Gardian and Vecsei, 2004; Leegwater-Kim and Cha, 2004). Moreover, clinical, epidemiological, imaging, and histological studies have provided valuable insights with regard to the severity and variability of clinical symptoms and the involvement of different brain systems.

Perspectively, a comprehensive model of HD must account for multiple pathogenic mechanisms and its interactions and, this way, explain the distribution of pathological changes throughout the brain. Therefore, precise knowledge on the distribution of pathological changes throughout the brain is essential for the understanding of HD. Until now, the distribution of tissue *loss* throughout the brain has been investigated intensively (Kassubek et al., 2004b, 2005; Peinemann et al., 2005; Rosas et al., 2001; Thieben et al., 2002; Vonsattel et al., 1985). In order to further characterize the pattern of grey-matter (GM) changes throughout the brain in HD, we searched for areas that, antipodal to the striatum, display relative preservation of GM or even absolute GM increase. For this purpose, we performed magnetic

Correspondence: Mark Mühlau, MD, Department of Neurology, Technische Universität München, Möhlstrasse 28, 81675 Munich, Germany
e-mail: m.muehlau@neuro.med.tu-muenchen.de

resonance imaging (MRI) and voxel-based morphometry (VBM) in HD patients and healthy controls. VBM enables the detection of subtle structural changes throughout the brain at the group level using MRI. The main idea of VBM comprises the following steps: 1) spatial normalization of all images to a standardized anatomical space to allow averaging; 2) segmentation of images into GM, white matter (WM) as well as cerebrospinal fluid (CSF); and 3) group comparison of GM across the whole brain. This way, both GM decrease and increase can be detected.

Subjects and methods

Subjects

Data and images were derived from routine diagnostics of our HD outpatient clinic that participates in the European Huntington Disease Network (http://www.euro-hd.net/html/network) and from healthy volunteers who had participated in other imaging studies at our department. The HD group consisted of 46 gene-positive subjects (woman, 23; left-handers, 2) (Oldfield, 1971) who did not generate motion artifacts during MRI. Seven patients were presymptomatic. Twenty eight patients were in stage I and 11 in stage II according to Shoulson and Fahn (1979). Further details on the HD group are given in the Table 1. Healthy controls were matched for age and sex in a pair-wise manner (woman, 23; left-handers, 2; mean age, 44 years; standard deviation of age, 10).

MRI

Each participant underwent MRI (magnetic field intensity, 1.5 Tesla; scanner, *Siemens Magnetom Symphony*; sequence, T1 magnetization prepared rapid gradient echo (MPRAGE); plane, sagittal; number of slices, 160; slice thickness, 1 mm; voxel size, $1 \times 1 \times 1\,mm^3$; flip angle, 15°; field of view, 256×256 mm). After 27 HD patients and 27 controls had undergone MRI (TR, 11.1 ms; TE, 4.3 ms; TI, 800 ms), *Siemens* performed a software upgrade by installing the "*syngo software*" which resulted in slightly different parameters of the standard MPRAGE sequence (TR, 8.9 ms; TE, 3.93 ms; TI, 800 ms). In order to certainly exclude an effect of this software upgrade, the sequence was included in each analysis of covariance (ANCOVA) as additional confounding covariate (see below).

Table 1. *Characterization of the HD patients*

	Min	Max	Median	Mean	SD
Age[a]	24	68	42	44	11
Onset age[b]	24	62	40	41	10
Time since onset	0	14	4.0	4.7	4.7
MMSE	18	30	28	27	3.0
mUHDRS[a]	0	62	13	18	17
CAG[c]	40	49	43	44	2.4

CAG Number of CAG trinucleotide repeats; *Max* maximum; *Min* minimum; *MMSE* mini-mental state examination (Folstein et al., 1975); *mUHDRS* motor score of the Unified HD Rating Scale (1996); *SD* standard deviation. [a] Age correlated significantly with mUHDRS (Spearman correlation coefficient, 0.74; 2-sided *P* value, <0.001). [b] Onset was defined as the occurrence of first motor symptoms. [c] CAG repeats correlated significantly with onset age (Spearman correlation coefficient, −0.52; 2-sided *P* value, 0.002).

Analyses of global volumes

Global volumes of GM, WM, and CSF of each subject were derived from the segmentation process of SPM2. Total intracranial volume (TIV) was defined as the sum of the global volumes of GM, WM, and CSF.

VBM parameters and statistical analyses

SPM2 software (Wellcome Department of Imaging Neuroscience Group, London, UK; http://www.fil.ion.ucl.ac.uk/spm) was applied for data processing. VBM was performed according to the "optimized" protocol (Good et al., 2001) using study-specific prior probability maps, the modulation step, and a Gaussian kernel of 8 mm for smoothing. Voxel-by-voxel analysis of covariance (ANCOVA) with MPRAGE-sequence, age, sex, and global GM volume as confounding covariates was used to detect GM differences between both groups.

As a result of nonlinear spatial normalization, the volumes of certain brain regions may grow, whereas others may shrink. Correction for these volume changes by another pre-processing step prior to smoothing has been recommended especially for the investigation of neurodegenerative diseases (Good et al., 2001, 2002).This additional step, the modulation, comprises multiplication of voxel values of the segmented images by the Jacobian determinants. In effect, an analysis of modulated data tests for regional differences in the absolute amount of GM (whereas analysis of unmodulated data tests for regional differences in concentration of GM) (Ashburner and Friston, 2000; Good et al., 2001).

VBM analyses aim to find regionally specific changes that cannot be explained by global effects. Compatible with general brain atrophy, the HD group showed significantly less total GM volume and significantly less total WM volume but significantly more total CSF volume whilst the total intracranial volumes did not differ significantly between both groups (Fig. 1). In order to correct for both brain size and global atrophy, we followed the suggestion of Good et al. (2001, 2002) and included the total GM volume of each participant as covariate in our ANCOVA. In this analysis, areas of GM decrease (in HD compared to controls) display GM loss above average (i.e., significantly less GM than estimated from global atrophy) whilst areas of GM increase display either GM gain or GM preservation (i.e., significantly more GM than estimated from global atrophy) (Good et al., 2001, 2002).

We applied a height threshold of $P < 0.05$ corrected with the family wise error and an extent threshold of $P < 0.05$ corrected (underlying voxel threshold, 0.001) (Friston et al., 1996). To visualize the extension of GM changes, significant clusters are displayed at a voxel threshold of $P < 0.001$.

Moreover, we investigated whether areas of relative GM preservation actually display absolute GM increase. For this purpose, we used the volume of

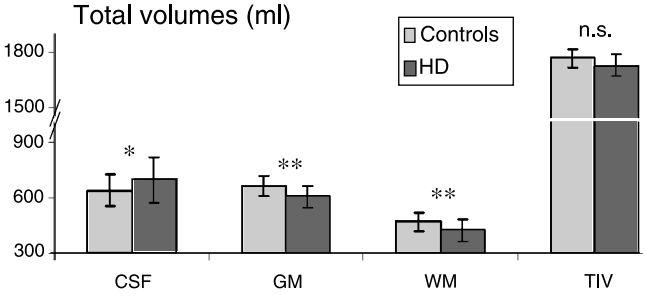

Fig. 1. Total volumes of HD patients and healthy controls. Total volumes of grey and white matter as well as cerebrospinal fluid (GM, WM, CSF) and total intracranial volume (TIV) are shown. Significance of the differences between both groups is indicated ($^{*}P < 0.05$; $^{**}P < 0.01$; *n.s.* not significant)

interest (VOI) function of SPM2 and extracted the raw values of each cluster (underlying voxel threshold, 0.001). These raw values were orthogonalized to brain size (TIV), sex, and MPRAGE sequence (using a Matlab routine). These orthogonalized data were compared between both groups with *t*-tests.

Finally, we investigated the influence of disease progression on the areas identified by our ANCOVA. In our sample of patients (Table 1), motor impairment significantly correlated with age (Spearman coefficient, 0.74; 2-sided *P* value, <0.001). Since different age-related changes between both groups had to be attributed to the progression of HD, we performed an interaction analysis of age with group. For this purpose, the extracted and orthogonalized values of each cluster (of all 96 participants) were fed in a step wise regression analysis (Statistical Package for the Social Sciences software (SPSS); version, 12.0.1; Chicago, Illinois, USA) as dependent variable. Age, group (controls, −1; HD, 1) and the interaction of age and group (product of age and group) served as independent variables.

Voxels included in the analyses

Accounting for possible misclassification of GM throughout the basal ganglia, we included all voxels of the caudate and lentiform nucleus (defined with the Wake Forest University (WFU)-Pick Atlas) (Maldjian et al., 2003). Apart from these regions, we included only voxels with a GM value greater than 0.2 (maximum value: 1) and greater than both the WM and CSF value in order to analyze only voxels with sufficient GM and to avoid possible edge effects around the border between GM, WM, and CSF.

Results

GM loss (Fig. 2, blue color; Table 2) was identified bilaterally in the striatum, thalamus, and insula. Further more, dorsolateral frontal regions as well as parietal and occipital regions displayed GM decrease. Accordingly, GM values of all clusters of GM loss were significantly lower in the HD group (2-sided *P* values, <0.001). Moreover, GM values of all clusters of GM loss showed significant interaction of group and age (2-sided *P* values, <0.001).

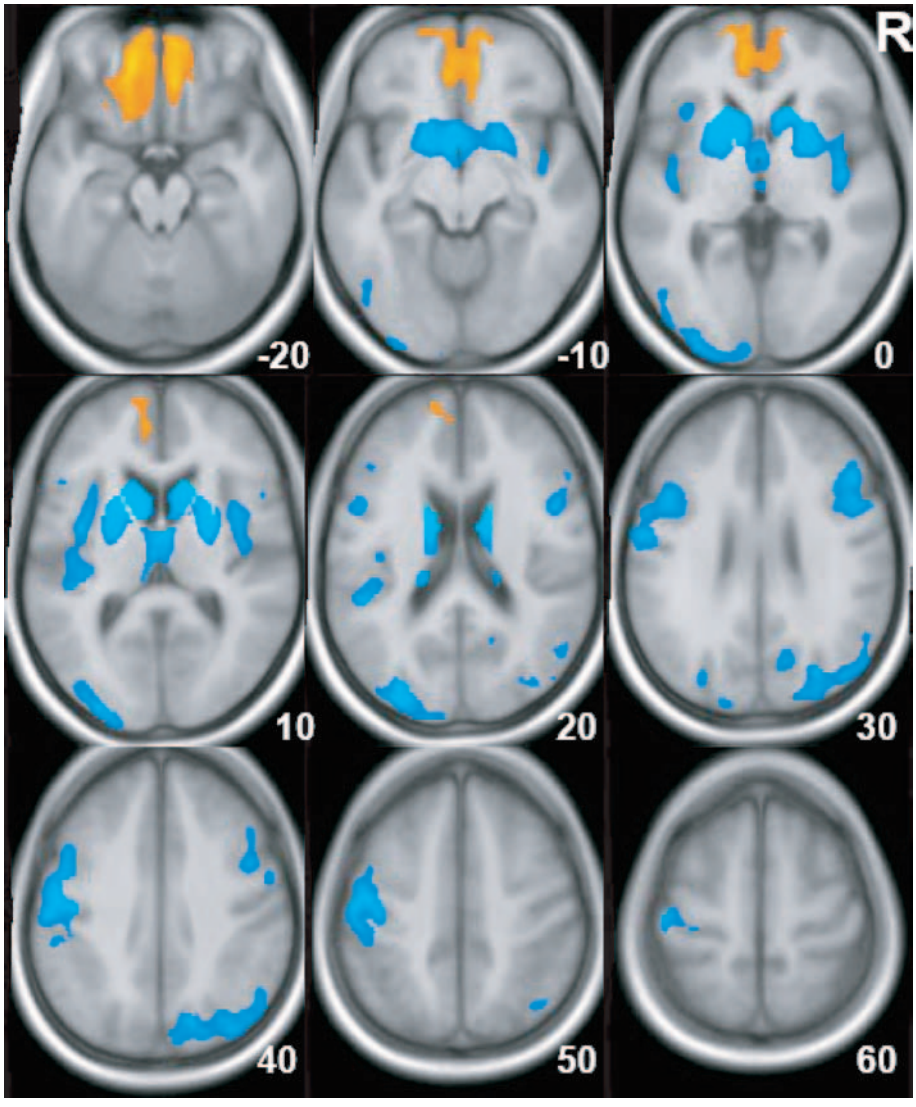

Fig. 2. Grey-matter changes in HD. At a voxel threshold of $P < 0.001$, significant GM changes throughout the whole brain are projected onto the study-specific averaged T1-image (orange color, GM preservation; blue color, GM loss). Increasing significance is color coded from dark to light. The right side of the image shows the right hemisphere. According to the Montreal Neurological Institute (MNI) standard brain, coordinates (Z axis) of axial slices are indicated in the right lower corner of each panel. Only clusters with a peak value of $P < 0.05$ corrected (Friston et al., 1996) and an extent threshold of $P < 0.05$ corrected at the cluster level (18) are shown

Table 2. *Areas of grey-matter changes in early Huntington disease*

Cluster size in voxels (1 × 1 × 1 mm)	MNI coordinates			Z values of peak voxels	Area
	x	y	z		
Grey-matter decrease					
51638	−11	10	6	>7.5	L caudate body
	15	19	10	>7.5	R caudate body
	−15	16	6	>7.5	L caudate head
	−18	12	6	>7.5	L putamen
	25	7	8	7.5	R putamen
	−39	−2	11	5.0	L insula
	42	−10	−2	5.2	R insula
	−2	−16	12	4.7	L thalamus
	3	−1	8	4.9	R thalamus
	−3	7	−11	5.2	L ventral striatum/subcallosal area
	15	4	−13	5.1	R ventral striatum/subcallosal area
	48	23	30	5.4	R frontal lobe, middle frontal g., BA46
	49	10	22	4.9	R frontal lobe, inferior frontal g., BA44
	43	10	35	4.8	R frontal lobe, middle frontal g., BA9
	50	10	28	4.8	R frontal lobe, inferior frontal g., BA9
16300	−46	13	32	5.4	L frontal lobe, middle frontal g., BA9
	−51	7	23	4.5	L frontal lobe, inferior frontal g., BA44
	−45	33	15	3.2	L frontal lobe, inferior frontal g., BA46
	−48	−11	46	6.1	L frontal lobe, precentral g., BA4
	−55	−17	42	5.9	L parietal lobe, postcentral g., BA4
	−47	−31	15	4.2	L inferior parietal lobule, BA40
1265	−13	−72	26	4.9	L parietal lobe, precuneus, BA31
9953	−30	−90	18	6.0	L occ. lobe, middle occ. g., BA19
	−26	100	1	4.5	L occ. lobe, middle occ. g., BA18
	−14	−99	22	4.2	L occ. lobe, cuneus, BA19
	−48	−78	−4	3.8	L occ. lobe, inferior occ. g., BA18
	−47	−68	−11	3.3	L occ. lobe, middle occ. g., BA37
1489	15	−73	37	5.2	R parietal lobe, precuneus, BA7
	28	−86	28	4.5	R occ. lobe, cuneus, BA19
	51	−63	43	4.3	R inferior parietal lobule, BA40
	49	−72	35	4.0	R parietal lobe, angular g., BA39
	39	−63	53	4.0	R superior parietal lobule, BA7
Grey-matter preservation					
22357	−13	45	−22	6.1	L frontal lobe, orbital g., BA11
	8	51	−18	4.9	R frontal lobe, orbital g., BA11
	−5	33	−23	4.2	L frontal lobe, rectal g., BA11
	9	39	−18	5.5	R frontal lobe, rectal g., BA11
	−6	44	−5	4.9	L anterior cingulate, BA10
	4	44	−7	4.7	R anterior cingulate, BA10
	−7	48	9	4.0	L anterior cingulate, BA10
	17	61	4	4.7	R medial frontal g., BA10
	−8	62	13	3.8	L medial frontal g., BA10

BA Brodmann area; *g*. gyrus; *L* left; *occ*. occipital; *R* right.

GM increase (Fig. 2, orange color; Table 2) was identified bilaterally in the anterior cingulate and orbitofrontal cortex of BA 10 and 11 (Z value of peak voxel, 6.1; cluster size at the voxel threshold of $P < 0.001$, 22357 voxels). Direct comparison of absolute GM values derived from this cluster did not reveal significant differences (2-sided P value, >0.2) indicating relative GM preservation rather than absolute GM increase. Interaction analysis of group and age did not indicate that GM preservation within this area changes in the course of the HD stages under examination (2-sided P value, >0.2).

Discussion

In this study, both GM decrease and increase was investigated in HD. To estimate the influence of disease progression

on the areas identified by our analysis, we performed an interaction analysis of age with group. We decided to perform this interaction analysis since age was closely correlated with motor impairment (Table 1) although this does not certainly imply a similarly close correlation of age with progression of higher cortical function impairment.

GM decrease (Fig. 2, blue color; Table 2) was well in accordance with earlier morphometric studies (Kassubek et al., 2004a, 2005; Peinemann et al., 2005; Rosas et al., 2001, 2002, 2003, 2005). Subcortical GM decrease was pronounced in the dorsal striatum but also found in the ventral striatum and thalamus. At the cortical level, GM loss was found in the insula, in dorsolateral frontal areas as well as in parietal and occipital areas. Since HD is a neurodegenerative disease, we expected GM decrease to progress in the course of the disease. Accordingly, we demonstrated significant interaction of age and group.

In contrast, the anterior cingulate and orbitofrontal cortex displayed GM preservation (Fig. 2, orange color; Table 2). Here the interaction analysis did not indicate changes of GM preservation in the course of the HD stages under examination. Correspondingly, we are not aware of studies that demonstrated involvement of these cortical areas in early HD. However, in one study, serial 11C-raclopride PET scans were performed in 12 patients that, at the first scan, were in later HD stages than our patients. In this study, a decreased 11C-raclopride binding potential (BP) was reported that also reached Brodmann area (BA)10 (Pavese et al., 2003). Moreover, we cannot exclude that, in later stages of HD or in patients with a genetic load higher than that of our HD group, this region might atrophy and, this way, contribute to cognitive and emotional symptoms (Cummings, 1993; Litvan et al., 1998).

The coexistence of GM loss and GM preservation in frontal cortical areas points to differential involvement of these areas in the pathophysiology of HD. Different portions of the frontal lobe are integrated in different circuits that link cortex, basal ganglia and thalamus (Alexander and Crutcher, 1990). Several of these distinct circuits have been described and different distinctions have been made (Alexander and Crutcher, 1990; Joel, 2001). Joel proposed a division of the striatum in 3 ''split circuits'' (Joel, 2001) each of them involving different frontal areas: 1) the motor circuit includes the primary and supplementary motor cortices that project to the ''motor striatum'' (i.e., primarily the putamen); 2) within the associative circuit, the dorsolateral prefrontal cortex projects to the ''associative striatum'' (i.e., primarily the caudate); 3) the limbic circuit comprises the limbic prefrontal cortex and the ''limbic (ventral) striatum.'' Notably, both areas that displayed GM preservation in the present study, namely, the orbitofrontal cortex and anterior cingulate, belong to the limbic prefrontal cortex and, hence, to the limbic circuit. In accordance with our data, striatal degeneration is commonly assumed to progress from dorsal to ventral and, probably, from medial to lateral (Fig. 2: color of GM loss, blue; coding of increasing significance, from dark to light) (Vonsattel et al., 1985). Therefore, the primary involvement of the associative circuit and motor circuit as well as the preservation of the limbic circuit has been postulated in early HD (Joel, 2001). However, our data do not simply demonstrate involvement of frontal cortical areas as suggested by the respective part of the striatum (Voorn et al., 2004). Though to different degrees, both the dorsal and ventral striatum show GM loss but frontal cortical areas display inverse changes: whilst areas that are related to the associative and motor circuit display GM loss, parts of the limbic prefrontal cortex resist the process of GM loss in early HD. This differential involvement of frontal cortical areas may rely on interactions between the distinct subcortical frontal circuits. These circuits are not only 'closed circuits' but are also interconnected via 'open pathways' (Joel, 2001). Theoretically, interconnectivity of subcortical frontal circuits accommodates the coexistence of a variety of symptoms that are related to different circuits but result from damage to only one station of one circuit (Joel, 2001). Therefore cognitive and emotional symptoms could also occur as a result of functional disruptions within the limbic circuit in the absence of GM loss in the limbic prefrontal cortex.

Moreover, another two assumptions are compatible with our data. 1) A compensatory role of the anterior cingulate in early HD has been suggested since HD patients showed an increased activation of the anterior cingulate while learning motor sequences (Rosas et al., 2004). 2) An active role for the generation of ''hyperactive behaviors'' has been attributed to the orbitofrontal cortex. An ''excitatory subcortical output through the medial and orbitofrontal circuits'' has been proposed to result in excitatory stimulation of the supplementary motor and premotor cortices (Kulisevsky et al., 2001; Litvan et al., 1998). Accordingly, a projection from the limbic circuit to the motor areas of the motor circuit has been postulated. This ''open limbic route'' (Joel, 2001) might constitute the neuroanatomical basis of such an excitatory stimulation.

Acknowledgements

We are indebted to Thorleif Etgen who provided most of the data and images of the control group.

References

Alexander GE, Crutcher MD (1990) Functional architecture of basal ganglia circuits: neural substrates of parallel processing. Trends Neurosci 13: 266–271

Ashburner J, Friston KJ (2000) Voxel-based morphometry – the methods. Neuroimage 11: 805–821

Cummings JL (1993) Frontal-subcortical circuits and human behavior. Arch Neurol 50: 873–880

Folstein MF, Folstein SE, McHugh PR (1975) ''Mini-mental state''. A practical method for grading the cognitive state of patients for the clinician. J Psychiatr Res 12: 189–198

Friston KJ, Holmes A, Poline JB, Price CJ, Frith CD (1996) Detecting activations in PET and fMRI: levels of inference and power. Neuroimage 4: 223–235

Gardian G, Vecsei L (2004) Huntington's disease: pathomechanism and therapeutic perspectives. J Neural Transm 111: 1485–1494

Good CD, Johnsrude IS, Ashburner J, Henson RN, Friston KJ, Frackowiak RS (2001) A voxel-based morphometric study of ageing in 465 normal adult human brains. Neuroimage 14: 21–36

Good CD, Scahill RI, Fox NC, Ashburner J, Friston KJ, Chan D, Crum WR, Rossor MN, Frackowiak RS (2002) Automatic differentiation of anatomical patterns in the human brain: validation with studies of degenerative dementias. Neuroimage 17: 29–46

Graveland GA, Williams RS, DiFiglia M (1985) Evidence for degenerative and regenerative changes in neostriatal spiny neurons in Huntington's disease. Science 227: 770–773

Huntington's Disease Collaborative Research Group (1993) A novel gene containing a trinucleotide repeat that is expanded and unstable on Huntington's disease chromosomes. Cell 72: 971–983

Huntington Study Group (1996) Unified Huntington's Disease Rating Scale: reliability and consistency. Mov Disord 11: 136–142

Joel D (2001) Open interconnected model of basal ganglia-thalamocortical circuitry and its relevance to the clinical syndrome of Huntington's disease. Mov Disord 16: 407–423

Kassubek J, Juengling FD, Ecker D, Landwehrmeyer GB (2005) Thalamic atrophy in Huntington's disease co-varies with cognitive performance: a morphometric MRI analysis. Cereb Cortex 15: 846–853

Kassubek J, Juengling FD, Kioschies T, Henkel K, Karitzky J, Kramer B, Ecker D, Andrich J, Saft C, Kraus P, Aschoff AJ, Ludolph AC, Landwehrmeyer GB (2004b) Topography of cerebral atrophy in early Huntington's disease: a voxel based morphometric MRI study. J Neurol Neurosurg Psychiatry 75: 213–220

Kassubek J, Landwehrmeyer GB, Ecker D, Juengling FD, Muche R, Schuller S, Weindl A, Peinemann A (2004a) Global cerebral atrophy in early stages of Huntington's disease: quantitative MRI study. Neuroreport 15: 363–365

Kulisevsky J, Litvan I, Berthier ML, Pascual-Sedano B, Paulsen JS, Cummings JL (2001) Neuropsychiatric assessment of Gilles de la Tourette patients: comparative study with other hyperkinetic and hypokinetic movement disorders. Mov Disord 16: 1098–1104

Leegwater-Kim J, Cha JH (2004) The paradigm of Huntington's disease: therapeutic opportunities in neurodegeneration. NeuroRx 1: 128–138

Litvan I, Paulsen JS, Mega MS, Cummings JL (1998) Neuropsychiatric assessment of patients with hyperkinetic and hypokinetic movement disorders. Arch Neurol 55: 1313–1319

Maldjian JA, Laurienti PJ, Kraft RA, Burdette JH (2003) An automated method for neuroanatomic and cytoarchitectonic atlas-based interrogation of fMRI data sets. Neuroimage 19: 1233–1239

Oldfield RC (1971) The assessment and analysis of handedness: the Edinburgh inventory. Neuropsychologia 9: 97–113

Pavese N, Andrews TC, Brooks DJ, Ho AK, Rosser AE, Barker RA, Robbins TW, Sahakian BJ, Dunnett SB, Piccini P (2003) Progressive striatal and cortical dopamine receptor dysfunction in Huntington's disease: a PET study. Brain 126: 1127–1135

Peinemann A, Schuller S, Pohl C, Jahn T, Weindl A, Kassubek J (2005) Executive dysfunction in early stages of Huntington's disease is associated with striatal and insular atrophy: A neuropsychological and voxel-based morphometric study. J Neurol Sci 239: 11–19

Rosas HD, Feigin AS, Hersch SM (2004) Using advances in neuroimaging to detect, understand, and monitor disease progression in Huntington's disease. NeuroRx 1: 263–272

Rosas HD, Goodman J, Chen YI, Jenkins BG, Kennedy DN, Makris N, Patti M, Seidman LJ, Beal MF, Koroshetz WJ (2001) Striatal volume loss in HD as measured by MRI and the influence of CAG repeat. Neurology 57: 1025–1028

Rosas HD, Hevelone ND, Zaleta AK, Greve DN, Salat DH, Fischl B (2005) Regional cortical thinning in preclinical Huntington disease and its relationship to cognition. Neurology 65: 745–747

Rosas HD, Koroshetz WJ, Chen YI, Skeuse C, Vangel M, Cudkowicz ME, Caplan K, Marek K, Seidman LJ, Makris N, Jenkins BG, Goldstein JM (2003) Evidence for more widespread cerebral pathology in early HD: an MRI-based morphometric analysis. Neurology 60: 1615–1620

Rosas HD, Liu AK, Hersch S, Glessner M, Ferrante RJ, Salat DH, van der Kouwe A, Jenkins BG, Dale AM, Fischl B (2002) Regional and progressive thinning of the cortical ribbon in Huntington's disease. Neurology 58: 695–701

Shoulson I, Fahn S (1979) Huntington disease: clinical care and evaluation. Neurology 29: 1–3

Thieben MJ, Duggins AJ, Good CD, Gomes L, Mahant N, Richards F, McCusker E, Frackowiak RS (2002) The distribution of structural neuropathology in pre-clinical Huntington's disease. Brain 125: 1815–1828

Vonsattel JP, Myers RH, Stevens TJ, Ferrante RJ, Bird ED, Richardson EP Jr (1985) Neuropathological classification of Huntington's disease. J Neuropathol Exp Neurol 44: 559–577

Voorn P, Vanderschuren LJ, Groenewegen HJ, Robbins TW, Pennartz CM (2004) Putting a spin on the dorsal-ventral divide of the striatum. Trends Neurosci 27: 468–474

Movement Disorders
Vol. 22, No. 8, 2007, pp. 1169–1201

Brief Reports

Striatal Gray Matter Loss in Huntington's Disease Is Leftward Biased

Mark Mühlau, MD,[1]* Christian Gaser, PhD,[2] Afra M. Wohlschläger, PhD,[1,3,4] Adolf Weindl, MD,[1] Michael Städtler,[1] Michael Valet, MD,[1] Claus Zimmer, MD,[3] Jan Kassubek, MD,[5] and Alexander Peinemann, MD[1]

[1]Department of Neurology, Technische Universität München, Munich, Germany; [2]Department of Psychiatry, University of Jena, Jena, Germany; [3]Department of Neuroradiology and [4]Department of Nuclear Medicine, Technische Universität München, Munich, Germany; [5]Department of Neurology, University of Ulm, Ulm, Germany

Abstract: **In Huntington's disease (HD), the distribution of pathological changes throughout the brain is incompletely understood. Some studies have identified leftward-biased lateralization, whereas others did not. We performed magnetic resonance imaging and a voxel-based asymmetry analysis in 44 right-handed HD gene carriers (presymptomatic, n = 5; stage I, n = 28; stage II, n = 11) and 44 right-handed healthy controls. The group comparison revealed leftward-biased gray matter loss in the striatum. Further analyses showed no indication of asymmetry in presymptomatic HD patients but an increase in asymmetry in the course of the HD stages under examination. Our study demonstrates and discusses leftward-biased gray matter loss in HD.** © 2007 Movement Disorder Society

Key words: gray matter loss; Huntington's disease; lateralization, striatum; voxel-based morphometry

Huntington's disease (HD) is an autosomal dominant neurodegenerative disease. Since the discovery that HD results from an expanded CAG trinucleotide,[1] HD has become an attractive model for the study of neurodegeneration. However, the pathomechanisms that lead to the typical distribution of pathological changes throughout the brain (i.e., neuronal loss and astrocytosis primarily in the striatum) and the clinical picture of HD are poorly understood. The development of animal models has led to numerous discoveries related to the mutant gene product huntingtin; however, far from arriving at a unifying mechanism, robust evidence suggests that multiple — probably interacting — pathomechanisms occur in HD. Therefore, a comprehensive model of HD must account for multiple pathomechanisms and interactions and, in this way, explain the distribution of pathological changes throughout the brain. However, data on this distribution are conflicting, even with respect to the basic question of lateralization.[2,3] Addressing this issue, we performed a whole-brain asymmetry analysis in HD based on voxel-based morphometry (VBM).

VBM enables the detection of subtle structural changes throughout the brain at group level using magnetic resonance imaging (MRI). The main idea of VBM asymmetry analysis comprises the following steps: (1) spatial normalization of all images to a symmetric anatomical space to allow averaging; (2) segmentation of images into gray matter (GM), white matter (WM), as well as cerebrospinal fluid (CSF); (3) calculation of difference images using the lateralization index; and (4) group comparison of GM asymmetry across the whole brain.

SUBJECTS AND METHODS

Subjects

Data and images were derived from routine diagnostics of our HD outpatient clinic that participates in the European Huntington Disease Network (http://www.euro-hd.net/html/network) and from healthy volunteers who had participated in other imaging studies at our department. The HD group (women, 23) consisted of 44 gene-positive right-handed subjects (lateralization index, >70%).[4] Five patients were presymptomatic (Motor score of the Unified HD Rating Scale [mUHDRS], 0; Mini-Mental State Examination, > 26). There were 28 patients who were in stage I and 11 who were in stage II according to Shoulson and Fahn.[5] Further details on the HD group are given in Table 1.

Healthy controls were matched for age (within 2 yr) and sex in a pair-wise manner (right-handers, 44;

*Correspondence to: Dr. Mark Mühlau, Technische Universität München, Department of Neurology, Möhlstrasse 28, D-81675 München, Germany. E-mail: m.muehlau@neuro.med.tum.de

Received 2 March 2006; Revised 26 June 2006; Accepted 26 June 2006

Published online 29 March 2007 in Wiley InterScience (www.interscience.wiley.com). DOI: 10.1002/mds.21137

TABLE 1. *Characterization of the HD patients*

	Min.	Max.	Median	Mean	SD
Age[a]	24	68	42	45	11
Onset age[b]	24	62	40	42	10
Time since onset	0	14	4.0	4.4	3.7
MMSE	18	30	28	27	3.1
mUHDRS[a]	0	62	13	18	17
CAG[c]	40	49	43	44	2.4

[a]Age correlated significantly with mUHDRS (Spearman correlation coefficient, 0.74; two-sided *P* value, <0.001).

[b]Onset was defined as the occurrence of first motor symptoms.

[c]CAG repeats correlated significantly with onset age (Spearman correlation coefficient, −0.52; two-sided *P* value, 0.002).

CAG, number of CAG trinucleotide repeats; Max., maximum; Min., minimum; MMSE, Mini-Mental State Examination;[15] mUHDRS, Motor score of the Unified Hutington's Disease Rating Scale.[12]

women, 23; mean age, 44 yr; standard deviation of age, 9.1).

Magnetic Resonance Imaging

Each participant underwent MRI in the same scanner (magnetic field intensity, 1.5 Tesla; scanner, *Siemens Magnetom Symphony*; sequence, T1 magnetization prepared rapid gradient echo (MPRAGE); plane, sagittal; number of slices, 160; slice thickness, 1 mm; voxel size, $1 \times 1 \times 1$ mm^3; flip angle, 15 degrees; field of view, 256×256 mm). After 27 HD patients and their corresponding controls had undergone MRI (TR, 11.1 msec; TE, 4.3 msec; TI, 800 msec), *Siemens* performed a software upgrade by installing the "*syngo software*," which resulted in slightly different parameters of the standard MPRAGE sequence (TR, 8.9 msec; TE, 3.93 msec; TI, 800 msec). To certainly exclude an effect of this software upgrade, the sequence was included in each analysis as confounding covariate (see below). SPM2 software (Wellcome Department of Imaging Neuroscience Group, London, UK; http://www.fil.ion.ucl.ac.uk/spm) was applied for data processing.

Voxels Included in the Analyses

We included only voxels with a GM value greater than 0.2 (maximum value, 1) and greater than both the WM and CSF value to analyze only voxels with sufficient GM and to avoid possible edge effects around the border between GM, WM, and CSF. Accounting for possible misclassification of GM throughout the basal ganglia, we also included all voxels of the caudate and lentiform nucleus as defined with the Wake Forest University (WFU) -Pick Atlas.[6]

"Conventional" Optimized VBM Analysis

At first, we performed "conventional" VBM according to the "optimized" protocol[7] using study-specific prior probability maps, the modulation step, and a Gaussian kernel of 8 mm for smoothing. The values of the resulting images indicate the voxel-wise probability of GM and are commonly interpreted as absolute GM.[7] Voxel-by-voxel analysis of covariance (ANCOVA) was used to detect absolute GM differences between both groups. In this analysis, age, sex, total GM volume (derived from the first segmentation process), and MPRAGE sequence of each participant were included as confounding covariates. Using the family wise error,[8] we applied a height threshold of $P < 0.05$ corrected for multiple comparisons at the voxel level and an extent threshold of $P < 0.05$ corrected at the cluster level. The areas identified by the "conventional" VBM analysis were used as a region of interest (ROI) for the asymmetry analysis.

Asymmetry Analysis

The asymmetry analysis is an extension of VBM and has been validated and described in detail elsewhere.[9] In accordance with this analysis, we used a study-specific symmetric template and study-specific symmetric probability maps for GM, WM, and CSF. Otherwise, the preprocessing steps were identical to the "conventional" optimized VBM analysis described above. In an additional step before smoothing, we generated a new set of GM images by calculating a difference image (DI) for each participant. For this purpose, the original GM images (origGM) were flipped along the midsagittal plane (flipGM). Then, we calculated the lateralization index of each voxel by applying the following formula: DI = (origGM − flipGM) / (0.5 [origGM + flipGM]).

To compare the brain asymmetry of HD patients with that of healthy controls, we used the smoothed DIs of all 88 participants for ANCOVA (ROI, voxels identified by the "conventional" VBM analysis; height threshold, $P < 0.05$ corrected; extent threshold, $P < 0.05$ corrected).[8] Because GM decreases with age in healthy subjects, age should be included as a confounding covariate in "conventional" VBM analyses.[7] Because motor impairment significantly correlated with age (Spearman coefficient, 0.74; two-sided *P* value, < 0.001) in our sample of patients, we, at first, tested the necessity to include age as confounding covariate in our asymmetry analysis. For this purpose, we performed a regression analysis of asymmetry with age in the control group. As we did not find age-related asymmetry, we included only sex and MPRAGE sequence but not age as confounding covariates in the asymmetry analysis. The applied contrast *Controls > HD* indicates areas that, in HD, contain less GM compared to the corresponding areas of the other hemisphere while also controlling for the asymmetry of both the control group and MRI sequence.

Finally, we analyzed asymmetry with regard to increase in the course of the disease and performed a multiple regression analysis (with constant) of GM asymmetry with motor impairment as determined with mUHDRS (ROI, voxels identified by the asymmetry analysis; height threshold, 0.05 corrected; extent threshold, 0.05 corrected; additional regressors, sex and MPRAGE sequence). To examine whether lateralization already exists at the presymptomatic stage or emerges in the course of the disease, we used the volume of interest function of SPM2 and extracted the raw values of the cluster showing significant correlation with motor impairment from both the HD and control group. The values of the HD group were then plotted against the mUHDRS and compared to the 5th and 95th percentile of the control group.

RESULTS

In accordance with previous studies,[2,10,11] the "conventional" VBM analysis (Fig. 1A; Table 2) demonstrated GM loss in the HD group that was most prominent in the striatum. Furthermore, regions with GM loss were identified in the frontal, parietal, and occipital lobe (Table 2). The asymmetry analysis (Fig. 1B) showed highly significant leftward-biased striatal GM loss in HD patients. Peak voxels were located in the putamen and in the head of the caudate nucleus (coordinates according to the Montreal Neurological Institute [MNI], −16, 11, −1 and −8, 10, 6; *Z* values, 6.9 and 6.6). Within the predefined ROI of GM asymmetry, regression analysis of GM asymmetry with motor impairment revealed the left putamen (MNI coordinates of peak voxel, −20, 5, −2; *Z* value, 3.9; Fig. 1C, left panels). The raw values of the cluster derived from both the HD and control group are shown in Figure 2. Without masking, regression analysis of GM asymmetry with motor impairment yielded a cluster that is also localized in the putamen (MNI coordinates of peak voxel, −16, 11, −1; *Z* value, 6.9) but posteriorly extends outside the ROI (Fig. 1C, right panels).

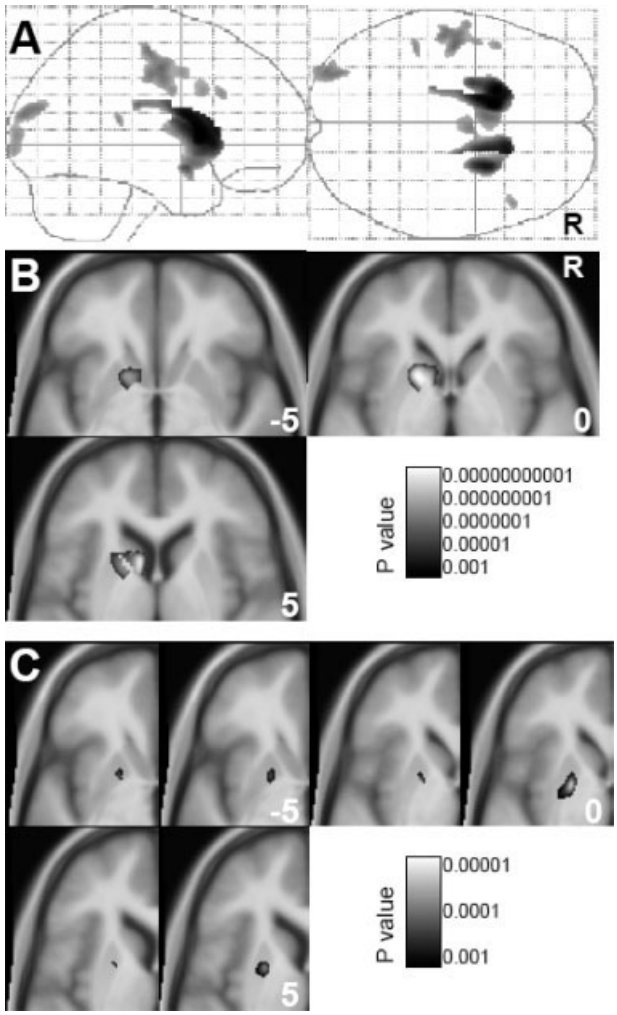

FIG. 1. Gray matter loss and its asymmetry in Huntington's disease. **A:** Shown are maximum intensity projections of gray matter (GM) decrease throughout the whole brain (height threshold, $P < 0.05$ corrected; extent threshold, $P < 0.05$ corrected; "conventional" voxel-based morphometry analysis). The right side of the images is indicated with "R". **B:** Gray matter asymmetry is projected onto axial slices of the study-specific averaged T1-image (region of interest [ROI], GM decrease as shown in A; height threshold, $P < 0.05$ corrected; extent threshold, $P < 0.05$ corrected). As indicated by the bar on the lower right, increasing significance is coded from black to white. According to the Montreal Neurological Institute standard brain, coordinates (*z* axis) of axial slices are indicated in the right lower corner of each slice. **C:** Correlation of GM asymmetry with the Motor score of the Unified Huntington's Disease Rating Scale is projected onto axial slices. Significant voxels of the predefined ROI (i.e., GM asymmetry as shown in B) are shown in the left panel of each slice, whereas the whole cluster that posteriorly extends outside the ROI is shown in the respective right panels.

DISCUSSION

In the present study, lateralization of pathological changes in HD throughout the whole brain was analyzed on a statistical basis. As we had no a priori hypothesis for asymmetries of areas apart from those displaying GM decrease (in HD compared to healthy controls), we first performed a "conventional" optimized VBM analysis (Fig. 1A) to derive a ROI for the asymmetry analysis. This asymmetry analysis revealed highly significant leftward-biased GM decrease in the striatum (Fig. 1B). In a further analysis, we investigated whether asymmetry of striatal GM loss changes in the course of the disease. For this purpose, we performed a regression analysis of asymmetry with motor impairment in the HD group. Again, we performed a ROI analysis because we had no a priori hypothesis for areas apart from that displaying

TABLE 2. *Areas of gray matter decrease in Huntington's disease*

Cluster size in voxels (1 × 1 × 1 mm)	MNI coordinates *x, y, z*	*Z* values of peak voxels	Area
10842	−11, 10, 7	<7.5	L caudate body
	−18, 12, 6	7.8	L putamen
	−15, 16, 6	7.6	L caudate head
	−17, 18, 2	7.6	L caudate head
	−24, −1, 14	6.9	L putamen
	−16, 6, 10	6.4	L putamen
	−14, 6, 6	6.1	L putamen
	−21, −25, 24	6.0	L caudate body
	−19, −18, 25	5.8	L caudate body
6608	15, 19, 10	7.5	R caudate body
	25, 7, 8	7.4	R putamen
	16, 5, 20	7.2	R caudate body
	18, −8, 25	6.4	R caudate body
	24, 13, −3	6.2	R putamen
	19, 6, 14	4.8	R putamen
	11, 19, 1	4.7	R caudate head
2997	−48, −11, 46	6.1	L frontal lobe, precentral g., BA4
	−53, −18, 56	5.9	L parietal lobe, postcentral g., BA3
	−55, −17, 41	5.8	L frontal lobe, postcentral g., BA4
1475	−30, −90, 18	5.9	L occ. lobe, middle occ. g., BA19
	−29, −83, 22	5.7	L occ. lobe, superior occ. g., BA19
	−31, −94, 5	5.4	L occ. lobe, middle occ. g., BA19
197	−44, −35, 14	5.4	L temp. lobe, superior temp. g., BA29
203	48, 23, 30	5.4	R frontal lobe, middle frontal g., BA46
239	−46, 13, 32	5.3	L frontal lobe, middle frontal g., BA9

MNI, Montreal Neurological Institute; BA, Brodmann area; g., gyrus; L, left; occ., occipital; R, right; temp., temporal.

GM asymmetry. In this way, leftward-biased GM loss was shown to significantly increase with motor impairment. In accordance with the primary role of the putamen in motor function, the respective cluster extended outside the ROI toward more posterior areas of the putamen (Fig. 1C). The comparison of the asymmetry values (derived from the cluster correlating with motor impairment) between the HD and control group (Fig. 2) indicated that leftward-biased striatal GM asymmetry is not present in presymptomatic HD but occurs with the development of symptoms.

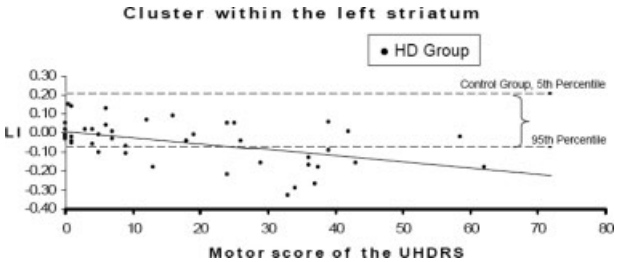

FIG. 2. Correlation of striatal asymmetry and motor impairment in Huntington's disease (HD). Asymmetry values (lateralization index, LI) of the HD group are plotted (black dots) against the motor score of the Unified Huntington's Disease Rating Scale (UHDRS; Spearman correlation coefficient, −0.45; two-sided *P* value, 0.002). For comparison, the 5th and 95th percentile of the respective values from the control group are indicated with dashed lines. Values were derived from the cluster (within the predefined region of interest) identified by the regression analysis of gray matter asymmetry with motor impairment.

So far, the only study reporting leftward-biased lateralization of pathological changes in HD on a statistical basis used MR spectroscopy. Jenkins and colleagues described a "curious" leftward-biased increase in lactate levels in the striatum. By the use of VBM, Thieben and associates[2] found GM decrease in the striatum bilaterally but this GM decrease showed "unexpected" asymmetry reaching only borderline significance on the right, whereas no particular analysis was performed to verify this leftward lateralization. In contrast, Kassubek and coworkers did not report leftward lateralization of GM loss but did not perform an asymmetry analysis either.[11]

The present study confirms the assumption that, in HD, pathological changes of the striatum are biased to the left (i.e., to the dominant hemisphere). This leftward biased GM asymmetry seems not to exist in presymptomatic stages of HD but to occur with symptoms (Fig. 2). Popular pathomechanisms that have been related to HD such as glutamatergic excitotoxicity[13] and mitochondrial dysfunction,[14] by nature, increase with neuronal activity. Therefore, we suggest that a surplus of cumulative life time activity in the left compared to the right striatum causes leftward-biased striatal GM loss in HD as also proposed by Jenkins and colleagues[3] and Thieben

and associates.[2] Such an asymmetry of overall striatal activity is well conceivable. All patients included in this study were right-handed; handedness displays the clearest example of behavioral lateralization, goes along with a more frequent use of the dominant hand and, hence, results in higher activity of cortical and subcortical motor areas of the dominant hemisphere. In future studies, left-handed HD patients should be investigated in presymptomatic and symptomatic stages to address the influence of handedness.

In summary, we evaluated the asymmetry of GM loss in HD and found leftward lateralization in the striatum. We propose that, primarily compatible with the pathomechanisms of excitotoxicity, a surplus of cumulative synaptic activity in the dominant striatum causes this leftward-biased GM loss.

REFERENCES

1. The Huntington's Disease Collaborative Research Group. A novel gene containing a trinucleotide repeat that is expanded and unstable on Huntington's disease chromosomes. Cell 1993;72:971–983.
2. Thieben MJ, Duggins AJ, Good CD, et al. The distribution of structural neuropathology in pre-clinical Huntington's disease. Brain 2002;125:1815–1828.
3. Jenkins BG, Rosas HD, Chen YC, et al. 1H NMR spectroscopy studies of Huntington's disease: correlations with CAG repeat numbers. Neurology 1998;50:1357–1365.
4. Oldfield RC. The assessment and analysis of handedness: the Edinburgh inventory. Neuropsychologia 1971;9:97–113.
5. Shoulson I, Fahn S. Huntington disease: clinical care and evaluation. Neurology 1979;29:1–3.
6. Maldjian JA, Laurienti PJ, Kraft RA, Burdette JH. An automated method for neuroanatomic and cytoarchitectonic atlas-based interrogation of fMRI data sets. Neuroimage 2003;19:1233–1239.
7. Good CD, Johnsrude IS, Ashburner J, Henson RN, Friston KJ, Frackowiak RS. A voxel-based morphometric study of ageing in 465 normal adult human brains. Neuroimage 2001;14:21–36.
8. Friston KJ, Holmes A, Poline JB, Price CJ, Frith CD. Detecting activations in PET and fMRI: levels of inference and power. Neuroimage 1996;4:223–235.
9. Luders E, Gaser C, Jancke L, Schlaug G. A voxel-based approach to gray matter asymmetries. Neuroimage 2004;22:656–664.
10. Rosas HD, Koroshetz WJ, Chen YI, et al. Evidence for more widespread cerebral pathology in early HD: an MRI-based morphometric analysis. Neurology 2003;60:1615–1620.
11. Kassubek J, Juengling FD, Kioschies T, et al. Topography of cerebral atrophy in early Huntington's disease: a voxel based morphometric MRI study. J Neurol Neurosurg Psychiatry 2004; 75:213–220.
12. Huntington Study Group. Unified Huntington's Disease Rating Scale: reliability and consistency. Mov Disord 1996;11:136–142.
13. DiFiglia M. Excitotoxic injury of the neostriatum: a model for Huntington's disease. Trends Neurosci 1990;13:286–289.
14. Schapira AH. Mitochondrial function in Huntington's disease: clues for pathogenesis and prospects for treatment. Ann Neurol 1997;41:141–142.
15. Folstein MF, Folstein SE, McHugh PR. "Mini-mental state". A practical method for grading the cognitive state of patients for the clinician. J Psychiatr Res 1975;12:189–198.

Myoclonus–Dystonia Syndrome With Severe Depression Is Caused by an Exon-Skipping Mutation in the ε-Sarcoglycan Gene

Anjum Misbahuddin, MRCP,[1] Mark Placzek, BSc,[1] Graham Lennox, FRCP,[2] Jan-Willem Taanman,[1] and Thomas T. Warner, FRCP[1]*

[1]Department of Clinical Neurosciences, Royal Free and University College Medical School, London, United Kingdom; [2]Department of Neurology, Addenbrookes Hospital, Cambridge, United Kingdom

Abstract: **We describe two affected individuals in a family with myoclonus–dystonia syndrome complicated with severe depression. One individual committed suicide. Molecular genetic analysis revealed a heterozygous point mutation in the ε-sarcoglycan gene, which we show leads to skipping of exon 5. This report suggests that the psychiatric spectrum of MDS includes more severe depression.** © 2007 Movement Disorder Society

Key words: myoclonus–dystonia syndrome; depression; ε-sarcoglycan mutation; exon skipping

Myoclonus–dystonia syndrome (MDS; OMIM 159900) is an autosomal dominant condition characterized by myoclonic jerks affecting the upper body and focal or segmental dystonia (e.g., cervical dystonia, writer's cramp).[1] Myoclonus affects proximal more than distal muscles and can be action-induced. Symptoms are often ameliorated by alcohol. There is also an association with obsessive–compulsive disorder, anxiety, and panic attacks.[1–3] These features are felt to be primary manifestations of the disease. Alcohol and benzodiazepine abuse is seen and thought to be secondary to use in alleviating symptoms.

This autosomal dominant disorder is caused by heterozygous mutations in the ε-sarcoglycan gene (*SGCE*) on chromosome 7q21.[4] MDS is 30% to 40% penetrant with evidence of maternal imprinting,[5] and RT-PCR has revealed expression of only the paternal allele in lymphocytes in most cases studied.[6] Numerous different mutations have been described in exons 2 to 9 in *SGCE*[4,7–10] and usually result in a truncated protein either

*Correspondence to: Dr. Thomas T. Warner, Department of Clinical Neurosciences, Royal Free and University College Medical School, Rowland Hill Street, London NW3 2PF, United Kingdom. E-mail: t.warner@medsch.ucl.ac.uk

Received 30 March 2006; Revised 9 September 2006; Accepted 10 September 2006

Published online 17 January 2007 in Wiley InterScience (www.interscience.wiley.com). DOI: 10.1002/mds.21297

PAPER

Bilateral grey-matter increase in the putamen in primary blepharospasm

T Etgen, M Mühlau, C Gaser, D Sander

J Neurol Neurosurg Psychiatry 2006;**77**:1017–1020. doi: 10.1136/jnnp.2005.087148

See end of article for authors' affiliations

Correspondence to: T Etgen, Department of Neurology, Klinikum Traunstein, Cuno-Niggl-Strasse 3, D-83278 Traunstein, Germany; thorleif.etgen@klinikum-traunstein.de

Received 27 December 2005
Revised version received 24 April 2006
Accepted 29 April 2006
Published Online First 11 May 2006

Background: Primary blepharospasm is a focal dystonia characterised by excessive involuntary closure of the eyelids. The pathophysiology of primary blepharospasm is unresolved.
Aim: To pinpoint grey-matter changes that are associated with primary blepharospasm.
Methods: 16 right-handed patients with primary blepharospasm (mean age 67.4 (SD 4.3) years; 12 women) were compared with 16 healthy volunteers matched for sex and age. High-resolution T1-weighted magnetic resonance imaging of each participant was obtained and analysed by voxel-based morphometry, a method to detect regionally specific differences in grey matter between patients and control group. To evaluate whether the identified grey-matter changes were correlated with the duration of primary blepharospasm or botulinum neurotoxin treatment (BoNT), separate regression analyses were carried out.
Results: In patients with primary blepharospasm, grey-matter increase in the putamina was observed, whereas regression analyses did not indicate a correlation between grey-matter increases and the duration of primary blepharospasm or BoNT. Grey-matter decrease was detected in the left inferior parietal lobule; here regression analyses of grey-matter decrease showed a significant ($p=0.013$) correlation of grey-matter decrease with the duration of BoNT.
Conclusions: The data suggest structural changes in primary blepharospasm and point to a crucial role of the putamen for the pathophysiology of this focal dystonia.

Blepharospasm is a common neurological disorder with a prevalence between 12 and 133 per million.[1] This focal dystonia is characterised by excessive involuntary closure of the eyelids, typically caused by spasms of the orbicularis oculi muscles. Primary blepharospasm is a disorder in which dystonia is the only clinical sign, without any identifiable exogenous cause or other inherited or degenerative disease. Accordingly, no lesions can be detected on routine magnetic resonance imaging (MRI). By contrast, secondary blepharospasm is an identifiable disorder and associated lesions have been documented in the basal ganglia, diencephalon, brain stem and cerebellum.[2–6]

The pathophysiology of primary blepharospasm is unclear. Therefore, we aimed at pinpointing grey-matter changes that are associated with primary blepharospasm. We compared a group of patients with a control group, matched for sex and age, using voxel-based morphometry (VBM), a method that allows averaging high-resolution MRI on people and hence comparisons at the group level.

VBM has been cross validated with region-of-interest measurements[7–9] and several studies have shown that structural changes identified by VBM are directly related to functional changes in brain activity.[10 11] Moreover, VBM has proved to be a powerful method in detecting regional differences in cerebral structure in various disorders such as narcolepsy,[12] restless legs syndrome,[13] idiopathic cervical dystonia[14] and focal hand dystonia.[15]

PARTICIPANTS AND METHODS

Patients and controls

Diagnosis of primary blepharospasm was established by a detailed history and a neurological examination carried out by an expert neurologist of our outpatient clinic for movement disorders (Department of Neurology, Technische Universität München, München, Germany). The severity of primary blepharospasm was assessed with the Blepharospasm Disability Scale and the Severity Rating Scale.[16] Secondary forms of blepharospasm were excluded by history, clinical examination, laboratory tests and neuroimaging. The 16 patients included were right-handed with primary blepharospasm. Table 1 summarises the demographic and clinical details.

All patients had no neurological abnormalities except for primary blepharospasm and were on regular botulinum neurotoxin treatment (BoNT). The 16 right-handed healthy controls were matched for age and sex. The study was carried out according to the *Declaration of Helsinki* and all participants had given prior written informed consent.

Data acquisition

High-resolution structural data were acquired on a 1.5-T Siemens Magnetom Symphony scanner (Erlangen, Germany) (standard two-channel birdcage head coil; magnetisation-prepared rapid gradient echo sequence; sagittal slices 160; repetition time (TR) 11.1 ms; echo time (TE) 4.3 ms; flip angle 15°; matrix size 224× 256 mm; voxel size 1×1×1 mm). A neuroradiologist, who was blinded to the study, detected neither abnormal nor unusual findings in all the screened images.

Image processing

VBM comprises the following steps:

- Spatial normalisation of all images to a standardised anatomical space to allow for spatial averaging
- Segmentation of images into grey and white matter as well as cerebrospinal fluid

Abbreviations: BoNT, botulinum neurotoxin treatment; FDG, ^{18}F-deoxyglucose; fMRI, functional magnetic resonance imaging; VBM, voxel-based morphometry

Table 1 Demographic data of patients with primary blepharospasm and controls

	Patients	Controls
Women:men	12:4	12:4
Age (years)	67.4 (4.3)	65.3 (4.9)
Duration of PB (years)	6.5 (4.9)	NA
Age at onset of PB (years)	61.5 (7.1)	NA
Time from last BoNT (days)	39.9 (30.2)	NA
BDS at onset of PB	9.5 (3.3)	NA
SRS at onset of PB	1.9 (1.0)	NA
Duration of BoNT (years)	3.0 (3.2)	NA

Values are given as mean (SD).
BDS, Blepharospasm Disability Scale (0–26); BoNT, botulinum neurotoxin treatment; NA, not applicable; PB, primary blepharospasm; SRS, Severity Rating Scale (0–4).

- Group comparison of local grey-matter values across the whole brain.[17]

We used standard statistical parametric mapping software (SPM2, Wellcome Department of Cognitive Neurology, London, UK) to preprocess and analyse our data.[18–20] Image preprocessing was carried out according to the optimised protocol described by Good *et al*.[21] The resulting grey-matter images were smoothed with a Gaussian kernel of 12 mm full-width at half-maximum.

Voxel-by-voxel analysis of covariance was used to detect grey-matter differences between the groups. In this analysis, we used the age of each participant as a covariate to control for age-related effects. To avoid edge effects around the border between grey and white matter, we excluded all voxels with a grey-matter value <0.1 (maximum value 1.0). We thresholded our results at a height threshold of $p<0.001$ uncorrected and, additionally, at an extent threshold of $p<0.05$, uncorrected (cluster level).[22] To evaluate whether the identified grey-matter changes were correlated with the duration of primary blepharospasm or BoNT, we carried out separate regression analyses. For this purpose, we extracted the raw values of each significant cluster (using the volume-of-interest function of SPM2). These raw values were fed as separate regression analyses (SPSS V.12.0.1). Grey-matter increases were controlled for a positive correlation, whereas grey-matter decreases were controlled for a negative correlation.

RESULTS

Grey-matter increase was identified in the right ($Z = 4.5$) and left ($Z = 4.2$) putamen (fig 1). In both clusters of grey-matter increase, regression analyses for the duration of primary blepharospasm and BoNT showed values of $p>0.7$ and, hence, did not indicate a correlation of the grey-matter increases with the duration of primary blepharospasm or BoNT.

Grey-matter decrease (fig 2) was found in the left inferior parietal lobule ($Z = 4.7$). Here regression analyses showed a trend towards a correlation of grey-matter decrease with the duration of primary blepharospasm ($p = 0.12$) and a significant correlation of grey-matter decrease with the duration of BoNT ($p = 0.013$; fig 3).

DISCUSSION

This study aimed at localising cerebral structures that play a crucial part in the pathophysiology of primary blepharospasm. By using VBM, we identified a bilateral grey-matter increase in the putamen and a grey-matter decrease in the left inferior parietal lobule.

Our finding of grey-matter increase in the putamen is consistent with other reports of striatal association with the pathophysiology of primary blepharospasm.

Animal models indicate an association of striatal structures with the pathogenesis of focal dystonias. In rhesus monkeys, unilateral lesions in the posterior putamen produce dystonia.[23] In a rat model, spasms of the lid-closing orbicularis oculi muscle similar to those found in primary blepharospasm are caused by the combination of a small depletion in striatal dopamine and slight weakening of the orbicularis oculi muscle.[24]

Studies on human lesions of secondary blepharospasm point to different regions including the basal ganglia, diencephalon, brain stem and cerebellum.[2–6] In idiopathic focal dystonia, conventional imaging showed changes in signal intensity in the putamen or globus pallidus, without gross radiological pathology.[25 26]

Some, but not all, neuroimaging studies suggest association of the putamen with the pathophysiology of primary blepharospasm. In a positron emission tomography (PET) study on patients with primary blepharospasm and hand dystonia, the in vivo binding of the dopaminergic radioligand (fluorine-18) spiperone was measured in the putamina and found to be decreased compared with that in unaffected controls.[27] ^{18}F-deoxyglucose (FDG)-PET and functional magnetic resonance imaging (fMRI) studies yielded conflicting results. In one FDG-PET study, patients with primary blepharospasm had hypermetabolism during wakefulness in the cerebellum and pons and hypometabolism during sleep in superior–medial frontal regions.[28] In contrast, another

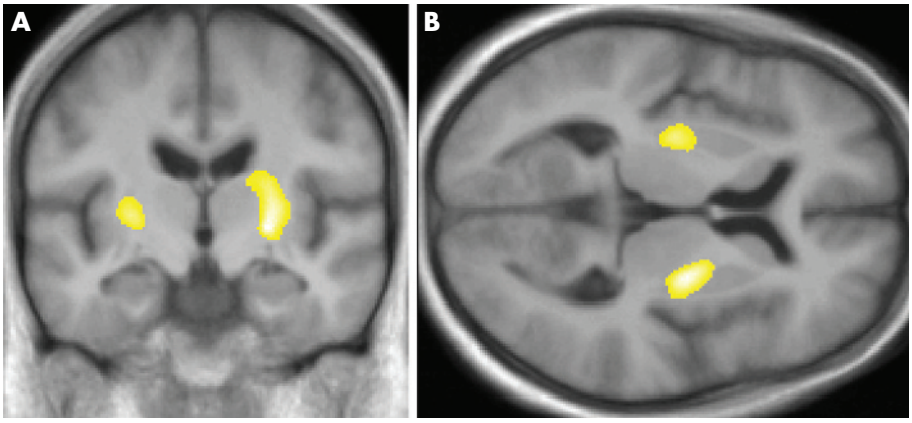

Figure 1 Grey-matter increase bilaterally in the putamen ($Z = 4.5$ on the right; Montreal Neurological Institute (MNI) coordinates: $x = 25$, $y = -8$, $z = 6$. $z = 4.2$; Z value, 4.2 on the left; MNI coordinates: $x = -26$, $y = -13$, $z = 4$). Results are projected on (A) coronal and (B) axial slices of the study-specific averaged T1-image in a standard stereotactic space derived from all the 32 study participants.

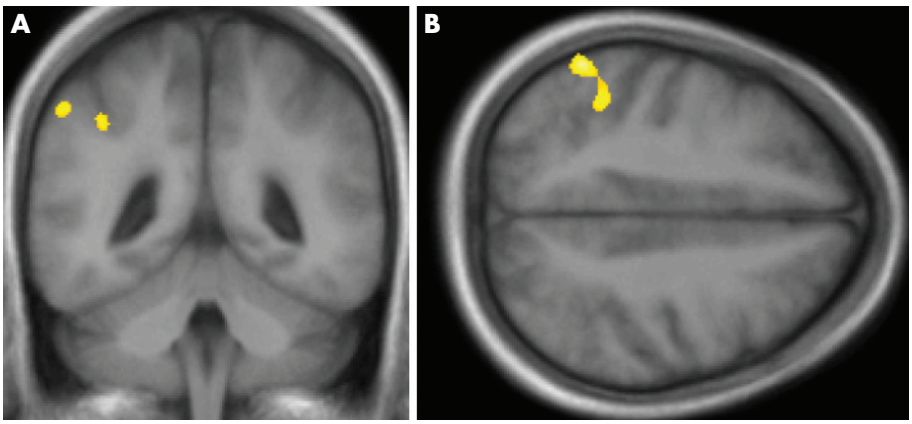

Figure 2 Grey-matter decrease in the left inferior parietal lobule (Z = 4.7; MNI coordinates: x = −55, y = −51, z = 49). Results are projected on (A) coronal and (B) axial slices of the study-specific averaged T1-image.

FDG-PET study showed striatal and thalamic hypermetabolism in patients with primary blepharospasm.[29] Using fMRI, one group reported a greater activation of the anterior visual cortex, anterior cingulate cortex, primary motor cortex, central region of the thalamus and superior cerebellum during spontaneous and voluntary blinking in patients with primary blepharospasm than in controls,[30] whereas another group compared spasms of the orbicularis oculi muscle in patients with primary blepharospasm with voluntary eye blinks of healthy controls and, notably, found spasms of the orbicularis oculi muscles in patients with primary blepharospasm accompanied by putaminal activation exactly at the site of grey-matter increase shown by our study.[31] In summary, several lines of evidence suggest a crucial role of the putamen in the pathophysiology of primary blepharospasm, which is confirmed by our structural data.

A functional putaminal change has been proposed that leads to a disturbance in the resistance of the blink system to environmental triggers and hence to lid spasms.[32] Such a functional putaminal change may go along with an increased number of neurones or synapses and, hence, grey-matter increase as shown by our VBM study. The neuronal correlate of changes in grey matter detectable by VBM is, however, unknown. An alternative explanation has been proposed in a VBM study on another focal dystonia (idiopathic cervical dystonia).[14] Here, changes in grey matter were seen as a result of neuronal plasticity—that is, synaptic remodelling that follows excessive involuntary movements. The major difficulty interpreting not only VBM but also PET and fMRI studies on primary blepharospasm remains the question, whether the putaminal changes reflect the primary cause or the secondary consequences of primary blepharospasm including its treatment.

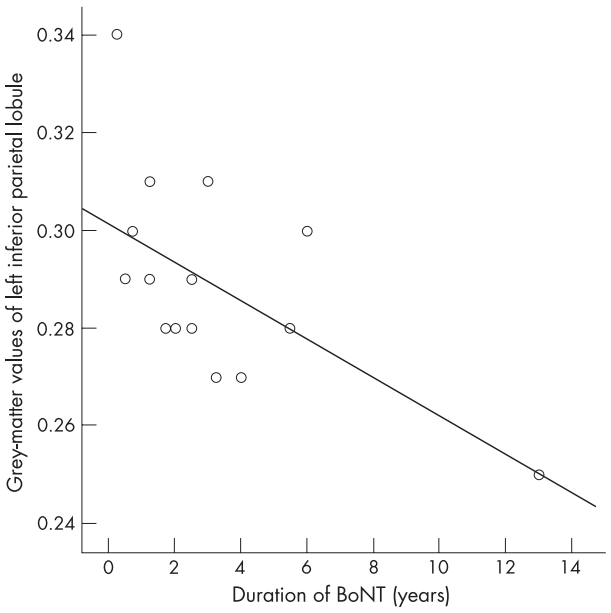

Figure 3 Regression analysis of the correlation between grey-matter values of the left inferior parietal lobule and the duration of botulinum neurotoxin treatment (BoNT).

We, however, assume that the grey-matter increase shown by our study is more likely to reflect a primary putaminal alteration for the following reason: the patients included in our study varied with regard to the duration of primary blepharospasm and duration of BoNT (table 1). If these variables were considerably related to the grey-matter increase of the putamina, we would expect at least some correlation of this increase with the duration of primary blepharospasm or BoNT, but none of the respective regression analyses showed even a trend towards such a correlation. Longitudinal studies on patients with primary blepharospasm may help to finally resolve this question.

Moreover, we found grey-matter decrease in the left inferior parietal lobule in primary blepharospasm. Several case studies have reported unilateral dystonia contralateral to parietal lesions,[33–35] but we are not aware of unilateral parietal lesions resulting in a symmetric dystonia such as blepharospasm. The finding of grey-matter decrease in the parietal region only on the left side indicates the involvement of functions that are primarily related to the left parietal cortex. Accordingly, cortical sensory processing, which may be presented in the parietal cortex in a leftward-biased manner, has been postulated to be abnormal in dystonia.[36 37] Several further functions have, however, been related to the parietal cortex in a leftward-biased manner (eg, motor attention and movement selection,[38] integration of time and space,[39] and imitation[40]). Therefore, it is also conceivable that frequent spasms of the eye-closing orbicularis oculi muscles as present in primary blepharospasm lead to neuroplastic changes detectable by VBM.[10 11] In fact, our data point in this direction, as regression analyses showed a trend towards correlation of the grey-matter decrease with the duration of primary blepharospasm and a significant correlation with the duration of the BoNT. Therefore, we conclude that the grey-matter decrease in the left inferior parietal lobule is more likely to reflect a secondary cause rather than the primary cause of primary blepharospasm.

Our data suggest in vivo morphological changes in the putamen in primary blepharospasm and, hence, support the hypothesis of a pivotal role for the putamen in the pathophysiology of this focal dystonia.

ACKNOWLEDGEMENTS

TE and his colleagues from the Department of Neurology (Technische Universität München) were supported by KKF-Fond 766160. We thank JP Rauschecker for reading an earlier version of this manuscript.

Authors' affiliations

T Etgen, M Mühlau, D Sander, Department of Neurology, Technische Universität München, München, Germany
C Gaser, Department of Psychiatry, University of Jena, Jena, Germany

Competing interests: None declared.

REFERENCES

1 **Hallett M**. Blepharospasm: recent advances. *Neurology* 2002;**59**:1306–12.
2 **Grandas F**, Lopez-Manzanares L, Traba A. Transient blepharospasm secondary to unilateral striatal infarction. *Mov Disord* 2004;**19**:1100–2.
3 **Jankovic J**, Patel SC. Blepharospasm associated with brainstem lesions. *Neurology* 1983;**33**:1237–40.
4 **Larumbe R**, Vaamonde J, Artieda J, *et al*. Reflex blepharospasm associated with bilateral basal ganglia lesion. *Mov Disord* 1993;**8**:198–200.
5 **Lee MS**, Marsden CD. Movement disorders following lesions of the thalamus or subthalamic region. *Mov Disord* 1994;**9**:493–507.
6 **Verghese J**, Milling C, Rosenbaum DM. Ptosis, blepharospasm, and apraxia of eyelid opening secondary to putaminal hemorrhage. *Neurology* 1999;**53**:652.
7 **Mummery CJ**, Patterson K, Price CJ, *et al*. A voxel-based morphometry study of semantic dementia: relationship between temporal lobe atrophy and semantic memory. *Ann Neurol* 2000;**47**:36–45.
8 **Vargha-Khadem F**, Watkins K, Price C, *et al*. Neural basis of an inherited speech and language disorder. *Proc Natl Acad Sci USA* 1998;**95**:12695–700.
9 **Woermann F**, Free S, Koepp M, *et al*. Voxel-by-voxel comparison of automatically segmented cerebral gray matter—a rater-independent comparison of structural MRI in patients with epilepsy. *Neuroimage* 1999;**10**:373–84.
10 **Gaser C**, Schlaug G. Brain structures differ between musicians and non-musicians. *J Neurosci* 2003;**23**:9240–5.
11 **Draganski B**, Gaser C, Busch V, *et al*. Neuroplasticity: changes in grey matter induced by training. *Nature* 2004;**427**:311–2.
12 **Draganski B**, Geisler P, Hajak G, *et al*. Hypothalamic gray matter changes in narcoleptic patients. *Nat Med* 2002;**8**:1186–8.
13 **Etgen T**, Draganski B, Ilg C, *et al*. Bilateral thalamic gray matter changes in patients with restless legs syndrome. *Neuroimage* 2005;**24**:1242–7.
14 **Draganski B**, Thun-Hohenstein C, Bogdahn U, *et al*. ''Motor circuit'' gray matter changes in idiopathic cervical dystonia. *Neurology* 2003;**61**:1228–31.
15 **Garraux G**, Bauer A, Hanakawa T, *et al*. Changes in brain anatomy in focal hand dystonia. *Ann Neurol* 2004;**55**:736–9.
16 **Fahn S**. The assessment of the primary dystonias. In: Munsat T, ed. *The quantification of neurologic deficit*. Boston: Butterworths, 1989:242–5.
17 **Ashburner J**, Friston KJ. Voxel-based morphometry—the methods. *Neuroimage* 2000;**11**:805–21.
18 **Ashburner J**, Friston K. Multimodal image coregistration and partitioning—a unified framework. *Neuroimage* 1997;**6**:209–17.
19 **Friston KJ**, Holmes A, Poline JB, *et al*. Statistic parametric maps in functional imaging: a general linear approach. *Hum Brain Mapp* 1995;**2**:189–210.
20 **Wright IC**, McGuire PK, Poline JB, *et al*. A voxel-based method for the statistical analysis of gray and white matter density applied to schizophrenia. *Neuroimage* 1995;**2**:244–52.
21 **Good CD**, Johnsrude IS, Ashburner J, *et al*. A voxel-based morphometric study of ageing in 465 normal adult human brains. *Neuroimage* 2001;**14**:21–36.
22 **Friston KJ**, Holmes A, Poline JB, *et al*. Detecting activations in PET and fMRI: levels of inference and power. *Neuroimage* 1996;**4**:223–35.
23 **Burns LH**, Pakzaban P, Deacon TW, *et al*. Selective putaminal excitotoxic lesions in non-human primates model the movement disorder of Huntington disease. *Neuroscience* 1995;**64**:1007–17.
24 **Schicatano EJ**, Basso MA, Evinger C. Animal model explains the origins of the cranial dystonia benign essential blepharospasm. *J Neurophysiol* 1997;**77**:2842–6.
25 **Iwata M**. MRI pathology of basal ganglia in dystonic disorders. *Adv Neurol* 1993;**60**:535–9.
26 **Schneider S**, Feifel E, Ott D, *et al*. Prolonged MRI T2 times of the lentiform nucleus in idiopathic spasmodic torticollis. *Neurology* 1994;**44**:846–50.
27 **Perlmutter JS**, Stambuk MK, Markham J, *et al*. Decreased [18F] spiperone binding in putamen in idiopathic focal dystonia. *J Neurosci* 1997;**17**:843–50.
28 **Hutchinson M**, Nakamura T, Moeller JR, *et al*. The metabolic topography of essential blepharospasm: a focal dystonia with general implications. *Neurology* 2000;**55**:673–7.
29 **Esmaeli-Gutstein B**, Nahmias C, Thompson M, *et al*. Positron emission tomography in patients with benign essential blepharospasm. *Ophthal Plast Reconstr Surg* 1999;**15**:23–7.
30 **Baker RS**, Andersen AH, Morecraft RJ, *et al*. A functional magnetic resonance imaging study in patients with benign essential blepharospasm. *J Neuroophthalmol* 2003;**23**:11–5.
31 **Schmidt KE**, Linden DE, Goebel R, *et al*. Striatal activation during blepharospasm revealed by fMRI. *Neurology* 2003;**60**:1738–43.
32 **Evinger C**, Perlmutter JS. Blind men and blinking elephants. *Neurology* 2003;**60**:1732–3.
33 **Nobbe FA**, Krauss JK. Subdural hematoma as a cause of contralateral dystonia. *Clin Neurol Neurosurg* 1997;**99**:37–9.
34 **Burguera JA**, Bataller L, Valero C. Action hand dystonia after cortical parietal infarction. *Mov Disord* 2001;**16**:1183–5.
35 **Khan AA**, Sussman JD. Focal dystonia after removal of a parietal meningioma. *Mov Disord* 2004;**19**:714–6.
36 **Tinazzi M**, Frasson E, Polo A, *et al*. Evidence for an abnormal cortical sensory processing in dystonia: selective enhancement of lower limb P37–N50 somatosensory evoked potential. *Mov Disord* 1999;**14**:473–80.
37 **Tinazzi M**, Priori A, Bertolasi L, *et al*. Abnormal central integration of a dual somatosensory input in dystonia. Evidence for sensory overflow. *Brain* 2000;**123**:42–50.
38 **Rushworth MF**, Johansen-Berg H, Gobel SM, *et al*. The left parietal and premotor cortices: motor attention and selection. *Neuroimage* 2003;**20**(Suppl 1):S89–100.
39 **Assmus A**, Marshall JC, Ritzl A, *et al*. Left inferior parietal cortex integrates time and space during collision judgments. *Neuroimage* 2003;**20**(Suppl 1):S82–8.
40 **Mühlau M**, Hermsdörfer J, Goldenberg G, *et al*. Left inferior parietal dominance in gesture imitation: an fMRI study. *Neuropsychologia* 2005;**43**:1086–98.

Cerebral Cortex September 2006;16:1283–1288
doi:10.1093/cercor/bhj070
Advance Access publication November 9, 2005

Structural Brain Changes in Tinnitus

M. Mühlau[1], J. P. Rauschecker[2], E. Oestreicher[3], C. Gaser[4], M. Röttinger[5], A. M. Wohlschläger[1,5,6], F. Simon[1], T. Etgen[1], B. Conrad[1] and D. Sander[1]

[1]Department of Neurology, Technische Universität München, D-81675 München, Germany, [2]Department of Physiology and Biophysics, Georgetown University Medical Center, Washington, DC 20007, USA, [3]Department of Otolaryngology, Technische Universität D-81675 München, Germany, [4]Department of Psychiatry, University of Jena, Jena D-07740, Germany, [5]Department of Radiology, Technische Universität München, D-81675 München, Germany and [6]Nuklearmedizinische Klinik und Poliklinik, Technische Universität München, München D-81675, Germany

Tinnitus is a common but poorly understood disorder characterized by ringing or buzzing in the ear. Central mechanisms must play a crucial role in generating this auditory phantom sensation as it persists in most cases after severing the auditory nerve. One hypothesis states that tinnitus is caused by a reorganization of tonotopic maps in the auditory cortex, which leads to an over-representation of tinnitus frequencies. Moreover, the participation of the limbic system in generating tinnitus has been postulated. Here we aimed at identifying brain areas that display structural change in tinnitus. We compared tinnitus sufferers with healthy controls by using high-resolution magnetic resonance imaging and voxel-based morphometry. Within the auditory pathways, we found gray-matter increases only at the thalamic level. Outside the auditory system, gray-matter decrease was found in the subcallosal region including the nucleus accumbens. Our results suggest that reciprocal involvement of both sensory and emotional areas are essential in the generation of tinnitus.

Keywords: medial geniculate nucleus, nucleus accumbens, subcallosal area, tinnitus, voxel-based morphometry

Introduction

Tinnitus is a common and often debilitating hearing disorder (Lockwood and others 2002). In addition, the study of tinnitus is of considerable interest for the understanding of basic brain mechanisms of hearing, especially with regard to reorganization and plasticity in the adult brain. Tinnitus is referred to as a phantom sensation because sound is perceived in the absence of a physical sound source and, in this respect, has also been compared with phantom pain (Jastreboff 1990; Flor and others 1995; Mühlnickel and others 1998; Rauschecker 1999). Despite extensive research, the neural mechanisms that cause tinnitus remain largely hypothetical (Eggermont and Roberts 2004). Tinnitus often arises through aging or from loud-noise exposure, both of which lead to loss of hair cells in the inner ear and subsequent hearing impairment.

However, several findings challenge purely cochlear models of tinnitus: 1) Tinnitus persists in most cases after severing of the eighth cranial nerve following surgical treatment of acoustic neuroma (Wiegand and others 1996; Andersson and others 1997). 2) Many patients with hearing loss do not suffer from chronic tinnitus (Lockwood and others 2002). 3) Psychometrically measured tinnitus loudness hardly correlates with tinnitus-related distress (Henry and Meikle 2000) or outcome of the treatment (Jastreboff and others 1994). 4) Most people occasionally experience "ringing in their ears" not only after irritation of the auditory system, such as after listening to loud music, but also in near-to-absolute silence (Heller and Bergman 1953).

Taken together, these observations have led to the view that tinnitus is caused by both peripheral and central mechanisms: 1) peripheral injury, 2) a reorganization of central auditory pathways, and 3) changes in parts of the limbic system that perform a valuation of the emotional content of sensory experiences. This hypothesis was first put forward in a comprehensive model by Jastreboff (1990). However, the exact localization of brain changes with tinnitus has remained controversial.

Animal studies point to different brain structures. Salicylate-induced tinnitus goes along with an increase of the spontaneous activity and the emergence of a bursting type of activity in the external nucleus of the inferior colliculus (Chen and Jastreboff 1995; Kwon and others 1999), whereas intense sound exposure leads to hyperactivity in the dorsal cochlear nucleus (Kaltenbach and others 2005). Moreover, tinnitus-evoking manipulations result in an increased activity of various structures in the auditory and limbic system, as revealed by various activity-dependent assays, such as the cytoskeleton-associated protein Arg3.1, [^{14}C]2-deoxyglucose, or c-fos expression (Wallhäusser-Franke and others 1996, 2003; Mahlke and Wallhäusser-Franke 2004).

In humans, functional imaging studies on tinnitus are hindered by the lack of an adequate control condition and have pointed to different structures within the auditory pathways. Changes at the level of the auditory cortex have been suggested by work using positron emission tomography (PET) (Arnold and others 1996; Lockwood and others 1998), magnetoencephalography (Mühlnickel and others 1998), and functional magnetic resonance imaging (MRI) (Giraud and others 1999; Mirz and others 1999), whereas the inferior colliculus has been implicated by others (Melcher and others 2000). Clear evidence for changes in a specific location of the limbic system is even sparser: Only 1 PET study so far has demonstrated abnormal activity within limbic structures, but only with a resolution insufficient to unequivocally identify a particular region and only in the rare form of tinnitus that can be altered by oral facial movements (Lockwood and others 1998).

This lack of decisive knowledge about the locus of tinnitus-related changes in the brain has held up an investigation of the mechanisms leading to tinnitus and, hence, approaches to successful treatment. We decided to employ a technique that is capable of pinpointing region-specific changes and that, on this basis, has already led to new therapeutic options in

a particular type of headache (May and others 1999; Leone and others 2004). This technique, voxel-based morphometry (VBM), is based on the use of high-resolution MRI revealing alterations in the concentration or volume of gray and white matter at the group level (Ashburner and Friston 2000; Good and others 2001). Although the technique is aimed primarily at revealing alterations in the concentration or volume of gray and white matter, several studies have demonstrated that these structural changes are directly related to functional changes in brain activity (Gaser and Schlaug 2003; Draganski and others 2004).

Materials and Methods

Participants

In accordance with the Declaration of Helsinki 2000, all subjects were informed about the purpose of the study before giving their written consent. The study had been approved by the local Ethics Committee of the Faculty of Medicine at the Technical University of Munich. Participants were recruited from tinnitus sufferers who consulted our outpatient ear, nose, and throat department between 2001 and 2003. Neither did the 28 tinnitus sufferers have a hearing loss that was detectable with standard audiometric testing (i.e., thresholds were <25 dB hearing level for all 6 standard audiometric frequencies) nor did any of them have a history of noise trauma or chronic noise exposure. Further features of the tinnitus sufferers are summarized in Table 1 including tinnitus-related distress as determined with a standard German questionnaire ("Tinnitus-Fragebogen") (Goebel and Hiller 1994; Hiller and others 1994). Apart from tinnitus, participants had neither audiological complaints (e.g., hyperacusis) nor neurological or psychiatric disorders. No patient localized his tinnitus exclusively to one side. Seven patients negated any lateralization of their sound. Thirteen patients had their tinnitus "in both ears" or "in the head" but could somehow distinguish a lateralization (5 to the right, 8 to the left). The remaining 8 patients could clearly indicate one side as paramount to the other (4 right > left, 4 left > right). The tinnitus percept was described as whistling (16), ringing (2), buzzing (9), or hissing (1). The pitch of the tinnitus was described as high in most (24) cases (intermediate, 3; low, 1). Eight patients heard more than 1 sound. Twenty-eight unaffected healthy controls were matched for age and sex in a pairwise manner (mean age: tinnitus sufferers, 40; controls, 39; ranges of both groups: 26–53, 15 females in each group).

Magnetic Resonance Imaging

Imaging was performed using a 1.5-T Siemens scanner (Magnetom Symphony) with a standard 8-channel birdcage head coil. A 3-dimensional, structural, high-resolution T_1-weighted MRI using a magnetization-prepared rapid gradient echo sequence was acquired on each subject (sagittal plane; picture matrix, 256 × 256 mm; time repetition, 1520 ms; echo time, 3.93 ms; time for inversion, 800 ms; flip angle, 15°; distance factor, 50%; number of slices, 160; slice thickness, 1 mm). These scans were screened by a neuroradiologist who detected neither abnormal nor unusual findings.

Table 1
Characterization of the tinnitus group

Item (maximal possible score)	Min.	Max.	Median	Mean	SD
1 Emotional distress (24)	0	18	8	7	5
2 Cognitive distress (16)	0	14	5	5	4
3 Em. + Cog. distress (40)	0	32	13	12	8
4 Intrusiveness (16)	0	15	7	7	4
5 Auditory complaints (14)	0	9	1	2	2
6 Sleep disturbances (8)	0	6	2	2	2
7 Somatic complaints (6)	0	5	0	1	1
8 Sum of items 1, 2, 4–7 (84)	1	58	26	25	16
9 Subjective loudness (10)	2	10	5	5	2
10 Duration in months	7	240	37	53	52

Note: Items 1–8 correspond to a standard German questionnaire ("Tinnitus-Fragebogen") (Goebel and Hiller 1994; Hiller and others 1994). Em. + Cog., emotional and cognitive; Min., minimum; Max., maximum; SD, standard deviation.

Data Processing and Statistical Analysis

SPM2 software (Wellcome Department of Cognitive Neurology, London, UK) was applied for data analysis. The main idea of VBM (Ashburner and Friston 2000; Good and others 2001) comprises the following steps: 1) spatial normalization of all images to a standardized anatomical space to allow spatial averaging, 2) segmentation of images into gray and white matter and cerebrospinal fluid, and 3) comparison of local gray-matter volume or concentration across the whole brain. Image preprocessing was performed as previously described (Good and others 2001) using study-specific prior probability maps. The resulting gray-matter images were smoothed with a Gaussian kernel of 8 mm full width at half maximum. The whole procedure yielded 2 images per subject, namely, gray-matter images that were either modulated or unmodulated. Analysis of modulated data tests for regional differences in the absolute amount (volume) of gray matter, whereas analysis of unmodulated data tests for regional differences in concentration of gray matter (per unit volume in native space) (Good and others 2001). In this study, we analyzed both modulated and unmodulated data. Voxel-by-voxel *t*-tests using the general linear model (Friston 1996) were used to detect gray-matter differences between tinnitus sufferers and control subjects. To account for unequal variance between both groups, we applied non-sphericity correction as implemented in SPM2. For the statistical analysis, we excluded all voxels with a gray-matter value less than 0.2 (maximum value: 1) to avoid possible edge effects around the border between gray and white matter and to include only voxels with sufficient gray matter. Statistical analyses for changes within the auditory system were corrected for the volume of the auditory system. For this purpose, we defined a region of interest that included the ventral and dorsal cochlear nuclei (sphere radius, 5 mm; Montreal-Neurological-Institute (MNI)-coordinates, ±10, −38, −45), superior olivary complex (sphere radius, 5 mm; MNI-coordinates, ±13, −35, −41), inferior colliculus (sphere radius, 5 mm; MNI-coordinates, ±6, −33, −11), medial geniculate nucleus (MGN) (sphere radius, 8 mm; MNI-coordinates, ±17, −24, −2), as well as the primary and secondary auditory cortices corresponding to Brodmann areas 41, 42, and 22 (defined with an extension of SPM2, the WFU-Pick Atlas [Maldjian and others 2003]). Statistical analyses for changes outside the auditory system were corrected for the volume of the whole brain. We applied a height threshold (voxel level) of $P < 0.05$ (corrected for multiple comparisons using false discovery rate [FDR] [Genovese and others 2002]). In addition, a spatial extent threshold (cluster level) of $P < 0.05$ (corrected for multiple comparisons [Friston and others 1996]) was applied.

Results

Whole-Brain Analysis

A highly significant decrease of gray-matter volume was identified in the subcallosal area (Fig. 1*A*,*B*; thesholded at $P < 0.05$, corrected at both voxel and cluster level; *Z* value of peak voxel, 4.9; *P* value of peak voxel corrected at the voxel level using FDR, 0.015; *P* value corrected at the cluster level, 0.0002). No other brain regions showed increases or decreases of either gray-matter volume or concentration that were significant at this *P* level. It was particularly surprising that no changes were found within the auditory system. We therefore performed a region-of-interest analysis.

Region-of-Interest Analysis

Within the auditory system, we encountered significant structural differences between tinnitus sufferers and normal controls only at the thalamic level (Fig. 2), although auditory brain stem structures and the auditory cortex were equally included in our analysis. The right posterior thalamus including the MGN showed an increase in gray-matter concentration (Fig. 1*A*,*B*;

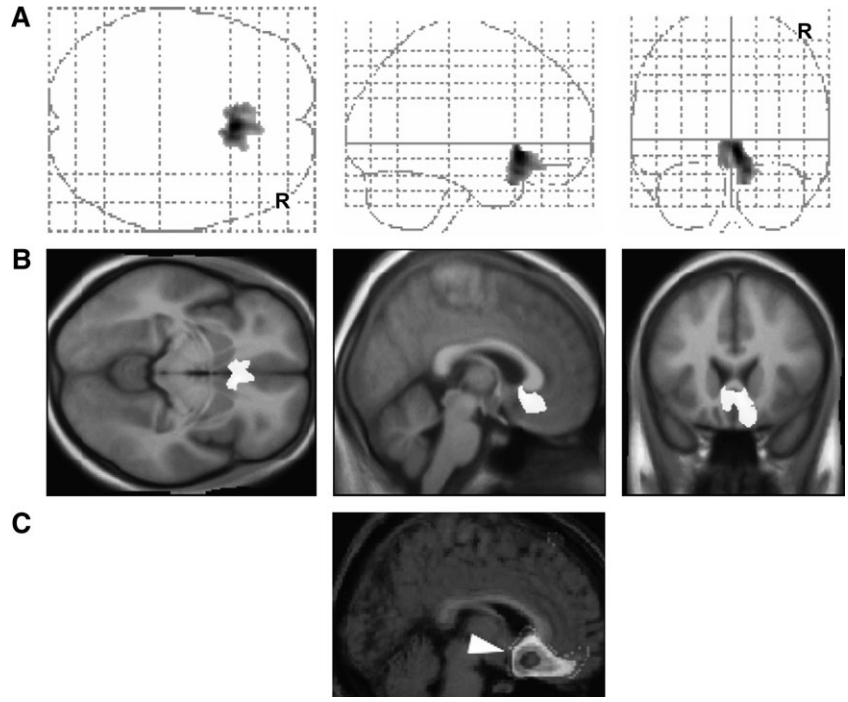

Figure 1. Gray-matter volume decreases. Changes throughout the whole brain are displayed. (*A*) Maximum intensity projection with a threshold of $P < 0.05$ corrected at both voxel and cluster level. (*B*) Gray-matter decrease of the subcallosal area is projected onto the study-specific averaged T_1 image. MNI-coordinates of peak value: $x = 4$, $y = 20$, $z = -6$; cluster size: 5234 voxels. (*C*) Data from Blood and others (1999) are shown for comparison. The subcallosal area displays significant negative correlation of regional cerebral blood flow with unpleasant emotions evoked by increasing musical dissonance.

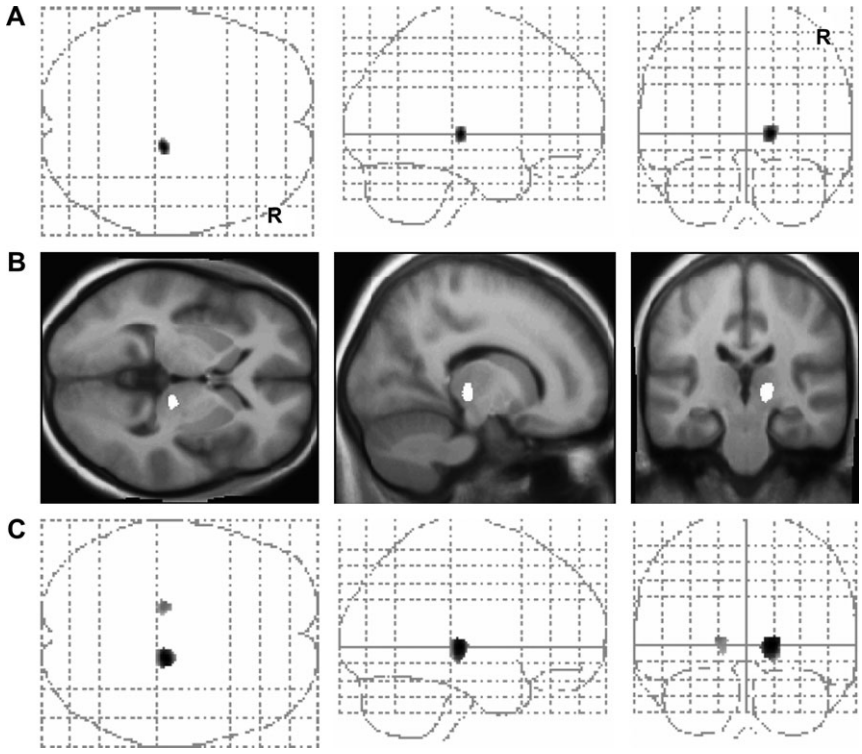

Figure 2. Gray-matter concentration increases. Only changes within the region of interest defined for the auditory system are displayed. (*A*) Maximum intensity projection with a threshold of $P < 0.05$ (corrected) at both voxel and cluster level. (*B*) Gray-matter increase of the right posterior thalamus including the MGN is projected onto the study-specific averaged T_1 image. MNI-coordinates of the peak value: $x = 15$, $y = -23$, $z = -1$; cluster size: 388 voxels. (*C*) Maximum intensity projection with the lower threshold of $P < 0.05$ (uncorrected) and the extent threshold of 30 contiguous voxels shows additional gray-matter increase only of the left posterior thalamus. MNI-coordinates of the peak value: $x = -15$, $y = -23$, $z = 5$; Z value, 2.4; cluster extent, 360 voxels.

thresholded at $P < 0.05$, corrected at both voxel and cluster level; Z value of peak voxel, 3.7; P value corrected at the voxel level using FDR, 0.04; P value corrected at the cluster level, 0.02). After relaxing the significance threshold to $P < 0.05$ uncorrected (extent threshold: 30 voxels), concentration increases surfaced also in the left posterior thalamus but not in any other structures of the auditory system (Fig. 2*C*).

Discussion

Although tinnitus is often considered a heterogeneous condition, all tinnitus sufferers share the complaint of an auditory phantom sensation. In terms of brain mechanisms of tinnitus, the present data suggest that, as a group, tinnitus sufferers share a highly significant gray-matter decrease in the subcallosal area. In addition, an increase of gray-matter concentration was found in the auditory thalamus of the tinnitus group.

The finding of structural tinnitus-related changes in the subcallosal region is intriguing for a variety of reasons: Activity in the subcallosal region is correlated with unpleasant emotions elicited by varying amounts of musical dissonance, exactly at the site where gray-matter decreases were identified by our results (Fig. 1*C*) (Blood and others 1999). Another study reports activation in the subcallosal region by aversive sounds (Zald and Pardo 2002). Furthermore, this area in the "limbic-related" (or paralimbic) ventral striatum, which includes the nucleus accumbens (NAc), plays a crucial role in the formation of adaptive behavioral responses to environmental stimuli. In humans, the NAc is active during instrumental as well as Pavlovian conditioning (O'Doherty and others 2004). In animal studies, the NAc has been shown to be involved in reward-directed as well as avoidance learning (McCullough and others 1993; Schultz 2004). Lesions of the NAc in rats impair the habituation to noise bursts preceded by a warning sound (McCullough and others 1993). The NAc receives glutamatergic input from the amygdala (Koob 2000) and serotonergic input from the brain stem raphe nuclei (Brown and Molliver 2000), which are involved in the regulation of sleep and arousal. Interconnected parallel circuits exist between NAc and thalamus, in particular the thalamic reticular nucleus (TRN) (O'Donnell and others 1997), where the NAc can exert an inhibitory gating influence over the thalamocortical relay. Decreased gray-matter volume in the NAc, as found here, would therefore reduce this inhibition normally conveyed by the NAc.

Within the auditory pathways, we identified gray-matter changes only at the thalamic level. At the FDR-corrected significance level of $P < 0.05$, increases in the posterior (auditory) thalamus were found only on the right; after relaxing the significance threshold, concentration increases were visible in both posterior thalami. The initial lateralization of this effect to the right hemisphere may reflect a lateralization of the tinnitus percept to the contralateral side throughout the tinnitus group, which was incompletely quantified by our questionnaires. Indeed, there was a trend for a lateralization of the tinnitus percept to the left.

The absence of VBM changes in the auditory cortex may at first seem surprising, given the observation of cortical involvement in tinnitus by several studies (Arnold and others 1996; Lockwood and others 1998; Mühlnickel and others 1998; Rauschecker 1999). However, subtle alterations at the cortical level, such as a distortion of the tonotopic map, may not be easily detectable by VBM. Alternatively, several lines of evidence demonstrate that adult sensory plasticity entails an interaction between the cortex and the thalamus (Ergenzinger and others 1998; Rauschecker 1998; Suga and Ma 2003; Chowdhury and others 2004). In the somatosensory system, peripheral deafferentation results in cortical map changes but causes even more massive reorganization at the thalamic level (Ergenzinger and others 1998; Rauschecker 1998; Chowdhury and others 2004). In these models, abnormal cortical activity (from a reduction in gamma-aminobutyric-acid (GABA)-mediated inhibition) leads to massive reassignment of projections at the thalamic level via (N-methyl-D-aspartate (NMDA)-receptor mediated) corticofugal modulation of thalamic neurons (Ergenzinger and others 1998; Chowdhury and others 2004). Further evidence for thalamic plasticity via top–down modulation comes from electrophysiological studies of the auditory system (Suga and Ma 2003). Within the MGN, greatest plasticity is found in its magnocellular division, which also receives somatosensory input and sends glutamatergic projections to the lateral amygdala (LeDoux 1992), a part of the limbic system involved in fear conditioning (Weinberger 2004). An important role in this plasticity is played by the TRN, which is a target of "nonspecific" modulatory input and has the ability to control thalamocortical transmission through inhibitory connections onto thalamic relay cells (Guillery and Harting 2003).

Taken together, the findings of decreased gray-matter volume in the subcallosal area (including the NAc) and increased gray-matter concentration in the posterior thalamus suggest a rather circumscribed model of tinnitus generation: 1) Reorganization in the MGN (possibly via corticofugal feedback loops) following a dysfunction in the auditory periphery (e.g., partial cochlear deafferentation) generates tinnitus-related neuronal activity in the central auditory pathways, which eventually leads to a permanent increase in thalamic gray-matter concentration. 2) The tinnitus-related activity in the MGN is relayed in parallel to limbic structures via the amygdala, which become involved in forming negative emotional associations with the tinnitus sound, as proposed by Jastreboff (1990, 2000). We hypothesize that long-term habituation mediated by the subcallosal region or, more specifically, the NAc normally helps to cancel out the tinnitus signal at the thalamic level (TRN) and prevents the signal from being relayed onto the auditory cortex. 3) Thus, in cases where the subcallosal region becomes impaired or disabled, a chronic tinnitus sensation would be the result. The subcallosal area contains dopaminergic and serotonergic neurons whose activity is modulated by stress and arousal (Brown and Molliver 2000). Both these factors are well known to affect the perception of tinnitus. Depression, insomnia, and aging are all associated with reduced serotonin levels in the brain (including the NAc) and are also correlated with tinnitus (Simpson and Davies 2000). It appears, therefore, that the perception of tinnitus may be related to the same humoral changes.

In summary, our findings suggest a pivotal role for the subcallosal area and the posterior thalamus in the pathogenesis of tinnitus. Only the combined changes in both regions seem to bring about the sensation of tinnitus. Our model suggests that 1) tinnitus-related neuronal activity is primarily perpetuated in the MGN, resulting from reorganization after peripheral hearing loss; 2) inhibitory feedback from the subcallosal area may normally help to tune out the tinnitus-related neuronal activity; and 3) a gray-matter decrease in the subcallosal area reduces this inhibitory feedback and, therefore, puts people with peripheral hearing loss at risk for developing tinnitus. Whether

the structural changes identified by our study precede the development of tinnitus or arise in the course of tinnitus remains open for further study. Group comparison of tinnitus sufferers and of hearing-impaired subjects without tinnitus will help to resolve this question. Studies in animals with artificially induced tinnitus (Jastreboff and Sasaki 1994) will also be helpful in testing our model in detail, and investigations of the transmitter systems involved in the subcallosal area can form a potential basis for specific drug treatment of tinnitus.

Notes

MM and his colleagues from the Department of Neurology (Technische Universität München) were supported by Fond 766160 of the *Kommission für Klinische Forschung (KKF) des Klinikums rechts der Isar der Technischen Universität München*. JPR was supported by the Tinnitus Research Consortium and a Research Award from the Alexander-von-Humboldt Foundation. We thank A. Meyer-Lindenberg and D. Steinbach for comments on an earlier version of the manuscript.

Address correspondence to Mark Mühlau, MD, Department of Neurology, Technische Universität München, Möhlstrasse 28, D-81675 München, Germany. Email: m.muehlau@neuro.med.tu-muenchen.de.

References

Andersson G, Kinnefors A, Ekvall L, Rask-Andersen H. 1997. Tinnitus and translabyrinthine acoustic neuroma surgery. Audiol Neurootol 2:403–409.

Arnold W, Bartenstein P, Oestreicher E, Romer W, Schwaiger M. 1996. Focal metabolic activation in the predominant left auditory cortex in patients suffering from tinnitus: a PET study with [18F]deoxyglucose. ORL J Otorhinolaryngol Relat Spec 58:195–199.

Ashburner J, Friston KJ. 2000. Voxel-based morphometry—the methods. Neuroimage 11:805–821.

Blood AJ, Zatorre RJ, Bermudez P, Evans AC. 1999. Emotional responses to pleasant and unpleasant music correlate with activity in paralimbic brain regions. Nat Neurosci 2:382–387.

Brown P, Molliver ME. 2000. Dual serotonin (5-HT) projections to the nucleus accumbens core and shell: relation of the 5-HT transporter to amphetamine-induced neurotoxicity. J Neurosci 20:1952–1963.

Chen GD, Jastreboff PJ. 1995. Salicylate-induced abnormal activity in the inferior colliculus of rats. Hear Res 82:158–178.

Chowdhury SA, Greek KA, Rasmusson DD. 2004. Changes in corticothalamic modulation of receptive fields during peripheral injury-induced reorganization. Proc Natl Acad Sci USA 101: 7135–7140.

Draganski B, Gaser C, Busch V, Schuierer G, Bogdahn U, May A. 2004. Neuroplasticity: changes in grey matter induced by training. Nature 427:311–312.

Eggermont JJ, Roberts LE. 2004. The neuroscience of tinnitus. Trends Neurosci 27:676–682.

Ergenzinger ER, Glasier MM, Hahm JO, Pons TP. 1998. Cortically induced thalamic plasticity in the primate somatosensory system. Nat Neurosci 1:226–229.

Flor H, Elbert T, Knecht S, Wienbruch C, Pantev C, Birbaumer N, Larbig W, Taub E. 1995. Phantom-limb pain as a perceptual correlate of cortical reorganization following arm amputation. Nature 375:482–484.

Friston KJ. 1996. Statistical parametric mapping and other analyses of functional imaging data. In: Toga AW, Mazziotta JC, editors. Brain mapping—the methods. New York: Academic Press. p 363–386.

Friston KJ, Holmes A, Poline JB, Price CJ, Frith CD. 1996. Detecting activations in PET and fMRI: levels of inference and power. Neuroimage 4:223–235.

Gaser C, Schlaug G. 2003. Brain structures differ between musicians and non-musicians. J Neurosci 27:9240–9245.

Genovese CR, Lazar NA, Nichols T. 2002. Thresholding of statistical maps in functional neuroimaging using the false discovery rate. Neuroimage 15:870–878.

Giraud AL, Chery-Croze S, Fischer G, Fischer C, Vighetto A, Gregoire MC, Lavenne F, Collet L. 1999. A selective imaging of tinnitus. Neuroreport 10:1–5.

Goebel G, Hiller W. 1994. [The tinnitus questionnaire. A standard instrument for grading the degree of tinnitus. Results of a multicenter study with the tinnitus questionnaire]. HNO 42:166–172.

Good CD, Johnsrude IS, Ashburner J, Henson RN, Friston KJ, Frackowiak RS. 2001. A voxel-based morphometric study of ageing in 465 normal adult human brains. Neuroimage 14:21–36.

Guillery RW, Harting JK. 2003. Structure and connections of the thalamic reticular nucleus: advancing views over half a century. J Comp Neurol 463:360–371.

Heller MF, Bergman M. 1953. Tinnitus aurium in normally hearing persons. Ann Otol Rhinol Laryngol 62:73–83.

Henry JA, Meikle MB. 2000. Psychoacoustic measures of tinnitus. J Am Acad Audiol 11:138–155.

Hiller W, Goebel G, Rief W. 1994. Reliability of self-rated tinnitus distress and association with psychological symptom patterns. Br J Clin Psychol 33(Pt 2):231–239.

Jastreboff PJ. 1990. Phantom auditory perception (tinnitus): mechanisms of generation and perception. Neurosci Res 8:221–254.

Jastreboff PJ. 2000. Tinnitus habituation therapy (THT) and tinnitus retraining therapy (TRT). In: Tyler R, editor. Handbook on Tinnitus. San Diego, CA: Singular Publishing Group. p 357–376.

Jastreboff PJ, Hazell JW, Graham RL. 1994. Neurophysiological model of tinnitus: dependence of the minimal masking level on treatment outcome. Hear Res 80:216–232.

Jastreboff PJ, Sasaki CT. 1994. An animal model of tinnitus: a decade of development. Am J Otol 15:19–27.

Kaltenbach JA, Zhang J, Finlayson P. 2005. Tinnitus as a plastic phenomenon and its possible neural underpinnings in the dorsal cochlear nucleus. Hear Res 206:200–226.

Koob GF. 2000. Neurobiology of addiction. Toward the development of new therapies. Ann N Y Acad Sci 909:170–185.

Kwon O, Jastreboff MM, Hu S, Shi J, Jastreboff PJ. 1999. Modification of single-unit activity related to noise-induced tinnitus in rats. In: Hazell J, editor. Proceedings of the sixth international tinnitus seminar, Cambridge, UK. London: THC. p 459–462.

LeDoux JE. 1992. Brain mechanisms of emotion and emotional learning. Curr Opin Neurobiol 2:191–197.

Leone M, May A, Franzini A, Broggi G, Dodick D, Rapoport A, Goadsby PJ, Schoenen J, Bonavita V, Bussone G. 2004. Deep brain stimulation for intractable chronic cluster headache: proposals for patient selection. Cephalalgia 24:934–937.

Lockwood AH, Salvi RJ, Burkard RF. 2002. Tinnitus. N Engl J Med 347:904–910.

Lockwood AH, Salvi RJ, Coad ML, Towsley ML, Wack DS, Murphy BW. 1998. The functional neuroanatomy of tinnitus: evidence for limbic system links and neural plasticity. Neurology 50: 114–120.

Mahlke C, Wallhäusser-Franke E. 2004. Evidence for tinnitus-related plasticity in the auditory and limbic system, demonstrated by arg3.1 and c-fos immunocytochemistry. Hear Res 195:17–34.

Maldjian JA, Laurienti PJ, Kraft RA, Burdette JH. 2003. An automated method for neuroanatomic and cytoarchitectonic atlas-based interrogation of fMRI data sets. Neuroimage 19:1233–1239.

May A, Ashburner J, Buchel C, McGonigle DJ, Friston KJ, Frackowiak RS, Goadsby PJ. 1999. Correlation between structural and functional changes in brain in an idiopathic headache syndrome. Nat Med 5:836–838.

McCullough LD, Sokolowski JD, Salamone JD. 1993. A neurochemical and behavioral investigation of the involvement of nucleus accumbens dopamine in instrumental avoidance. Neuroscience 52:919–925.

Melcher JR, Sigalovsky IS, Guinan JJ Jr, Levine RA. 2000. Lateralized tinnitus studied with functional magnetic resonance imaging: abnormal inferior colliculus activation. J Neurophysiol 83: 1058–1072.

Mirz F, Pedersen B, Ishizu K, Johannsen P, Ovesen T, Stodkilde-Jorgensen H, Gjedde A. 1999. Positron emission tomography of cortical centers of tinnitus. Hear Res 134:133–144.

Mühlnickel W, Elbert T, Taub E, Flor H. 1998. Reorganization of auditory cortex in tinnitus. Proc Natl Acad Sci USA 95:10340–10343.

O'Doherty J, Dayan P, Schultz J, Deichmann R, Friston K, Dolan RJ. 2004. Dissociable roles of ventral and dorsal striatum in instrumental conditioning. Science 304:452–454.

O'Donnell P, Lavin A, Enquist LW, Grace AA, Card JP. 1997. Interconnected parallel circuits between rat nucleus accumbens and thalamus revealed by retrograde transynaptic transport of pseudorabies virus. J Neurosci 17:2143–2167.

Rauschecker JP. 1998. Cortical control of the thalamus: top-down processing and plasticity. Nat Neurosci 1:179–180.

Rauschecker JP. 1999. Auditory cortical plasticity: a comparison with other sensory systems. Trends Neurosci 22:74–80.

Schultz W. 2004. Neural coding of basic reward terms of animal learning theory, game theory, microeconomics and behavioural ecology. Curr Opin Neurobiol 14:139–147.

Simpson JJ, Davies WE. 2000. A review of evidence in support of a role for 5-HT in the perception of tinnitus. Hear Res 145:1–7.

Suga N, Ma X. 2003. Multiparametric corticofugal modulation and plasticity in the auditory system. Nat Rev Neurosci 4:783–794.

Wallhäusser-Franke E, Braun S, Langner G. 1996. Salicylate alters 2-DG uptake in the auditory system: a model for tinnitus? Neuroreport 7:1585–1588.

Wallhäusser-Franke E, Mahlke C, Oliva R, Braun S, Wenz G, Langner G. 2003. Expression of c-fos in auditory and non-auditory brain regions of the gerbil after manipulations that induce tinnitus. Exp Brain Res 153:649–654.

Weinberger NM. 2004. Specific long-term memory traces in primary auditory cortex. Nat Rev Neurosci 5:279–290.

Wiegand DA, Ojemann RG, Fickel V. 1996. Surgical treatment of acoustic neuroma (vestibular schwannoma) in the United States: report from the Acoustic Neuroma Registry. Laryngoscope 106:58–66.

Zald DH, Pardo JV. 2002. The neural correlates of aversive auditory stimulation. Neuroimage 16:746–753.

Article

Gray Matter Decrease of the Anterior Cingulate Cortex in Anorexia Nervosa

Mark Mühlau, M.D.
Christian Gaser, Ph.D.
Rüdiger Ilg, M.D.
Bastian Conrad, M.D.
Carl Leibl, M.D.
Marian H. Cebulla, Ph.D.
Herbert Backmund, M.D.
Monika Gerlinghoff, M.D.
Peter Lommer, Dipl.-Soz.
Andreas Schnebel, Dipl.-Psych.
Afra M. Wohlschläger, Ph.D.
Claus Zimmer, M.D.
Sabine Nunnemann, M.D.

Objective: The brain regions that are critically involved in the pathophysiology of anorexia nervosa have not been clearly elucidated. Moreover, decrease in cerebral tissue during extreme malnutrition has been demonstrated repeatedly in anorexia nervosa, but data regarding the reversibility of this cerebral tissue decrease are conflicting. The authors examined region-specific gray matter changes and global cerebral volumes in recovered patients with anorexia nervosa.

Method: High-resolution, T1-weighted magnetic resonance imaging (MRI) and voxel-based morphometry were performed in 22 recovered women with anorexia nervosa and in 37 healthy comparison women. Recovery was defined as a body mass index above 17.0 kg/m^2 and regular menses for at least 6 months.

Results: The global volumes of gray matter (but not white matter) were decreased in patients with anorexia nervosa by approximately 1%. Analyses of region-specific gray matter changes revealed a gray matter decrease bilaterally in the anterior cingulate cortex of approximately 5%, which remained significant after correction for global effects. This gray matter decrease correlated significantly with the lowest body mass index of lifetime but not with other clinical variables.

Conclusions: In anorexia nervosa, part of the global gray matter loss persists over the long run. Region-specific gray matter loss in the anterior cingulate cortex is directly related to the severity of anorexia nervosa, indicating an important role of this area in the pathophysiology of the disorder. Further research is warranted to determine the cause, specificity, and functional consequences of this structural brain change in anorexia nervosa.

(Am J Psychiatry 2007; 164:1–9)

Eating disorders are an important cause of physical and psychosocial morbidity in adolescent girls and young adult women, while they are much less frequent in men. These disorders are characterized as a primary disturbance of eating habits or weight-control behavior resulting in significant impairment of physical health or psychosocial functioning. According to DSM-IV, the diagnostic group of anorexia nervosa is defined by the refusal to maintain body weight at or above a minimal normal weight. This is combined with an intense fear of gaining weight or becoming overweight, with a disturbance in the way in which body weight or shape is experienced, and amenorrhea. Anorexia nervosa is divided into the following two types: 1) the restricting type, in which patients primarily restrict their eating, and 2) the binge eating/purging type, in which patients are regularly engaged in binge eating or purging behavior (1). Nevertheless, there is frequently a combination of symptoms over time, and a number of patients with anorexia nervosa develop bulimia nervosa or an atypical eating disorder.

The brain regions critically involved in the pathophysiology of anorexia nervosa are a question of continuing debate. This lack of decisive knowledge about the locus of anorexia nervosa-related changes in the brain has not only hampered the investigation of the mechanisms leading to anorexia nervosa but also approaches to more successful treatment.

Various lines of imaging studies have aimed to identify the brain regions critically involved in the pathophysiology of anorexia nervosa. A systematic review of lesion studies on patients who developed an eating disorder subsequent to cerebral damage concluded that "complex syndromes, including characteristic psychopathology of eating disorders, are associated with right frontal and temporal lobe damage" (2). In studies that used single photon emission computed tomography (SPECT), anorexia ner-

TABLE 1. Clinical and Morphometric Variables of the Participants

Clinical/Morphometric Variable	Minimum		Median		Maximum	
	Comparison Subjects	Anorexia Nervosa Subjects	Comparison Subjects	Anorexia Nervosa Subjects	Comparison Subjects	Anorexia Nervosa Subjects
Age (years)	18.3	18.4	23.8	22.3	40.2	40.8
Body mass index at the time of scanning (kg/m^2)	18.3	17.0	20.1	19.5	24.8	22.8
Total intracranial volume (ml)	1,473	1,516	1,780	1,781	2,223	2,129
Fraction of white matter (global volume of white matter [ml] divided by the total intracranial volume [ml])	0.22	0.22	0.24	0.25	0.27	0.27
Fraction of CSF (global volume of cerebrospinal fluid [ml] divided by the total intracranial volume [ml])	0.30	0.34	0.36	0.37	0.41	0.42
Fraction of gray matter (global volume of gray matter [ml] divided by the total intracranial volume [ml])	0.36	0.36	0.39	0.38	0.44	0.40
Anterior cingulate cortex (ml)[a]	12.1	11.4	13.0	12.3	14.3	13.5
Lowest body mass index of lifetime (kg/m^2)		10.0		13.5		16.1
Age at onset (years)		12.5		15.6		24.8
Duration of anorexia nervosa (years)[b]		1		5		23
Length of recovery (months)		6		15.5		60

[a] Gray matter content (sum of all 21,421 voxel values) of the only cluster of region-specific gray matter decrease that was located in the anterior cingulate cortex.
[b] Time from first symptoms to latest recovery, i.e., latest recurrence of menses.

vosa patients showed hypoperfusion in the medial prefrontal cortex and anterior cingulate cortex (3, 4), even after weight restoration (5). Using functional magnetic resonance imaging (fMRI), patients with restricting anorexia nervosa, who were either recovered or chronically ill, were compared with healthy comparison subjects with respect to brain activation in response to food stimuli. This study revealed increased medial prefrontal and anterior cingulate cortex activation as well as a lack of activity in the inferior parietal lobule in the recovered group relative to the healthy comparison group. The comparison of the recovered group with chronically ill patients showed increased activation of the right lateral prefrontal, frontopolar, and dorsal anterior cingulate cortices (6). In another fMRI study, nonrecovered patients suffering from either bulimia or anorexia nervosa were confronted with food stimuli (7). Patients with both eating disorders also displayed increased activation in the anterior cingulate cortex (7). Studies using positron emission tomography (PET) with serotonin (5-HT)-specific radioligands have implicated alterations of 5-HT$_{1A}$ and 5-HT$_{2A}$ receptors and the 5-HT transporter in the frontal, cingulate, temporal, and parietal cortices (8), which persist after physical recovery.

Another approach to identify the brain regions critically involved in the pathophysiology of anorexia nervosa constitutes the analysis for structural brain changes. In recent years, morphometric techniques have been developed that allow the localization of subtle gray matter changes at the group level. One of these techniques, voxel-based morphometry, is based on high-resolution magnetic resonance imaging (MRI). Although the technique reveals alterations in the local concentration of gray matter, several studies have demonstrated that these structural changes are directly related to functional changes in brain activity (9, 10). However, applying voxel-based morphometry in anorexia nervosa requires caution, since at low weight global changes in the brain structure exist that are commonly attributed to malnutrition (11–14).

Against this background, we applied voxel-based morphometry in recovered anorexia nervosa patients to study both global and regional structural brain changes.

Method

Sample Collection

The present study was approved by the local ethics committee. Since anorexia nervosa occurs much less frequently in men than in women and it is unclear whether the pathophysiology of the disorder in men equals that in women (15), we examined female anorexia nervosa patients exclusively. We examined recovered patients, since we expected the global brain tissue decrease at low weight to conceal region-specific gray matter changes. Recovery was defined by a body mass index (i.e., weight in kilograms divided by the square of height in meters) above 17.0 kg/m^2 and regular menstrual cycles for at least 6 months. Participants were recruited from three therapy centers for eating disorders. We included 22 patients. For the patient group, the following inclusion criteria were predefined: between 18 and 48 years of age, anorexia nervosa restricting type during the first year of the disease (according to DSM-IV), and exclusion of comorbidity. The following lifetime diagnoses were predefined as exclusion criteria: posttraumatic stress disorder (PTSD), manic episodes, schizophrenia, obsessive-compulsive disorder (OCD), substance use disorders, and borderline personality disorder. The diagnosis of major depressive episodes only constituted an exclusion criterion when it occurred not only at times of low weight but also at times of recovery. We used the diagnostic items of a modified version of the Structured Interview for Anorexic and Bulimic Disorders for DSM-IV and ICD-10 (16). All patients who were included fulfilled the diagnostic criteria for anorexia nervosa in the past but not at the time of scanning. PTSD, manic or major depressive episodes, schizophrenia, OCD, and substance use disorders were excluded by international diagnosis checklists according to DSM-IV (17). Borderline personality disorder was ruled out by the Structured Clinical Interview for DSM-IV Axis II Personality Disorders (SCID II) (18). Only patients who were likely to fulfill the inclusion criteria according to their patient records were asked by their therapists in writing whether they were willing to participate in a telephone interview with the aim to identify appropriate anorexia

All				Analysis
All Comparison Subjects		Anorexia Nervosa Subjects		Two-Sided p Values of Independent t Tests
Mean	SD	Mean	SD	
24.7	4.3	23.7	6.0	0.5
20.7	1.8	19.7	1.6	0.03
1,799	154	1,811	156	0.8
0.247	0.01	0.247	0.01	0.8
0.361	0.02	0.375	0.02	0.03
0.392	0.02	0.379	0.01	0.004
13.0	0.5	12.3	0.5	<0.001
		13.5	1.6	
		16.4	2.8	
		5.2	5.1	
		19.3	12.8	

nervosa patients for an imaging study. Fifty-one patients agreed to participate in the interview by completing a form accordingly and sending it to the imaging center. Among the patients interviewed, 25 were invited to participate in the study. After complete description of the study to the subjects, written informed consent was obtained. Prior to scanning, the subjects were interviewed in detail by an experienced investigator who was specifically trained to use the diagnostic tools applied. This resulted in the identification of psychiatric comorbidity in two patients and, hence, to their exclusion from the study. To further characterize the anorexia nervosa patients, the following parameters were required: body mass index at the time of scanning, lowest body mass index of lifetime, age at onset (i.e., when anorexia nervosa symptoms resulted in significant impairment of physical health or psychosocial functioning for the first time), duration of anorexia nervosa (i.e., time from anorexia nervosa onset to latest recovery defined by latest recurrence of menses), and length of recovery (i.e., time from latest recurrence of menses).

After providing written informed consent, all comparison women were interviewed as described above and only included when there was no indication of any psychiatric disorder in their lifetime.

MRI Acquisition

Two MRI sequences were acquired from every participant using the same scanner (Siemens Magnetom Symphony; magnetic field intensity, 1.5 Tesla). For voxel-based morphometry, sequence 1 was used (sequence=T1 MPRAGE; plane=sagittal; number of slices=160, slice thickness=1 mm, voxel size=1×1×1 mm^3, flip angle=15°; field of view=256×256 mm, time to repeat=8.9 msec, echo time=3.93 msec, T1=800 msec). Sequence 2 was used to support the detection of abnormal or unusual findings (sequence=fluid attenuated inversion recovery; plane=axial; slice thickness=6 mm). Apart from one patient who was excluded from the study because of very large artifacts, probably resulting from her dental braces, neither abnormal nor unusual findings were detected.

Voxel-Based Morphometry: Preprocessing

Voxel-Based Morphometry 2 software (http://dbm.neuro.uni-jena.de/vbm), an extension of Statistical Parametric Mapping (SPM)2 software (http://www.fil.ion.ucl.ac.uk/spm), was applied. Voxel-Based Morphometry 2 applies the "optimized" protocol and a hidden Markov random field model (19). We used study-specific prior probability maps and a Gaussian kernel of 14 mm for smoothing.

Calculation of Global Volumes

Gray matter, white matter, and CSF were derived from the non-normalized segmented images as provided by SPM2 after the first segmentation process. Total intracranial volume was approximated by the sum of the global volumes of gray matter, white matter, and CSF. To correct for head size, brain tissue fractions of gray matter, white matter, and CSF were calculated by dividing the respective volumes by the total intracranial volume.

Analysis of Global Volumes

For group comparisons of global values, two-sided independent t tests were performed using standard software (SPSS, version, 14.0.1). Within the anorexia nervosa group, the following correlation analyses were performed: fraction of gray matter with the duration of anorexia nervosa, age of first diagnosis, length of recovery as well as lowest body mass index of lifetime, and body mass index at the time of scanning. Moreover, a univariate analysis of variance (ANOVA) was performed with fraction of gray matter as a dependent variable and the parameters mentioned above as independent variables.

Voxel-Based Morphometry: Statistical Analyses

We included only voxels with a gray matter value greater than 0.2 (maximum value=1) and greater than both the white matter and CSF values to analyze only voxels with sufficient gray matter and to avoid possible edge effects around the border between gray matter, white matter, and CSF. Because the analysis of fraction of gray matter revealed significant differences, we performed two voxel-by-voxel analyses of covariance (ANCOVA). In the first ANCOVA, only age was included as a confounding covariate (to remove variance explained by age). We will refer to this approach as "analysis for the regional distribution of gray matter changes." In the second ANCOVA, age and fraction of gray matter values were included as confounding covariates in order to exclusively identify changes that cannot be explained by global effects. We will refer to this approach as "analysis for region-specific gray matter changes." Within the anorexia nervosa group, the following correlation analyses were performed: gray matter content (sum of all voxel values) of the clusters of region-specific gray matter changes with lowest body mass index of lifetime, body mass index at the time of scanning, duration of anorexia nervosa, age at the time of scanning, age at first diagnosis, length of recovery, fraction of gray matter, occurrence of major depressive episodes at low weight (no=0; yes=1), and occurrence of an eating disorder other than the restricting type of anorexia nervosa in the course of the disorder (no=0; yes=1). Moreover, an ANOVA was performed with gray matter content of the clusters of region-specific gray matter changes as a dependent variable and the parameters mentioned above as independent variables.

We applied a height threshold of $p<0.05$, corrected for all voxels included in the analysis applying the family-wise error (20). To indicate the extension of gray matter changes, significant clusters were displayed at a voxel threshold of $p<0.01$.

Results

Characteristics of the Participants

Both groups were similar in age. Body mass index at the time of scanning differed significantly. After the first year of disease onset, 10 anorexia nervosa patients had fulfilled the diagnostic criteria for eating disorders other than the restricting type of anorexia nervosa (i.e., binge eating/

TABLE 2. Correlations of Morphometric and Clinical Variables Within the Anorexia Nervosa Group

	Morphometric Variable								
Clinical Variable	Anterior Cingulate Cluster[a]	Fraction of Gray Matter[b]	Age	Age at Onset	Body Mass Index	Lowest Body Mass Index of Lifetime	Length of Recovery	Duration[c]	Only Anorexia Restricted Type[d]
Anterior cingulate cortex cluster[a]									
Pearson correlation coefficient	1								
2-second p value									
Fraction of gray matter[b]									
Pearson correlation coefficient	0.7**	1							
2-second p value	<0.01								
Age at the time of scanning (years)									
Pearson correlation coefficient	–0.3	0.0	1						
2-second p value	>0.2	>0.2							
Age at onset (years)									
Pearson correlation coefficient	–0.0	0.2	0.5*	1					
2-second p value	>0.2	>0.2	0.02						
Body mass index at the time of scanning (kg/m^2)									
Pearson correlation coefficient	0.1	–0.0	0.0	–0.0	1				
2-second p value	>0.2	>0.2	>0.2	>0.2					
Lowest BMI of lifetime (kg/m^2)									
Pearson correlation coefficient	0.5*	0.2	0.0	0.2	0.6**	1			
2-second p value	0.02	>0.2	>0.2	>0.2	<0.01				
Length of recovery (months)									
Pearson correlation coefficient	–0.1	–0.0	–0.1	–0.4*	–0.3	–0.2	1		
2-second p value	>0.2	>0.2	>0.2	0.04	0.2	>0.2			
Duration (years)[c]									
Pearson correlation coefficient	–0.2	–0.0	0.9**	0.1	0.1	0.0	–0.1	1	
2-second p value	>0.2	>0.2	<0.01	>0.2	>0.2	>0.2	>0.2		
Only anorexia restricted type[d]									
Pearson correlation coefficient	0.1	0.2	–0.2	–0.1	0.2	0.2	–0.1	–0.2	1
2-second p value	>0.2	>0.2	>0.2	>0.2	>0.2	>0.2	>0.2	>0.2	
Depressive episode at low weight (yes=1; no=0)									
Pearson correlation coefficient	0.1	0.2	–0.2	–0.1	0.2	0.2	–0.1	0.3	0.1
2-second p value	>0.2	>0.2	>0.2	>0.2	>0.2	>0.2	0.1	>0.2	>0.2

[a] Gray matter content of the cluster of region-specific gray-matter decrease within the anterior cingulate cortex.
[b] Global volume of gray matter (ml) divided by the total intracranial volume (ml).
[c] Time from first symptoms to latest recovery (i.e., latest recurrence of menses).
[d] Only the restricting type of anorexia nervosa occurred in the course of the disorder (yes=1; no=0).

purging type of anorexia nervosa: eight; binge eating/purging type of anorexia nervosa and bulimia nervosa: two). During episodes of low weight, 16 patients met the criteria for a major depressive episode at least once. Further variables of the participants are given in Table 1.

Global Brain Changes

The anorexia nervosa group showed a significant decrease of 1.3% in fraction of gray matter (95% confidence interval [CI]=0.2%–2.6%), while fraction of white matter was nearly equal in both groups (Table 1). Within the anorexia nervosa group, fraction of gray matter did not show a tendency toward correlation (Table 2) with any of the clinical variables. Accordingly, the corrected model derived from the ANOVA with fraction of gray matter as the dependent variable was not significant (two-sided p value=0.9).

Analysis for the Regional Distribution of Gray Matter Changes in Anorexia Nervosa Patients Relative to Healthy Comparison Subjects

Applying the voxel-wise ANCOVA with only age as a confounding covariate, no gray matter increase was identified. Decrease in gray matter was detected in frontal, temporal, parietal, occipital, and subcortical areas. At the voxel level of p<0.01, gray matter decreases merged to large clusters (extents>5000 voxels; p values corrected at the cluster level<0.001) that spread throughout the whole brain (Figure 1).

Anterior Cingulate Cortex-Specific Gray Matter Changes in Anorexia Nervosa Patients Relative to Healthy Comparison Subjects

Applying the voxel-wise ANCOVA with both age and fraction of gray matter as confounding covariates, region-specific gray matter decrease was identified in a cluster of 45 voxels exclusively located within the left dorsal anterior cingulate cortex. At the voxel level of p<0.01 (Figure 2, Table 1), this cluster within the anterior cingulate cortex (anterior cingulate cortex cluster) was the largest throughout the whole brain (cluster extent, 21,421 voxels; p value corrected at the cluster level=0.0002) and extended bilaterally from the dorsal to the rostral anterior cingulate cortices. The gray matter volume content of the anterior cingulate cortex clus-

ter was decreased by 5.4% in anorexia nervosa patients relative to comparison subjects (95% CI=3.2%–7.1%).

Correlations of Clinical Variables and Anterior Cingulate Cortex-Specific Gray Matter Changes in Anorexia Nervosa Patients

The gray matter content of the anterior cingulate cortex cluster correlated significantly with the lowest body mass index of lifetime (Figure 3) and with fraction of gray matter (Table 2). None of the remaining variables showed a tendency toward correlation with the gray matter content of the anterior cingulate cortex cluster (Table 2). The significance value of the corrected model derived from the ANOVA with the gray matter content of the anterior cingulate cortex cluster as a dependent variable was 0.003. Again, only fraction of gray matter and the gray matter content of the anterior cingulate cortex cluster correlated significantly with the lowest body mass index of lifetime (partial correlation coefficient=0.6; two-sided p value=0.02).

Discussion

This study aimed at identifying both global and regional structural brain changes in recovered anorexia nervosa patients. First, we analyzed our data for global changes and found that global gray matter (i.e., fraction of gray matter) but not white matter was significantly decreased in the anorexia nervosa group. This finding complies with the results of two previous longitudinal studies (13, 14). In these studies, patients were scanned at low weight and displayed decreased global gray and white matter. In the patients who underwent rescanning after recovery, only global gray matter remained significantly lower. By contrast, Swayze et al. (11, 12) found only reduced global white matter but not gray matter in anorexia nervosa patients at low weight relative to comparison subjects, although follow-up scans of the anorexia nervosa patients revealed significant increase in both global white and gray matter. Another cross-sectional MRI study (21) found normal brain tissue volumes after long-term recovery in anorexia nervosa patients who were slightly less affected than our patients (lowest body mass index of lifetime: 14.1 [SD= 1.4] versus 13.5 [SD=1.6]). In addition, the mean length of recovery was longer (28.7 months versus 19.3 months) and the body mass index at the time of scanning was higher (21.1 [SD=2.0] versus 19.7 [SD=1.6]) in this group of patients than in our anorexia nervosa group. This raises the question of whether restoration of brain morphology was incomplete in our anorexia nervosa group at the time of scanning. If this were the case, the global gray matter should have increased with the length of recovery, but our correlation analysis does not support this assumption (Table 2). Conversely, we did not find a clear association of global gray matter with any of the clinical variables, including the severity of anorexia nervosa estimated with the lowest body mass index of lifetime and the duration of anorexia nervosa (Table 2). Another question that emerges from our data is whether functional deficits can be assumed merely because of a global gray matter decrease of approximately 1% at the group level. This seems very unlikely, since there are no compelling links between brain size and behavioral capacity within the range of brain size observed in our study groups (22). However, our data do not exclude the possibility of specific cognitive impairments in anorexia nervosa, which is still a matter of debate (23, 24) but beyond the scope of the present study.

Second, we analyzed our data for the regional distribution of gray matter changes and found that gray matter loss spread across the whole brain (Figure 1), indicating

FIGURE 1. Regional Distribution of Gray Matter Decrease in Patients With Anorexia Nervosa[a]

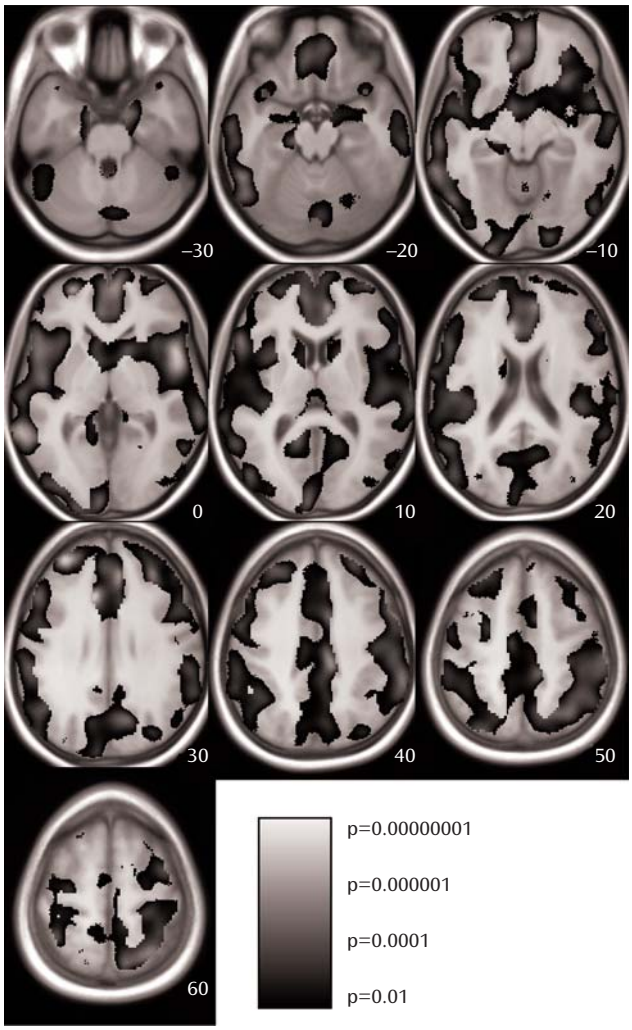

[a] At a voxel threshold of p<0.01, significant gray matter decrease in patients with anorexia nervosa relative to healthy comparison subjects throughout the whole brain are projected onto the study-specific-averaged T1 image. According to the bar in the lower right, increasing significance is coded from dark to light. The right side of the image shows the right hemisphere. According to the standard brain of the Montreal Neurological Institute, coordinates (z axis) of axial slices are indicated in the right lower corner of each panel.

FIGURE 2. Region-Specific Gray Matter Decrease in Patients With Anorexia Nervosa[a]

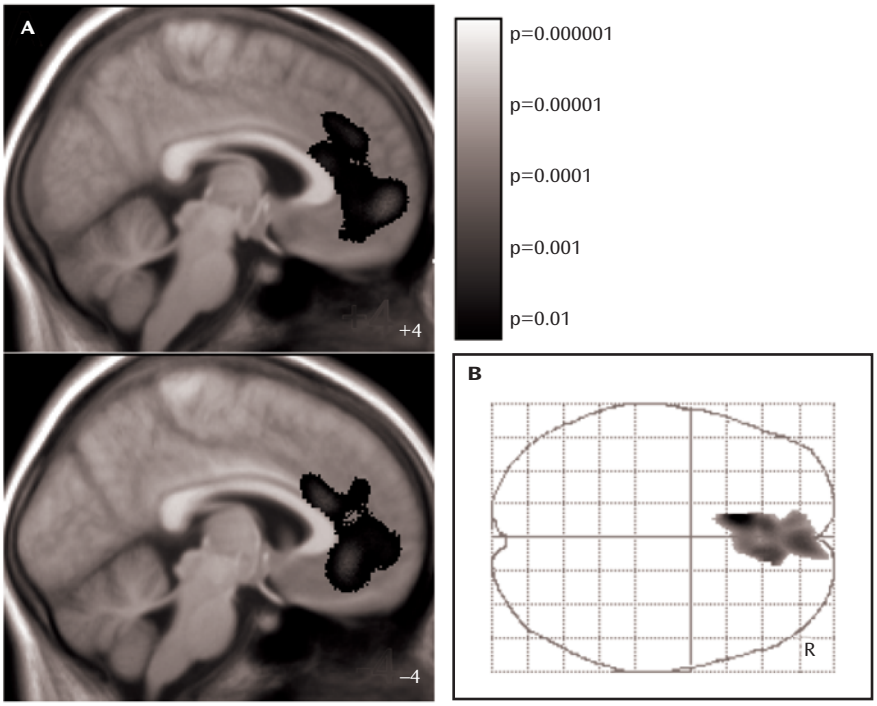

[a] Voxel level=p<0.01 uncorrected. A) Region-specific gray matter decrease in patients with anorexia nervosa relative to healthy comparison subjects is projected onto the study-specific averaged T1 image. Coordinates of the x axis (Montreal Neurological Institute) are indicated in the right lower corner of each slice. The bar in the upper right encodes increasing significance from dark to light. B) The maximum intensity projection is shown. The cluster within the anterior cingulate cortex was the largest throughout the brain (cluster extent=21,421 voxels; p value corrected at the cluster level=0.0002). Only this cluster contained voxels that were significant at a significance threshold of p<0.05 corrected at the voxel level (Montreal Neurological Institute coordinates of peak voxel=–11, 24, 23; z=4.9).

that the magnitude of gray matter loss is generalized rather than specific to particular brain regions.

Third, we searched for region-specific gray matter changes (i.e., regional changes that cannot be explained by global gray matter decrease) by additionally including fraction of gray matter as a confounding covariate in the ANCOVA model. In this analysis, only one small cluster of gray matter loss within the left anterior cingulate cortex was identified. Since both the ANCOVA-model applied and correction for multiple comparisons with the family-wise error (20) constitute very conservative approaches, we displayed this result at a voxel level of p<0.01. To exclude that the enlargement of this cluster at this liberal threshold occurred by chance, we considered the significance at the cluster level (corrected p value=0.0002). Moreover, we analyzed the gray matter content of the anterior cingulate cortex cluster for a correlation with several clinical variables. We used the lowest body mass index of lifetime to estimate the severity of anorexia nervosa and not the duration of anorexia nervosa, since this parameter was correlated with the age of our patients (Table 2). Notably, the severity of anorexia nervosa was the only clinical variable that correlated with the gray matter content of the anterior cingulate cortex cluster (Figure 3, Table 2). This effect was robust and remained significant after correction for global gray matter volume and the remaining clinical variables. These findings allow for two interpretations. Either gray matter decrease within the anterior cingulate cortex is an effect of anorexia nervosa, indicating that the anterior cingulate cortex is more vulnerable than the rest of the brain to conditions associated with anorexia nervosa such as malnutrition, or gray matter decrease within the anterior cingulate cortex is a cause of anorexia nervosa, indicating that the anterior cingulate cortex plays an original role in the pathophysiology of the disorder. We are not aware of scientific data indicating a particular vulnerability of the anterior cingulate cortex. In contrast, given the complex clinical picture of anorexia nervosa, it seems well conceivable that the functionally heterogenic structure of the anterior cingulate cortex plays an important role in the pathophysiology of this eating disorder.

In the 19th century, Broca already postulated that the anterior cingulate cortex integrates internal drives and emotions with higher cognitive functions (25). Today, the anterior cingulate cortex is regarded as a pivotal component of circuits that underlie functions such as attention, learning, language, and motor behavior (26). There are at least three functional subdivisions of the anterior cingulate cortex, of which the first two (rostral affective/visceral region and dorsal cognitive region) overlap with our anterior cingulate cortex cluster. The rostral affective/visceral region is located inferior and anterior to the genu of the

callosum. Strongly interconnected with the orbitofrontal cortex and amygdala, this region is not only involved in autonomic and endocrine functions but also in higher-order functions such as conditioned emotional learning, assessments of motivational content, and assigning emotional valence to internal and external stimuli. The dorsal cognitive region, the site of the peak voxel of the anterior cingulate cortex cluster, lies superior to the callosum, has extensive reciprocal connections with temporal and other frontal areas, and participates in response selection and cognitively demanding information processing (27, 28).

Evidence for an original role of the anterior cingulate cortex in the pathophysiology of anorexia nervosa derives not only from our structural data but also from other imaging studies. Applying SPECT, anorexia nervosa patients showed hypoperfusion in the anterior cingulate cortex (3–5), indicating an impaired or inhibited activity of this region. A PET study with specific radioligands was performed to localize alterations of the serotonin system and, notably, identified the anterior cingulate cortex (8). Further, fMRI studies indicate altered activation in the anterior cingulate cortex of anorexia nervosa patients specific to food stimuli (6, 7). In summary, converging evidence suggests that in anorexia nervosa the anterior cingulate cortex is altered with regard to both structure and function. However, we are far from arriving at a unifying model for the pathophysiology of anorexia nervosa, given the fact that the anterior cingulate cortex constitutes a multimodal region where complex phenomena, such as emotion, internal drives, reward seeking, attention, higher cognitive function, and learning, are functionally integrated. Moreover, some results of the imaging studies described above seem contradictory (e.g., hypoperfusion versus hyperactivation), and a considerable proportion of the brain regions that were additionally identified do not correspond. Yet, these data indicate that the pathophysiology of anorexia nervosa can almost certainly not be reduced to just a dysfunction of the anterior cingulate cortex. In addition, morphometric changes of the anterior cingulate cortex have also been reported in further psychiatric disorders such as OCD (29), PTSD (30), and schizophrenia (31), and thus it remains open for study whether changes of the anterior cingulate cortex in various psychiatric disorders result from common root causes of these disorders or from the involvement of different functional subdivisions of the anterior cingulate cortex.

Our study has some methodological limitations. Since recovery of our patients might have been incomplete and since we did not examine morphological changes longitudinally, the conclusion regarding the reversibility of global gray matter decrease remains speculative. Although we could show that region-specific gray matter decrease in the anterior cingulate cortex is directly related to the severity of anorexia nervosa, it remains to be elucidated whether this abnormality is a vulnerability marker and predictor (of relapse or chronicity) of anorexia nervosa.

FIGURE 3. The Relationship Between Lowest Body Mass Index of Lifetime and Gray Matter Decrease Within the Anterior Cingulate Cortex in Patients With Anorexia Nervosa[a]

[a] Correlation of lowest body mass index of lifetime and region-specific gray matter decrease (gray matter content of the cluster within the anterior cingulate cortex) is shown. The Spearman correlation coefficient was 0.5 (two-sided p value=0.01). This correlation remained significant after correcting for various variables such as age, duration of anorexia nervosa, body mass index at the time of scanning, and fraction of global gray matter volume (partial correlation coefficient=0.6; two-sided p value=0.02).

Correlation analyses of structural brain changes with the genetic load derived from anorexia nervosa patients with numerous siblings or from genetic testing (32) constitute a possible approach regarding the question of whether gray matter decrease in the anterior cingulate cortex results from genetic or environmental factors. Last, further neuroimaging studies are warranted to assess the anterior cingulate cortex in anorexia nervosa patients with regard to both structure and function.

Received Nov. 15, 2006; revisions received Feb. 3 and April 1, 2007; accepted April 13, 2007 (doi: 10.1176/appi.ajp.2007.06111861). From the Department of Neurology, Technische Universität München, Munich; Department of Psychiatry, University of Jena, Jena, Germany; Medizinisch-Psychosomatische Klinik Roseneck (Hospital for Behavioral Medicine), Prien am Chiemsee, Germany; TCE (Therapie-Centrum für Ess-Störungen, Therapy Center for Eating Disorders) München, Munich; ANAD (Anorexia Nervosa and Associated Disorders) e.V. Beratungsstelle für Essstörungen (Counselling Center for Eating Disorders), Munich; Department of Neuroradiology, Technische Universität München, Munich; Department of Nuclear Medicine, Technische Universität München, Munich. Address correspondence and reprint requests to Dr. Mühlau, Department of Neurology, Technische Universität München, Ismaninger Str. 22, 81675 München, Germany; m.muehlau@neuro.med.tum.de (e-mail).

The authors report no competing interests.

Supported by Fond 766160 of the Kommission für Klinische Forschung (KKF) des Klinikums rechts der Isar der Technischen Universität München.

References

1. American Psychiatric Association: Diagnostic and Statistical Manual of Mental Disorders, Fourth Edition (DSM-IV-TR). Washington DC, American Psychiatric Publishing, 2000

2. Uher R, Treasure J: Brain lesions and eating disorders. J Neurol Neurosurg Psychiatry 2005; 76:852–857
3. Takano A, Shiga T, Kitagawa N, Koyama T, Katoh C, Tsukamoto E, Tamaki N: Abnormal neuronal network in anorexia nervosa studied with I-^{123}-IMP SPECT. Psychiatry Res 2001; 107:45–50
4. Naruo T, Nakabeppu Y, Deguchi D, Nagai N, Tsutsui J, Nakajo M, Nozoe S: Decreases in blood perfusion of the anterior cingulate gyri in anorexia nervosa restricters assessed by SPECT image analysis. BMC Psychiatry 2001; 1:2
5. Kojima S, Nagai N, Nakabeppu Y, Muranaga T, Deguchi D, Nakajo M, Masuda A, Nozoe S, Naruo T: Comparison of regional cerebral blood flow in patients with anorexia nervosa before and after weight gain. Psychiatry Res 2005; 140:251–258
6. Uher R, Brammer MJ, Murphy T, Campbell IC, Ng VW, Williams SC, Treasure J: Recovery and chronicity in anorexia nervosa: brain activity associated with differential outcomes. Biol Psychiatry 2003; 54:934–942
7. Uher R, Murphy T, Brammer MJ, Dalgleish T, Phillips ML, Ng VW, Andrew CM, Williams SC, Campbell IC, Treasure J: Medial prefrontal cortex activity associated with symptom provocation in eating disorders. Am J Psychiatry 2004; 161:1238–1246
8. Kaye WH, Frank GK, Bailer UF, Henry SE, Meltzer CC, Price JC, Mathis CA, Wagner A: Serotonin alterations in anorexia and bulimia nervosa: new insights from imaging studies. Physiol Behav 2005; 85:73–81
9. Gaser C, Schlaug G: Brain structures differ between musicians and non-musicians. J Neurosci 2003; 23:9240–9245
10. Draganski B, Gaser C, Busch V, Schuierer G, Bogdahn U, May A: Neuroplasticity: changes in grey matter induced by training. Nature 2004; 427:311–312
11. Swayze VW II, Andersen A, Arndt S, Rajarethinam R, Fleming F, Sato Y, Andreasen NC: Reversibility of brain tissue loss in anorexia nervosa assessed with a computerized Talairach 3-D proportional grid. Psychol Med 1996; 26:381–390
12. Swayze VW II, Andersen AE, Andreasen NC, Arndt S, Sato Y, Ziebell S: Brain tissue volume segmentation in patients with anorexia nervosa before and after weight normalization. Int J Eat Disord 2003; 33:33–44
13. Katzman DK, Zipursky RB, Lambe EK, Mikulis DJ: A longitudinal magnetic resonance imaging study of brain changes in adolescents with anorexia nervosa. Arch Pediatr Adolesc Med 1997; 151:793–797
14. Lambe EK, Katzman DK, Mikulis DJ, Kennedy SH, Zipursky RB: Cerebral gray matter volume deficits after weight recovery from anorexia nervosa. Arch Gen Psychiatry 1997; 54:537–542
15. Fairburn CG, Harrison PJ: Eating disorders. Lancet 2003; 361: 407–416
16. Fichter MM, Herpertz S, Quadflieg N, Herpertz-Dahlmann B: Structured Interview for Anorexic and Bulimic Disorders for DSM-IV and ICD-10: updated (third) revision. Int J Eat Disord 1998; 24:227–249
17. Hiller W, Zaudig M, Mombour W: Development of diagnostic checklists for use in routine clinical care: a guideline designed to assess DSM-III-R diagnoses. Arch Gen Psychiatry 1990; 47: 782–784
18. Spitzer RL, Williams JBW, Gibbon M, First MB: Instruction Manual for the Structured Clinical Interview for DSM-III-R (SCID). New York, New York State Psychiatric Institute, Biometrics Research, 1988
19. Cuadra MB, Cammoun L, Butz T, Cuisenaire O, Thiran JP: Comparison and validation of tissue modelization and statistical classification methods in T1-weighted MR brain images. IEEE Trans Med Imaging 2005; 24:1548–1565
20. Friston KJ, Holmes A, Poline JB, Price CJ, Frith CD: Detecting activations in PET and fMRI: levels of inference and power. Neuroimage 1996; 4:223–235
21. Wagner A, Greer P, Bailer UF, Frank GK, Henry SE, Putnam K, Meltzer CC, Ziolko SK, Hoge J, McConaha C, Kaye WH: Normal brain tissue volumes after long-term recovery in anorexia and bulimia nervosa. Biol Psychiatry 2006; 59:291–293
22. Peters M: Sex differences in human brain size and the general meaning of differences in brain size. Can J Psychol 1991; 45: 507–522
23. Kingston K, Szmukler G, Andrewes D, Tress B, Desmond P: Neuropsychological and structural brain changes in anorexia nervosa before and after refeeding. Psychol Med 1996; 26:15–28
24. Neumarker KJ, Bzufka WM, Dudeck U, Hein J, Neumarker U: Are there specific disabilities of number processing in adolescent patients with anorexia nervosa? evidence from clinical and neuropsychological data when compared to morphometric measures from magnetic resonance imaging. Eur Child Adolesc Psychiatry 2000; 9(suppl 2):II111–121
25. Broca P: Anatomie compare des circonvolutions cerebrales: le grande lobe limbique. Rev Anthropol 1878; 1:385–498 (French)
26. Yucel M, Wood SJ, Fornito A, Riffkin J, Velakoulis D, Pantelis C: Anterior cingulate dysfunction: implications for psychiatric disorders? J Psychiatry Neurosci 2003; 28:350–354
27. Bush G, Vogt BA, Holmes J, Dale AM, Greve D, Jenike MA, Rosen BR: Dorsal anterior cingulate cortex: a role in reward-based decision making. Proc Natl Acad Sci U S A 2002; 99:523–528
28. Carter CS, Braver TS, Barch DM, Botvinick MM, Noll D, Cohen JD: Anterior cingulate cortex, error detection, and the online monitoring of performance. Science 1998; 280:747–749
29. Valente AA Jr, Miguel EC, Castro CC, Amaro E Jr, Duran FL, Buchpiguel CA, Chitnis X, McGuire PK, Busatto GF: Regional gray matter abnormalities in obsessive-compulsive disorder: a voxel-based morphometry study. Biol Psychiatry 2005; 58:479–487
30. Yamasue H, Kasai K, Iwanami A, Ohtani T, Yamada H, Abe O, Kuroki N, Fukuda R, Tochigi M, Furukawa S, Sadamatsu M, Sasaki T, Aoki S, Ohtomo K, Asukai N, Kato N: Voxel-based analysis of MRI reveals anterior cingulate gray-matter volume reduction in posttraumatic stress disorder due to terrorism. Proc Natl Acad Sci U S A 2003; 100:9039–9043
31. Honea R, Crow TJ, Passingham D, Mackay CE: Regional deficits in brain volume in schizophrenia: a meta-analysis of voxel-based morphometry studies. Am J Psychiatry 2005; 162:2233–2245
32. Grice DE, Halmi KA, Fichter MM, Strober M, Woodside DB, Treasure JT, Kaplan AS, Magistretti PJ, Goldman D, Bulik CM, Kaye WH, Berrettini WH: Evidence for a susceptibility gene for anorexia nervosa on chromosome 1. Am J Hum Genet 2002; 70: 787–792